LBL-10712

Lawrence Berkeley Laboratory
UNIVERSITY OF CALIFORNIA

ENERGY & ENVIRONMENT DIVISION

AIR INFILTRATION IN BUILDINGS

Max Howard Sherman
(Ph.D. thesis)

October 1980

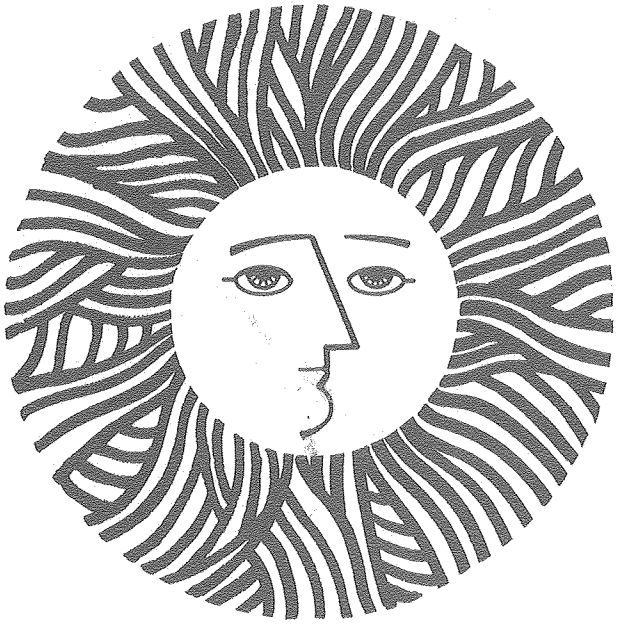

Prepared for the U.S. Department of Energy under Contract DE-AC03-76SF00098

DISCLAIMER

This document was prepared as an account of work sponsored by the United States Government. While this document is believed to contain correct information, neither the United States Government nor any agency thereof, nor the Regents of the University of California, nor any of their employees, makes any warranty, express or implied, or assumes any legal responsibility for the accuracy, completeness, or usefulness of any information, apparatus, product, or process disclosed, or represents that its use would not infringe privately owned rights. Reference herein to any specific commercial product, process, or service by its trade name, trademark, manufacturer, or otherwise, does not necessarily constitute or imply its endorsement, recommendation, or favoring by the United States Government or any agency thereof, or the Regents of the University of California. The views and opinions of authors expressed herein do not necessarily state or reflect those of the United States Government or any agency thereof or the Regents of the University of California.

AIR INFILTRATION IN BUILDINGS

Max Howard Sherman
Energy & Environment Division
Lawrence Berkeley Laboratory
University of California
Berkeley, CA 94720

ABSTRACT

Since the 1973 embargo by the oil producing and exporting countries (OPEC), this nation has been aware of the need to save energy. Many sectors of the economy, notably transportation, have been critically studied, but until recently, one of the largest sectors — the buildings sector — has been virtually neglected. In the last few years, researchers have recognized that infiltration (the flow of air though leaks in the building envelope) is a critical factor in energy loss in buildings and merits concentrated research effort if national energy conservation goals are to be served. It has been established, for example, that the energy loss due to infiltration is between 6 percent and 9 percent of the total energy budget for the nation.

This paper presents a physical model of infiltration in buildings that can be used to predict the infiltration for a wide range of construction types and climate regions. The the problems associated with commonly-used tracer gas methods for measuring infiltration were examined in detail so that results obtained from the model could be properly compared with actual measurements. In addition, a simple model of the hydrodynamics of typical leaks in the building envelope was devised in order to study the physical processes of infiltration (i.e., the flow of

---

The work described in this report was funded by the Office of Buildings and Community Systems, Assistant Secretary for Conservation and Solar Applications of the U.S. Department of Energy under contract No. DE-AC03-76SF00098.

TABLE OF CONTENTS

CHAPTER I	INTRODUCTION
CHAPTER II	MEASUREMENT TECHNIQUES
CHPATER III	HYDRODYNAMICS OF LEAKS
CHAPTER IV	WHOLE BUILDING LEAKAGE
CHAPTER V	PREDICTIVE MODEL
CHAPTER VI	CONCLUSION
APPENDIX A	MULTICHAMBER INFILTRATION DERIVATION
APPENDIX B	AC PRESSURIZATION DERIVATION
APPENDIX C	MODEL DERIVATION
APPENDIX D	TEST SITE MEASUREMENTS
APPENDIX E	LINEAR LEAKAGE INFILTRATION MODEL

CHAPTER I

INTRODUCTION

Since the 1973 oil embargo by the OPEC members, energy supply has been a major concern to all industrialized nations. Many solutions to the global energy problem have been suggested, but, as shown by a study made by the Harvard Business School,[1] the most cost effective supply alternative with the greatest probability for widespread implementation before the turn of the century is conservation. Currently, the United States spends about 1/4 of a trillion dollars on energy; thus, a small percentage decrease in annual energy use would translate into substantial monetary savings. The following chart displays a breakdown of energy end use by sectors:[2]

U.S. RESOURCE ENERGY ANNUAL CONSUMPTION (QUADS)	
Residential Buildings	17
Commercial Buildings	11
Industry	29
Transportation	21
Total	78
1 QUAD = 10^{15} Btu	

While a considerable amount of work has been done to improve the energy efficiency of the automobile, (i.e., the mpg rating), the transportation sector, as indicated above, accounts for only 27 percent of the annual energy budget of the United States. Buildings, however, consume 36 percent of U.S. energy, but far less has been done to improve the energy efficiency. The reasons for this dichotomy are not hard to

---

* Most of the data in this section has been extracted from the Building Energy Use Data Book produced for the Department of Energy (See reference 1.).

understand: since the transportation industry is dominated by the three large auto companies, policies can be simply stated and enforced; whereas, since the building industry is diffuse, it is quite difficult to define and execute effective policy measures. Additionally, large centralized industries, such as the automakers, are able to take advantage of their oligopolistic positions in order to do a significant amount of research and development work privately; but decentralized industries, such as construction, do not have the capital or facilities to invest in R&D efforts.

The largest single energy end-use in buildings is space heating and cooling, which accounts for over half the energy use in the building sector. (See the "pie charts" at the end of this section for the actual breakdown of energy use.) In the residential sector 50 percent of the energy is consumed by space heating and 6 percent is consumed by cooling. (While residential cooling might be a much smaller energy consumer than residential heating, cooling loads tend to be near electrical demand peaks, thus using more costly resources.)

The space conditioning load (i.e., the energy consumed by both space heating and cooling) is due to two main components: conduction and infiltration. Conduction causes direct heat loss through materials in the building envelope because of a temperature difference across it:

$$E = U\,A\,\Delta T \qquad (I.1)$$

where

E	is the heat loss due to conduction [W],
U	is the conductivity of the envelope [$W/m^2/K$],
A	is the envelope area [m^2] and
ΔT	is the inside-outside temperature difference [K].

The conductivity(U) and the area(A) are often combined into a single term called the conductance or UA value of the envelope.

Infiltration is the mass transport of air through leaks in the building envelope and is caused by pressure differences across the envelope. The heat loss due to infiltration is the product of the infiltration and the temperature difference:

$$E = Q \rho C_p \Delta T \tag{I.2}$$

where

E	is the energy loss due to infiltration [W],
Q	is the infiltration [m^3/s],
ρ	is the density of air [1.2 kg/m^3],
C_p	is the heat capacity of air [1000 J/kg/K] and
ΔT	is the inside-outside temperature difference [K].

Infiltration, unlike conductivity, is a function of weather; this, infiltration is nonlinear and difficult to model. Accordingly, fewer attempts have been made to quantify infiltration than to quantify conduction. Nevertheless, infiltration remains an important component of the space-conditioning load. For a structure built before 1979, the ventilation load is currently estimated to be in the range of 1/3 to 1/2 the total load; the total infiltration energy load is estimated to range from 6 percent to 9 percent of the total energy bill of the country. Thus, the cost of infiltration is estimated to be 20 billion dollars per year.

In commercial buildings, only part of the total ventilation load is due to infiltration, most of the load is due to mechanical ventilation. The substantive difference between infiltration and mechanical ventilation is that mechanical ventilation, unlike infiltration, is assumed to be independent of weather and controlled by the operators of the building. But, in a residence, virtually all of the ventilation load is due to infiltration. The table below displays annual heating costs attributed to infiltration for an average home in Boston (6000 degree ^oF-days -- excluding any cooling load) having a volume of 250 m^3 and an infiltration rate of 200 m^3/hr.):

RESIDENTIAL INFILTRATION IN BOSTON*

Fuel Type	Efficiency	Amount	Unit Price	Cost
Natural Gas	.60	450 therms	40¢	$180
Oil	.60	340 gallons	$1	$340
Electric	1.00	13000 kWh	5¢	$650

Since infiltration is both an important fraction of the space conditioning load of a structure and a difficult quantity to calculate, many have suggested abandoning infiltration model research, and proceed to tighten the shell of the building (i.e. remove leaks) until infiltration is no longer an important factor in estimating building energy use. The notion is not only intellectually unsatisfactory, it is neither possible nor desirable.

While infiltration can be costly in terms of energy use, too little ventilation may be hazardous to health. Recent studies have shown that pollution levels inside a building may be much higher than outside levels. Carbon monoxide, Carbon dioxide, oxides of nitrogen, particulates, unburnt hydrocarbons, etc., are released as combustion by-products[3] i.e., from normal activities like cooking and heating; aldehydes, e.g. formaldehyde, may be given off by building materials[4] i.e.,from components of the structure like walls, furniture etc., that may contain glues. Less common but more serious in terms of human health may be the presence of radon.[5]

Radon is emitted durng the decay-chain of the uranium-235 atom. Radon, a noble gas, is chemically inert. This renders it dangerous because radon can diffuse several inches through concrete, and get easily into the air. Radon itself decays by alpha emission to form a series of chemically active daughters that attach themselves to fine

---

* See the Table of Conversions at the end of this section to compare units.

particulates that could be inhaled into the lungs.

Some studies suggest[6] that a significant fraction of lung cancers in nonsmokers may be attributed to the presence of radon in indoor air. There remain, however, many open questions concerning the extrapolation of long-term low-dose health hazards from the short-term high-dose data that currently exist. All researchers, however, agree that radon research, as well as research into other pollutants, is necessary.

For building-energy use models, infiltration is not a simple quantity to be ignored. On the other hand, if insufficient ventilation air were supplied to the structure, the air quality of the interior of the structure will be inadequate to maintain the health of the occupants; on the other hand, each cubic meter of air brought into the structure must be conditioned (heated, cooled, etc.) in order to maintain the comfort level of the occupants.

The United States is paying approximately 20 billion dollars each year to condition air that is leaking into homes, office buildings and factories, yet little is known about the infiltration process. If the United States could recover even half of the energy lost to infiltration, the country as a whole would be saved the cost of ten new nuclear power plants or six Chrysler loan guarantees every year; from the energy saved by decreasing infiltration the United States could cut its oil consumption by 2 million barrels per day, or, equivalently, could shut down or cancel 100 power plants throughout the nation.

As noted above, decreasing infiltration in buildings, while desirable from the point of view of saving the energy component of a building's life-cycle cost, does affect indoor air quality. Minimum ventilation standards should be maintained in order to insure the health of the buildings occupants. These two considerations appear at odds. The development of air-to-air heat exchangers,[7] however, would provide the possibility for adequate ventilation without necessarily increasing infiltration loads. An air-to-air heat exchanger permits an exchange between two streams of air, the air entering the building, and the exhaust air. Thus, during the heating season, for example, the escaping air warms the entering stream of air sufficiently so that the incoming

air requires no further conditioning (heating) and energy requirements are lowered by approximately 75 percent. The same process, reversed, occurs in hot weather and allows cooling costs to be similarly reduced.

Even though it has been demonstrated that reducing infiltration need not be incompatible with the increased ventilation needed to assure indoor air quality, it is insufficient to assume that infiltration will be reduced when the leaks in a structure are sealed. It is still necessary to be able to predict the infiltration on a short-term basis: construction quality standards ought to be implemented, requiring mechanical ventilation when the average infiltration is below an appropriate value and requiring an upper limit on the infiltration costs of the structure. Furthermore, a model of infiltration would be required in order to predict infiltration changes that might occur after an existing building has been retrofitted. The purpose of this paper is to describe the physics associated with infiltration, and to describe the techniques required for its measurement. In addition, it is important that physical models of the processes involved are developed — models that are simple enough and accurate enough to apply to real situations. In order to develop an accurate model, infiltration in a structure must be measured directly.

The first techniques for measuring infiltration were developed by Dick in the 1940s.[8-10] Much of that work is still used today, although the limits on its accuracy and the assumptions underlying its use are not well known. Thus, it is necessary to begin by developing equations describing the measurement techniques themselves, in order to expose the assumptions underlying the equations.

Infiltration is the flow of air through leaks in the building envelope, thus the hydrodynamics of such leaks must be studied and applied to actual structures. Although hydrodynamics encompasses a large body of research and knowledge, in this case, principles of hydrodynamics would be applied to very restricted conditions: the pressure range across the leaks (principally within a single order of magnitude), the air (a single fluid) within a small band of pressure and temperature conditions, and the dimensions of the leaks.

Once the hydrodynamics of infiltration have been understood, the principles can be applied macroscopic structures composed of distributed leaks often having different geometric identities. Techniques for measuring macroscopic leakage properties need to be developed in a manner that allows the information to be used in infiltration modelling. Having characterized the response of a building under known pressures, it is then necessary to be able to predict the pressures that cause infiltration, by finding a model that uses the leakage information and pressure distribution to predict infiltration. Finally, predictions will be compared to direct measurements of infiltration. The purpose of this paper is to place these problems in a cohesive perspective, in order to assess the work that remains to be done.

REFERENCES

1. "Energy Future," Report of the Energy Project at the Harvard Business School, R. Stogaugh, D. Yergin Editors, Random House, N.Y. (1979)

2. Blue et al., "Buildings Energy Use Data Book: Edition 2," Oak Ridge National Laboratory No. 5552 Oak Ridge, Tenn., (1979)

3. J.V. Berk, C.D. Hollowell, J.H. Pepper, R.A. Young, "The impact of Reduced Ventilation on Indoor Air Quality in Residential Buildings," Lawrence Berkeley Laboratory Report LBL-10527 (1980)

4. C. Lin, R.N. Anaclerio, D.W. Anthon, L.Z. Fanning, C.D. Hollowell, "Indoor/Outdoor Measurements of Formaldehyde and Total aldehydes," Lawrence Berkeley Laboratory Report LBL-9397 (1979)

5. C.D. Hollowell, J.V. Berk, M.L. Boegal, J.G. Ingersoll, D.L. Krinkel, W.W. Nazaroff, "Radon in Energy-Efficient Residences," Lawrence Berkeley Laboratory Report LBL-9560 (1979)

6. R.J. Budnitz, J.V. Berk, C.D. Hollowell, W.W. Nazaroff, A.V. Nero,

A.H. Rosenfeld, "Human Disease from Radon Exposers: The Impact of Energy Conservation in Residential Buildings," Lawrence Berkeley Laboratory Report LBL-7809 Revised (1979)

7. G.D. Roseme, J.V. Berk, M.L. Boegel, H.I. Halsey, C.D. Hollowell, A.H. Rosenfeld, I. Turiel, "Residential Ventilation with Heat Recovery: Improving Indoor Air Quality and Saving Energy," Lawrence Berkeley Laboratory Report LBL-9749 (1980)

8. J.B. Dick, "Experimental Studies in Natural Ventilation of Houses," J. Inst. Heat. Vent. Eng. 17,420 (1949)

9. J.B. Dick & D.A. Thomas, "Ventilation Research in Occupied Houses," J. Inst. Heat. Vent. Eng. 19,306 (1941)

10. J.B. Dick, "The Fundamental of Natural Ventilation of Houses," J. Inst. Heat. Vent. Eng., p. 123, (1950)

TABLE OF CONVERSIONS

1 quad	1.0×10^{15} Btu
1 mbd[a]	2.5×10^{15} Btu
1 therm	1.0×10^{5} Btu
1 kWh	3.4×10^{3} Btu
1 Joule	1.0×10^{-3} Btu
1 ft^3 gas	1.0×10^{3} Btu[b]
1 ton coal	2.5×10^{7} Btu[b]
1 barrel oil	5.8×10^{6} Btu[b]
1 barrel	42 gallons

a mbd stands for million barrels per day oil equivalent

b approximate heating value

FIGURE CAPTIONS

FIG. I:1 Building energy consumption for 1976 for total US stock.

FIG. I:2 Residential energy consumption for California in 1979.

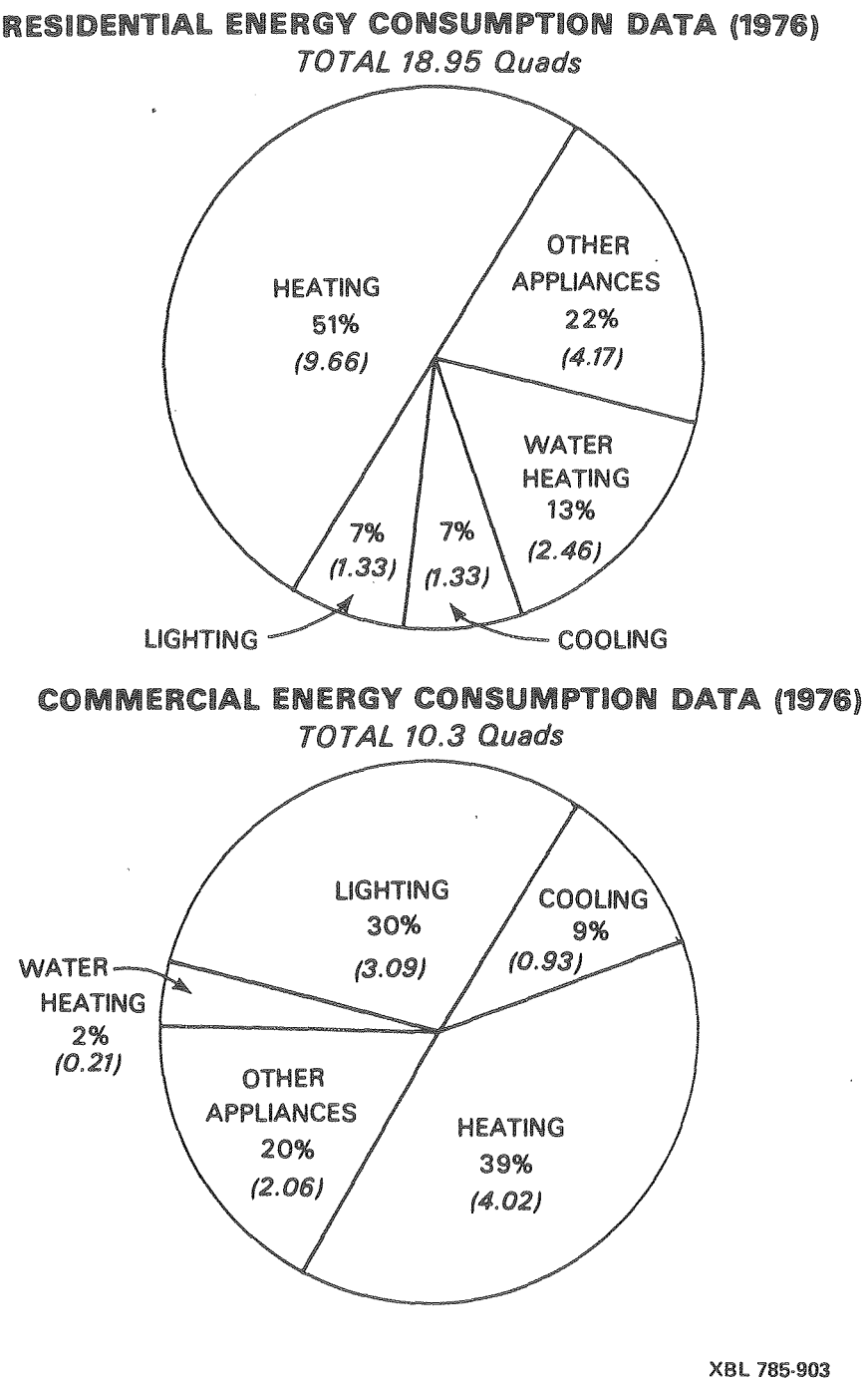

FIG. I:1 Building energy consumption for 1976 for total US stock.

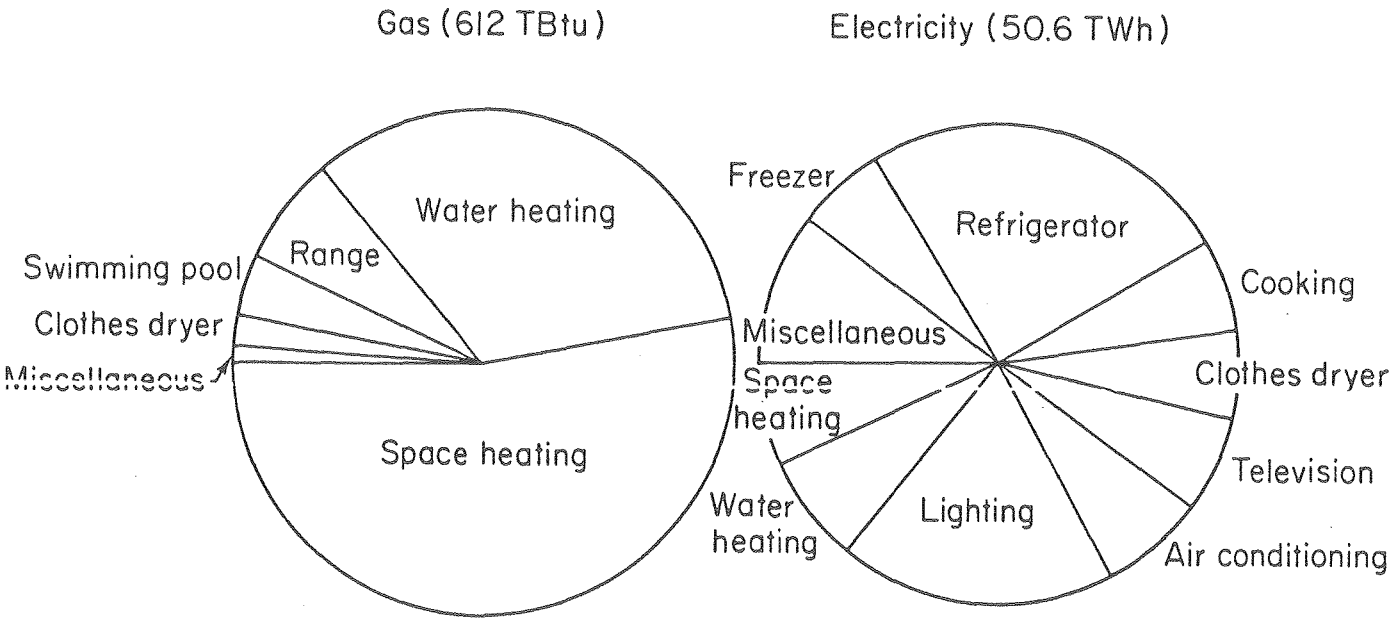

FIG. I:2 Residential energy consumption for California in 1979.

CHAPTER II

INFILTRATION MEASUREMENT TECHNIQUES

The most straightforward method of quantifying infiltration is to measure it directly. There are many direct-measurement schemes used to measure infiltration, and virtually all involve the use of a tracer gas. A tracer gas permits the air in a structure to be tagged so that air movement can be followed; dilution of the tracer gas is associated with the exfiltration of air. Other, more esoteric, methods for measuring air infiltration (e.g., particulate tagging, ratios of radioactive daughters, etc) have been proposed, but none are actively being pursued. The techniques described here are concerned with tracer gas methods exclusively.

TRACER GAS COMPARISIONS

Hunt[1] in his review of current techniques lists some of the the qualities of an ideal tracer gas

(1) inexpensive,

(2) easily measurable at low concentrations,

(3) nontoxic and nonallergenic,

(4) nonflammable,

(5) have approximately the same molecular weight as air,

(6) not absorbed on any surfaces within the space under test,

(7) not a normal constituent of the air in the test space,

(8) yield results independent of tracer gas.

No tracer gas meets all these requirements; thus, many researchers have compared tracer gases to find those that most closely approach the ideal. An excellent review of the experimental techniques used to measure air infiltration is that of Hitchin and Wilson .[2] This review

has been extended by Hunt's careful review of current techniques, to include work through 1978.

Many researchers have compared many different gases in the course of intercomparison work. Warner[3] compared coal gas (a mixture of H_2 and CO obtained by passing steam over hot carbon), detected using a Katharometer with CO_2 measured by Haldane gas analysis.

Collins and Smith[4] used the radioactive argon isotope ^{41}A as a tracer, measuring concentration with a geiger counter and a ratemeter. They made a direct comparison of the infiltration rate using H_2 as detected by a katharometer and ^{41}A; agreement within ±8 percent was seen in two trials.

Howland, Kimber and Littlejohn[5] compared radioactive isotope ^{85}Kr, measured using a geiger counter and a ratemeter with CO_2. The carbon dioxide concentration was determined by drawing samples of air periodically and using chemical analysis (the Haldane apparatus), to find the amount of tracer remaining in the test space. Three separates tests showed agreement to within ±9 percent.

Lidwell[6] compared nitrous oxide, N_2O, with acetone, C_3H_6O. Infrared absorption was used to measure the concentration of nitrous oxide; acetone concentration was determined by measuring the change in pH which occurred when air containing acetone is absorbed into solutions of hydroxylamine hydrochloride. A single measurement (judged to be accurate to within ±10 percent) produced ±3 percent agreement.

Howard[7] compared N_2O with both H_2 and O_2. N_2O concentrations were determined with an infrared analyzer, H_2 concentrations with a katharometer, and O_2 by absorption in aqueous chromous chloride. Although specific results are not reported, the author states that close agreement between decay rates using N_2O and O_2 were seen over wide ranges of wind speeds. On the other hand, H_2 decay rates were substantially higher than those of N_2O. The evidence suggests that the source of the discrepancy was diffusion of H_2 through the walls of the unpainted gypsum. The hypothesis was tested by repeating tests after the walls were sealed with two coats of latex paint, and repeating the tests

again in a laboratory with masonry walls. The discrepancy was not present in the latter tests.

Using as their test space a 4-bedroom townhouse constructed within an environmental test chamber, Hunt and Burch[8] compared air change rates using He and SF_6 to examine the influence of molecular diffusion on the infiltration process. If molecular diffusion were important in the infiltration process, the air change rate measured with He would be significantly larger than that measured with SF_6. In fact, slightly larger air change rates were seen when SF_6 was used as the tracer. Six trials were made, and the ratio of the air change rate measured with SF_6 to that measured with He was 1.17 with a standard deviation of 0.14.

The most recent study of tracer gases was made by Grimsrud, Sherman, Janssen, Pearman and Harrje[9] who compared SF_6, N_2O, C_2H_6 and CH_4 (sulfur hexafluoride, nitrous oxide, ethane, and methane). The SF_6 was measured by means of gas chromatography with electron capture, and the light gasses were measured by infrared absorbency techniques. The test took place in a ranch style house in Walnut Creek (see Appendix D for details of "Haven" house). No differences were detected among the light gases, but a statistically significant, although numerically small difference appeared between the light gases and SF_6.

All of the data to date is compared in this paper by Grimsrud et al. However, the conclusions are simple; the very light gases (e.g. H_2, He) and the very heavy gases (e.g. SF_6) have anomalous behavior when compared with other gases, but there are a wide variety of acceptable gases for tracer studies.

CONTINUITY EQUATION

Before measurement techniques can be evaluated, equations used for data analysis must be derived. For infiltration, the continuity equation describing the flow of air among a set of chambers was derived. When considering the general case of several interconnecting chambers, each of which may communicate, i.e., exchange air with each other, as well as the outside, a matrix of airflows can be defined, that contains

as its elements, the flow from one chamber to another. (Note that unlike heat or electrical charge, the flow of air from chamber a to chamber b is not directly related to the flow from chamber b to chamber a.) The infiltration matrix is the matrix containing the airflows between chambers and appears in the continuity equation as derived in Appendix A:

$$\bar{\bar{V}} \cdot \frac{d\bar{C}}{dt} + \bar{\bar{Q}} \cdot \bar{C} = \bar{F} \qquad \text{(II.1)}$$

where

$\bar{\bar{V}}$	is the effective volume matrix [m^3],
$\bar{C}$	is the concentration vector,
$\bar{\bar{Q}}$	is the infiltration matrix [m^3/s] and
$\bar{F}$	is the effective flow matrix of injected tracer [m^3/s].

The volume matrix is assumed to be diagonal, i.e.,

$$V_{kj} = V_k \, \delta_{kj} \qquad \text{(II.2)}$$

where

δ_{kj}	is the Kronecker delta function.
V_k	is the effective volume of the kth chamber [m^3],
C_j	is the concentration in the jth chamber,
$-Q_{jk}$	is the air flow from kth to jth chamber [m^3/s],
Q_{jj}	is the total exfiltration from the jth chamber [m^3/s] and
F_j	is the effective flow of the jth chamber [m^3/s]).

Although the off-diagonal elements of the infiltration matrix contain information about the flow from one chamber to another, they do not contain any information about the flow to, or from the outside; to recover that information, the continuity equation for air must be derived. Since the diagonal elements contain the total exfiltration (thus, total infiltration), the flows to and/or from the outside can be recovered by taking the difference between the total exfiltration/infiltration and

the sum of the individual chamber exfiltrations/infiltrations:

$$\sum_{k=1}^{N} Q_{kj} = -Q_{0j} \qquad j=1 \ldots N \qquad \text{(II.3.1)}$$

$$\sum_{k=1}^{N} Q_{jk} = -Q_{j0} \qquad j=1 \ldots N \qquad \text{(II.3.2)}$$

where

$-Q_{j0}$ is the infiltration from the outside to the jth chamber and

$-Q_{0j}$ is the exfiltration from the jth chamber to the outside.

Because of imperfect mixing, the effective volume (the volume that takes part in the air exchange) might not be equal to the physical volume of a particular chamber. Likewise, the effective flow, (of the flow that is "felt" by the chamber), may not be equal to the physically injected flow of tracer gas. While it is possible to measure the effective volume and mixing function* directly, it is better to use a measurement technique that minimizes their effects.

TECHNIQUES

The following discussion outlines the techniques currently used for measuring infiltration.[10] While many researchers have used these methods on single-chamber systems, very little data have been acquired for multichamber systems. Accordingly, the discussion focuses on measurement techniques as actually used in the field, and concludes with a short discussion of how techniques could be generalized to include measurement in multichamber situations. Since the largest single source of error in tracer measurements is the violation of the assumption of perfect

---

* The mixing function is the relationship between the physical injected flow and the effective injected flow. See Appendix A for details.

mixing, the techniques will be compared for their sensitivity with regard to mixing problems. The single-chamber continuity equation is simply a special case of the general equation, i.e., when N=1:

$$V \dot{C} + Q C = F \qquad \text{(II.4)}$$

where

V	is the effective volume [m^3],
$\dot{C}$	is the time rate of change of concentration [s^{-1}],
Q	is the infiltration [m^3/s],
C	is the concentration and
F	is the effective injected flow rate [m^3/s].

Some form of this equation will be used in each of the techniques discussed below.

Decay technique

The tracer decay technique is by far the most widely used method for measuring air infiltration. In the decay technique tracer gas is first released in order to bring the concentration of tracer gas in the room up to some value; then the flow of tracer gas is discontinued and the concentration is allowed to decay. During this period of decay, there is no source term in the continuity equation:

$$V \dot{C} + Q C = 0 \qquad \text{(II.5)}$$

and the solution to the homogeneous differential equation described the concentration:

$$C(t) = C_o e^{-At} \qquad \text{(II.6)}$$

where

C_o is the concentration at t=0 and

A=Q/V is the infiltration rate [hr^{-1}].

Procedure: The tracer detector is connected to a single-channel chart recorder (or data may be taken by hand).

A volume of tracer gas sufficient to bring the concentration of tracer to near the full scale of the analyzer is released. (Additional mixing may be used at this point to assure even distribution of the tracer.)

The system is allowed to stabilize and data is recorded until the concentration drops well below its starting value (1/2 to 2 hr).

The data is analyzed by fitting the concentration data to a simple exponential. The time constant (coefficient of the time variable) yields the infiltration rate.

If longer-term measurements are required, the procedure is repeated.

This system is simple, uses the minimum amount of equipment and is well suited for making short-term measurements, or spot checks at many sites. The analysis calculates the infiltration rate (the ratio of the infiltration (in m^3/hr) to the effective volume) used, in turn, to calculate the infiltration by multiplying it by the physical volume of the space. Therefore, the calculated infiltration would be in error by the ratio of the effective volume to the physical volume, a ratio which could be as large as 50 percent.

Because a given decay rarely lasts longer than a few hours, in order to get long term information, it is necessary to repeat the entire procedure frequently. In addition, a significant time period must be spent waiting for the mixing to be complete after each injection. For those

reasons, the system is inappropriate to use for long-term continuous measurements.

Multichamber: In a multichamber decay all of the flows are set to zero. Accordingly, the solution is analogous to the single chamber solution:

$$\bar{\bar{C}}(t) = e^{-\bar{\bar{A}}t} \cdot \bar{\bar{C}}_o \qquad \text{(II.7)}$$

where

$\bar{\bar{C}}_o$ is the initial set of concentrations

$\bar{\bar{A}} = \bar{\bar{V}}^{-1} \cdot \bar{\bar{Q}}$ is the infiltration rate matrix and

Care must be taken in defining the infiltration rate matrix; although all elements are well defined, only the diagonal elements have easily interpretable meanings: they are the rate of total infiltration from all spaces, including outside.

Constant concentration / Constant flow

The best way to eliminate the problem of finding the effective volume is by finding a way to eliminate it from the continuity equation used to calculate infiltration. Because the coefficient of the effective volume is the time rate of change of the concentration, any uncertainties about the effective volume could be removed by maintaining a constant concentration. If automatic injection with a feedback system were used to keep the concentration at a desired level, the infiltration could be simply:

We have used a matrix as the exponent; this has meaning only through the context of an infinite series and cannot be expressed in simple terms otherwise.

$$Q = \frac{F}{C} \tag{II.8}$$

where F and Q may be time-varying but C is a constant.

In practice, however, this technique is impossible because of the mixing function. The mixing function causes a delay in the response of the concentration to a change in the flow. When sensing no appreciable concentration change, the measurement continues to change the flow even further, causing an overshoot in the constant concentration level. In other words, if the automated system were to attempt to keep the concentration constant, the delay would cause an unstable oscillation in the concentration and a breakdown in the experimental design.

The only way to prevent instability in the feedback system is to make the update time of the system long compared to any mixing time. If the update time were long enough, i.e., the loop gain of the system is small enough, the instabilities could be avoided. In that case, however, the concentration could be considered constant only for time scales that are long compared to the update time, which in turn must be long compared to the mixing times. Therefore, the assumption of constant concentration would be violated for all but the most highly mixed conditions. A modification to the constant concentration technique that might avoid this instability would be to make the flow constant. Using a constant flow technique minimizes mixing problems because after the initial warm-up period (a time long compared to any mixing time), the mixing function has no effect and the effective flow is equal to the actual flow (See Fig. 1). However, since the concentration is not constant, the volume term would be present; that is,

$$Q = \frac{F}{C} - \frac{V}{C}\dot{C} \tag{II.9}$$

<u>where</u>

V is the effective volume [m^3].

Care must be taken in interpreting the volume used in any of these infiltration equations. In most cases, the volume to which symbol, V, refers, is the effective volume and not the physical one.

If the system were near equilibrium, the concentration would be slowly varying, and the time rate of change of concentration would be quite small. In that case, the last term in the above equation would be a small correction term and the error introduced by replacing the effective volume with the physical volume would be negligible.

Procedure: The tracer detector and a mass-flow controller (or other flow-metering device) are connected to a two-pen chart recorder and started.

Enough tracer-gas is released to bring the concentration up to mid-scale on the analyzer.

Infiltration is estimated and this value is used to set the flow so that at equilibrium the concentration should be mid-range on the gas analyzer.

The system is allowed to run continuously and data is considered to be valid once the time rate of change of the concentration is small.

The data is analyzed by means of the above equation.

This technique has the advantage of being relatively insensitive to the mixing function and minimizes the effect of the unknown, effective volume. The automatic feedback system will run for days and give continuous infiltration measurements. This does have some disadvantages, however. If the infiltration were to deviate significantly from the estimate, the gas analyzer will go off scale and data would be lost. If the infiltration were to change rapidly, a rapid change in the concentration would occur, emphasizing any effects due to effective volume. The system requires some warm-up time (approximately 1 hour) before the data can be considered valid.

Multichamber: In a constant concentration experiment, the concentration of gas in each space is held constant.

$$\bar{\bar{Q}} \cdot \bar{C} = \bar{F} \qquad \text{(II.10)}$$

This experiment cannot be done using only one gas, unless several completely independent runs are made. Using separate runs makes the rather poor assumption that the air flows will be the same for each run. In either case, a concentration matrix is constructed; an injected flow matrix is constructed (whose columns are either different runs, or different gases, and whose rows, as before, are different chambers); and an injected tracer flow matrix is constructed having the same properties, i.e.,

$$\bar{\bar{Q}} \cdot \bar{\bar{C}} = \bar{\bar{F}} \qquad \text{(II.11)}$$

Solving for the infiltration, directly, yields,

$$\bar{\bar{Q}} = \bar{\bar{F}} \cdot \bar{\bar{C}}^{-1} \qquad \text{(II.12)}$$

As can be seen from this expression, the requirement for independent runs, or different gases would be necessary to keep the concentration matrix from becoming singular.

A special case of the multichamber constant concentration technique would be encountered if all of the concentrations were held constant to the same value, for which the continuity equation becomes,

$$C_o \sum_{k=1}^{N} Q_{jk} = F_j \qquad j=1 \ldots N \qquad \text{(II.13)}$$

where

C_o is the constant concentration.

Due to the derivation of the infiltration matrix, the sum could be

replaced by infiltration from the outside:

$$-Q_{j0} = \frac{F_j}{C_o} \qquad j=1 \ldots N \qquad \text{(II.14)}$$

where

$-Q_{j0}$ is the infiltration from the outside $[m^3/s]$.

Thus, if the only quantity desired were the infiltration of fresh air into each chamber, this method would become practical as long as feedback instabilities could be handled. A version of this technique is being used currently by British Gas.[11]

In the constant flow case, the diagonal physical volume matrix is used as a correction term for the above expression:

$$\bar{\bar{Q}} = \bar{\bar{F}} \cdot \bar{\bar{C}}^{-1} - \bar{\bar{V}} \cdot \frac{d\bar{\bar{C}}}{dt} \cdot \bar{\bar{C}}^{-1} \qquad \text{(II.15)}$$

where

$\bar{\bar{V}}$ is the physical volume matrix

Long-term average technique

In order to characterize any nation's housing stock, it would be necessary to make a survey of infiltration rates averaged over long periods of time e.g., a month. In theory, one of the techniques described above could be used for a month and an average of the results could be taken; however, it would be much more desirable to have a simpler, low-cost system available for such a purpose.

To measure long-term average infiltration rates, average the continuity equation divided by the infiltration.

$$\left[\frac{V}{Q}\dot{C}\right] + \left[C\right] = \left[\frac{F}{Q}\right] \qquad \text{(II.16)}$$

where

$\left[\cdots\right]$ indicates a time average.

If the flow were kept constant,

$$\left[\frac{F}{Q}\right] \rightarrow F\left[\frac{1}{Q}\right] \tag{II.17}$$

If the averaging interval were long enough, i.e., long compared to the inverse infiltration rate,

$$\left[\frac{V}{Q}\dot{C}\right] \rightarrow 0 \tag{II.18}$$

Combining terms gives an expression for the average of the reciprocal infiltration:

$$\left[\frac{1}{Q}\right] = \frac{\left[C\right]}{F} \tag{II.19}$$

If the infiltration were held constant, then the inverse of the average infiltration would be equal to the average of the inverse infiltration; however, over the long term, infiltration would not be constant. A correction factor, k, must be defined that allows the conversion of the average of the inverse infiltration to the average infiltration:

$$\left[\frac{1}{Q}\right] = \frac{k}{\left[Q\right]} \tag{II.20}$$

where

$$k = \sqrt{1 + 2\sigma^2} \tag{II.21}$$

and σ is the fractional standard deviation of either the infiltration or the inverse infiltration.

Since the inverse average weights small infiltration values more than large ones (and more would be weighted if a simple average were taken), the correction factor would always be greater than unity.

Procedure: A two-channel sampling pump and accessories are brought to the site of interest.

The pump is set so that one channel is used to inflate an empty bag with room air; and the other channel is used to evacuate a bag full of tracer gas.

The pump speed and tracer-gas concentration in the initially full bag are set so that the concentration of gas in the initially empty bag will be within the range of the analyzer.

A volume of tracer-gas sufficient to bring the analyzer up to half scale is released, and the pump is started.

The equipment is left unattended on site for the duration of the experiment and then picked up and brought back to the laboratory for analysis.

The total amount of gas dispensed is measured by comparing the volume of the initially full bag to its volume after the experiment; the concentration in the initially empty bag is also measured and the results are used to calculate the average inverse infiltration.

This technique is currently being used in actual field measurements. Because its concentration can be measured in the range of one part in 10^{12} to one part in 10^{9}, the tracer chosen for use in this experiment is SF_6. This provides both high sensitivity, and large dynamic range; and is, thus, useful for long-term average measurements. The analyzer costs about $7000 but the total equipment cost for each field site is about $500. Thus, it is inexpensive to do several long-term average

infiltration measurements simultaneously.

The trade off for low-cost is found in the correction term required to convert the average inverse infiltration into the average infiltration. A large set of data[12] were used to find values for parameters from the previous equation:

Site	$\left[\frac{1}{Q}\right]$	$\left[Q\right]$	σ	k
HTSG	1.22	.85	.21	1.05
HSLG	2.79	.38	.24	1.06

Note that the site designations are from the original work.

From this set of data, it might be concluded that the correction factor would be near unity for typical infiltration values, indicating that an independent measurement of the standard deviation of the infiltration would not be necessary.

It is interesting to note that the necessity of the correction factor becomes moot if the purpose of the long-term measurement were to access indoor air pollutant levels. If it were assumed that the source of the pollutants could be treated as quasi-steady-state entities, then the average concentration of the resultant pollutant would be proportional to the average inverse of the infiltration — the quantity we measured. In fact, the average concentration of a pollutant would be equal to the average concentration of the tracer, times the ratio of the sources:

$$\left[C_p\right] = \left[C\right] \frac{F_p}{F} \qquad \text{(II.22)}$$

where

C_p is the concentration of the pollutant and

F_p is the source of the pollutant [m^3/s].

Multichamber: Although long-term average multichamber infiltration could be considered, infiltration should be measured with separate gasses, since it would be impossible to do several independent runs over a long period of time. As in the single-chamber case, it would be the inverse of the infiltration that would be calculated,

$$\left[\bar{\bar{Q}}^{-1} \right] = \bar{\bar{F}} \left[\bar{\bar{C}}^{-1} \right] \qquad \text{(II.23)}$$

and there could be a correction factor, k. In the multichamber case, however, k would be a matrix, and, without actual infiltration measurements, it would be difficult to interpret the importance of this correction factor. As in the single-chamber case, the correction factor is unimportant to the assessment of indoor air quality.

Continuous flow

The researchers at LBL have attempted to develop a highly accurate, continuous, infiltration monitoring system, capable of running unattended for significant periods of time, e.g. a week. Thus, microprocessor-based, continuous-flow infiltration system has been designed.

Continuous-flow and constant-flow techniques are quite similar except that in continuous flow systems, the effective volume is treated as an unknown parameter, in a constant-flow system, the effective volume is approximated by the physical volume. In order to assist in eliminating random error in continuous flow systems, nonlinear search routines are used to find the "best fit" of the unknown parameter over a cycle period.

During a cycle the flow is held constant; if infiltration and effective volume were treated as constants during one cycle period (typically half an hour), the continuity equation could be solved for the concentration as a function of time.

$$C(t) = \frac{F}{Q} + \left(C_o - \frac{F}{Q} \right) e^{-\frac{Q}{V}t} \tag{II.24}$$

This expression contains three unknown parameters — V, Q, and C_o. C_o, the "best fit" to the initial concentration, is a parameter that is of no real interest; but, nevertheless, must be found simultaneously with the other two parameters.

Procedure: The flow rate for a cycle is set equal to a target concentration, times the calculated infiltration from the previous cycle. This choice of flow assures that the concentration would always be near the target (usually chosen to be about 2/3 of full scale). If it were the very first cycle, the previous infiltration would be assumed to be one physical volume per hour. This assumption is not critical, since it would be used only to determine what the flow rate for the first cycle should be.

For the first few minutes after the flow has been changed, the analyzer is re-zeroed using outside air. Aside from checking the zero drift of the analyzer, this time allows for delay due to the mixing function. Since, in general, the flow would not change very much from cycle to cycle, the wait-time necessary to overcome the mixing delays would be quite small.

The flow rate is held constant for the remainder of the cycle period by the use of a mass-flow controller, and concentration data is collected at regular intervals from the tracer-gas analyzer.

At the end of the cycle period, the concentration data is used in a simplex* search routine to find the three parameters. The simplex algorithm contains constraints that do not allow the effective volume to vary much from cycle to cycle. The slow updating of the volume has the

effect of "homing in" on the effective volume over a period of several cycles. Thus, this method can accurately measure the effective volume.

The calculated values are stored on a floppy disk for later use.

The computer monitors both the analyzer and the mass-flow controller, sets the mass-flow controller, and activates the solenoid valves used to control the flow of sample or zeroing gas to the analyzer. While the infiltration system is in use, the computer can still be used to perform other functions, such as further data reduction or display. Figure 2 presents a block diagram of the continuous flow system.

The operating system for the microprocessor is a single-user time-sharing system called TORX (Task Oriented Real-time eXecutive), developed at the Lawrence Berkeley Laboratory for use on Z-80 based microprocessor systems. This system solves the problems of effective volume, mixing and continuous operation; however, it costs about $20,000 to build and, therefore, would be unsuitable for long-term or short-term measurements.

Multichamber: The continuous flow method uses the full solution to the multichamber continuity equation.

$$\bar{\bar{C}}(t) = \bar{\bar{Q}}^{-1}\,\bar{\bar{F}} + e^{-\bar{\bar{V}}^{-1}\bar{\bar{Q}}t}\left[\bar{\bar{C}}_o - \bar{\bar{Q}}^{-1}\,\bar{\bar{F}}\right]$$

The single-chamber algorithm could be adapted for use in the multichamber problem. One and only one gas would be injected in each room, and the diagonal element corresponding to that chamber would control the injection rate, much as in the single-chamber case. The simplex* algorithm could be adapted to include the $3N^2$ unknown parameters in the above

---

* The simplex algorithm is a standard type of nonlinear search routine which finds the set of parameters that have the maximum likelihood of fitting a set of data.

equation.

FUTURE DIRECTIONS

A large body of data exists for most of the single-chamber measurement techniques described above; little work, however, has been done on the measurement or monitoring of multichamber infiltration. The theory, as derived herein, is adequate to describe infiltration but, as yet, no instrumentation exists to measure it. LBL proposes to develop an automated controlled flow measurement technique for monitoring multichamber infiltration, as found, for example, in an office building.

The effect of mixing on the continuity equation requires further study. As described in Appendix A, mixing effects could appear in the mixing function, and the S matrix and, while the theoretical description of them gives them some physical meaning, there is little experimental corroboration of these effects. Some effects, e.g. the mixing function, could be measured in single-chamber measurements but others, e.g. the S matrix, have meaning only in a multichamber experiment.

SUMMARY

Each of the tracer techniques presented (Decay, Constant Concentration, Constant Flow, Long Term Average, and Continuous Flow) could be used in either a single or multichamber mode. The methods have varying degrees of popularity and effectiveness depending on the mixing problems associated with a particular site. Below is a listing of the techniques and their relative merits.

METHOD	COMMENTS
DECAY	most popular; most susceptible to effective volume problems; can be susceptible to effective flow problems if insufficient wait time allotted; least expensive; difficult to use in multichamber mode; good choice for spot measurements.
CONSTANT CONCENTRATION	insensitive to effective volume problems; most sensitive to effective flow problems can lead to instabilities; used in multichamber mode to find outside infiltration; requires long start-up period; useful for long-term unattended measurements if adequate mixing supplied.
CONSTANT FLOW	relatively insensitive to effective volume problems; insensitive to effective flow problems; cannot run unattended; useful for long-term measurements.
LONG-TERM AVERAGE	little field data; least expensive for large samples; simulates constant flow technique; ideal for air quality studies.
CONTINUOUS FLOW	relatively insensitive to effective volume problems; relatively insensitive to effective flow problems; requires use of on-line microprocessor; treats effective volume as an undetermined parameter; ideal for long-term unattended operation; multichamber mode with multiple tracer gasses.

REFERENCES

1. Hunt, C.M. (1978), "Air Infiltration: A Review of Some Existing Measurement Techniques and Data," NBS Report, to be published in the Proceedings of the Symposium on Air Infiltration and Air Change Measurements, ASTM, Washington, D.C., (1978).

2. Hitchin, E.R., Wilson, C.B. , "Review of Experimental Techniques for the Investigation of Natural Ventilation in Buildings," Build. Sci. 2: 59-82 (1967).

3. Warner, C.G. (1940), "Measurements of the Ventilation of Dwellings," J. Hyg. 40: 125-15

4. Collins, B.G., Smith, D.B. (1955), "Measurements of Ventilation Rates Using a Radioactive Tracer," J. Inst. Heat Vent. Eng. 23, 270-274.

5. Howland, A.H., Kimber, D.E., Littlejohn, R.F. (1960), "Measurements of Air Movements in a House Using a Radioactive Tracer Gas," J. Inst. Heat. Vent. Eng. 28: 57-71.

6. Lidwell, C.M. (1960), "The Evaluation of Ventilation," J. Hyg. 58: 297-305.

7. Howard, J.S. (1966), "Ventilation Measurements in Houses and the Influence of Wall Ventilators," Build. Sci. 1: 251-257.

8. Hunt, C.M., Burch, D.M., "Air Infiltration Measurements in a Four-Bedroom Townhouse Using Sulfur Hexaflouride as a Tracer Gas," ASHRAE Trans. 81:I, 186-201 (1975).

9. D.T. Grimsrud, M.H. Sherman, J.E. Janssen, A.N. Pearman, D.T. Harrje, "An intercomparison of Tracer Gases Used for Air Infiltration," ASHRAE Trans. 86, (1980), Lawrence Berkeley Laboratory Report, LBL-8394 (1979)

10. M.H. Sherman, D.T. Grimsrud, P.E. Condon, B.V. Smith, "Air Infiltration Measurement Techniques," Proc. 1st IEA Symp. of Air Infiltration Centre Instrumentation and Measuring Techniques, Windsor, UK (1980); Lawrence Berkeley Laboratory Report LBL-10705 (1980)

11. D.K. Alexander, D.W. Etheridge R. Gale, "Theoretical and Exper-

imental Studies of Heat Loss Due to Ventilation," Proc. XXI Int. Cong. Building Services Eng. (1980)

12. G. Reeves, M. McBride, C. Sepsy, "Air Infiltration Model for Residences," ASHRAE Trans. 85 Part 1, (1979)

FIGURE CAPTIONS

FIG. II:1 The response of the concentration of tracer gas to a step function in flow is plotted vs. time.

FIG. II:2 Block diagram of the continuous flow infiltration system using a Z80 microprocessor, floppy disk, mass-flow controller and gas analyzer.

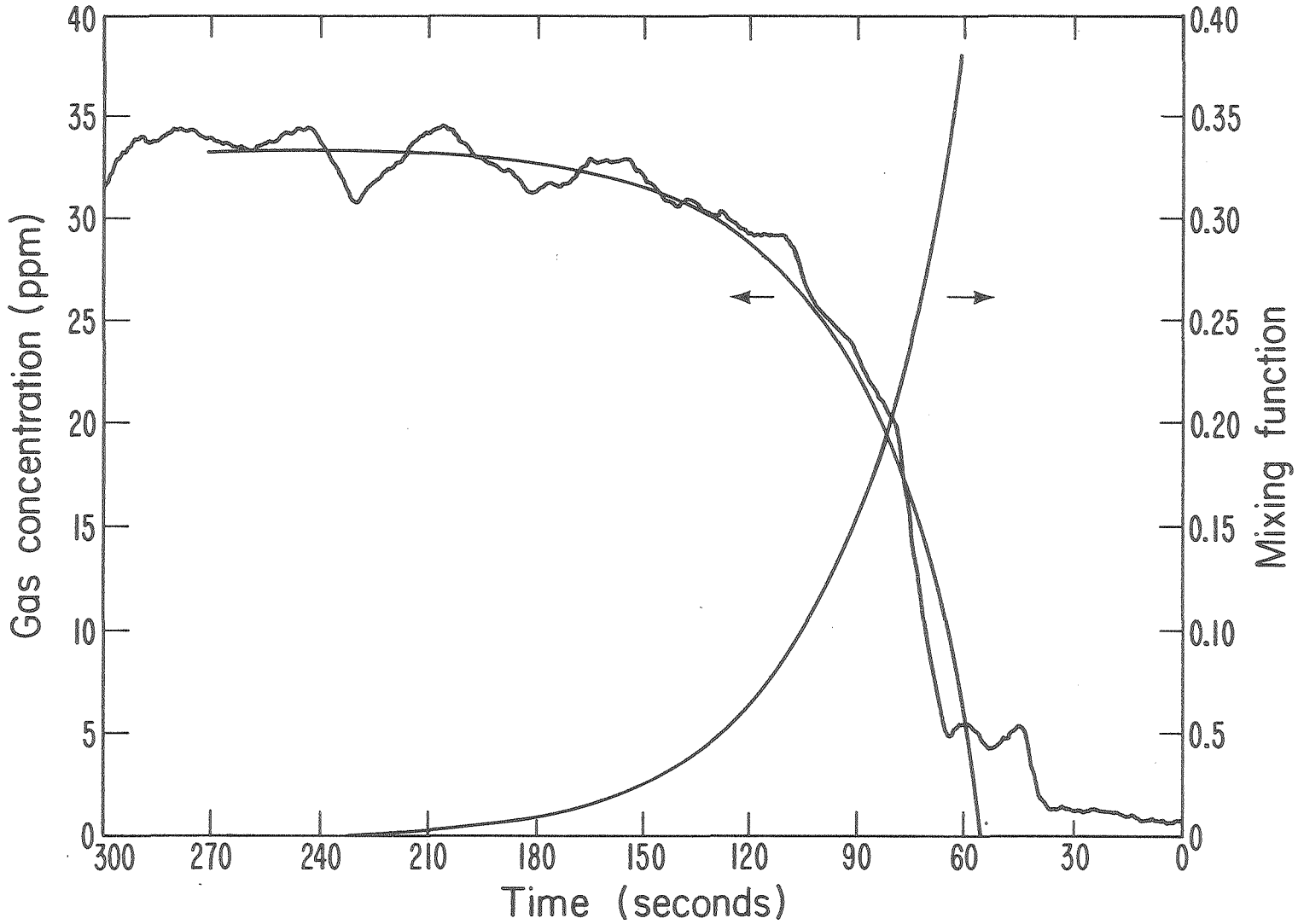

XBL783-460

FIG. II:1 The response of the concentration of tracer gas to a step function in flow is plotted vs. time.

AUTOMATED INFILTRATION SYSTEM

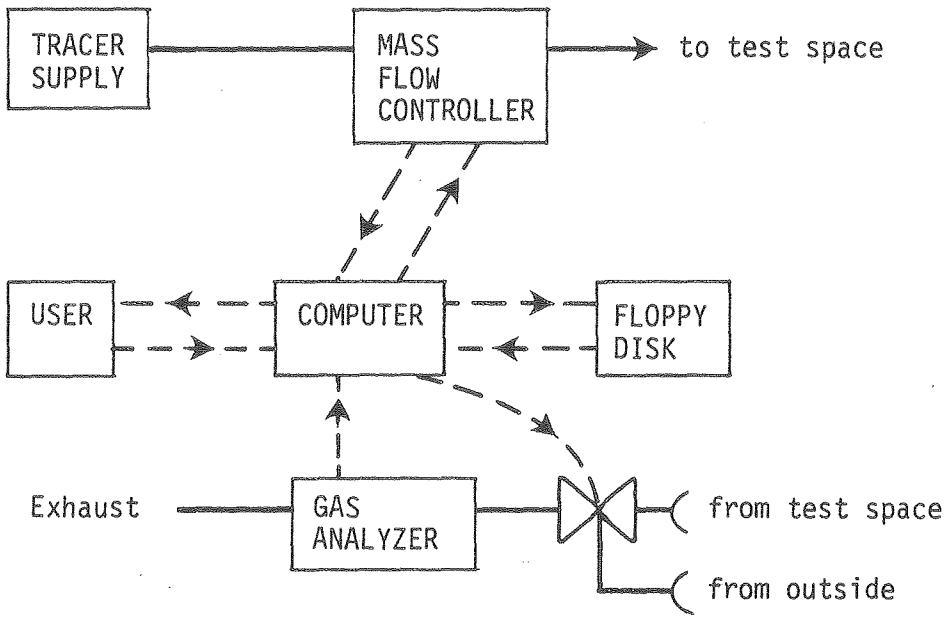

XBL 802-375

FIG. II:2 Block diagram of the continuous flow infiltration system.

CHAPTER III

THE HYDRODYNAMICS OF LEAKS

To develop an effective model for predicting the infiltration in a given building, the basic physics of infiltration need to be understood. Measurement techniques discussed in Chapter 2 might then be applied and results compared with those generated by the model. In this chapter, the laws of hydrodynamics are derived as they apply to the rather restricted conditions involved in the problem of infiltration in buildings. Infiltration is the air flow through the envelope of a structure in response to externally applied pressures (caused primarily by weather, i.e., wind and temperature difference) through leaks or cracks in the building shell. This study focuses on finding the flow response to an applied pressure, not necessarily on finding the velocity profile. Furthermore, the effects of the inlet or the exhaust jet are not of interest, except insofar as they would affect the pressure-flow relation. The physical process we should examine, therefore, is the pressure-induced flow or air through pipes.*

The pipes in actual buildings vary widely in geometry. Small pipes could have a radius near 1 mm and a length of 1 cm, while large pipes, e.g. kitchen vents, chimneys, could have a radius of 10 cm and a length of several meters; thus a particular geometry would be limiting. We could, however, limit assumptions about a particular pressure range. Because the typical differential pressures across the surface of the building envelope are in the range 0-10 Pascals, we would not expect to see velocities over 1 m/s in the pipe. (This assertion is an <u>a posteriori</u> consequence of applying our results to this pressure range.)

---

* We use the term "pipe" to mean any tube, pathway, or conduit than connects the interior to the exterior of the structure. We do not wish to imply that the 'pipe' is either straight, smooth or circular; nor need it be of constant cross-section.

The pressure-flow relation needs to derived and because we need only derive it within a reasonably small pressure range, we can use a simplier description of hydrodynamics as our model of pipe flow; this simple model will be developed along side of a more standard description of standard hydrodynamics.

HISTORICAL PERSPECTIVE

Since the hydrodynamics of viscous materials is a complex topic of study, it behooves us to quickly outline the history of the art. The summary below was extracted from an excellent text by White [1] on viscous theory.

> "The exact solution for the problem of the viscous fluid at rest was correctly given by the Greek mathematician Archimedes (287-212 B.C.) as his two postulates of buoyancy. Subsequently, in order to derive expressions for the buoyant force on various-shaped bodies, Archimedes actually developed a version of the differential calculus. At about the same time, the Romans were building their magnificent water-supply systems and in so doing demonstrated some intuitive understanding of the effect of viscous resistance in long conduits. However, the Romans contributed little to a systematic solution of this problem, and in fact no significant progress on channel resistance was made until Chezy's work in 1768.
>
> "The period from the birth of Christ to the fifteenth century produced the same impact on viscous flow analysis as it did on other fields of science, i.e., little if any. But the mountains of conjecture and superstition accumulated in these unscientific centuries certainly contained nuggets of fact which the great thinkers of the Renaissance finally mined. In 1500, the equation of conservation of mass for incompressible one-dimensional viscous flow as correctly deduced by Leonardo da Vinci, the Italian painter, sculptor, musician, philosopher, anatomist, botanist, geologist, architect, engineer, and scientist. Leonardo's notes also contain accurate sketches and descriptions of wave motion, hydraulic jumps, free jets, eddy formation behind bluff bodies, reduction of drag by streamlining, and the velocity distribution in a vortex.
>
> "The next notable achievement was by Evangelista Torricelli (1608-1647), who in 1644 published his theorem that the velocity of efflux of a (viscous) liquid from a hole in a tank is equal to the velocity which a liquid particle would attain in free fall from its surface. Torricelli termed his discovery "almost useless," but history has seen fit to disagree. From the point of view of this text, the efflux principle is unusually interesting, since it is one of the few flow phenomena for which viscous effects are often negligible.

"The above achievements do not relate directly to viscous motion. That is, these early workers were probably studying a fluid they thought to be inviscid, or perfect; it happens that their results are also true for a viscous, or real fluid. The first to make a direct study of fluid friction was probably Edme Mariotte (1620-1684), who invented a balance system to measure the drag of a model held stationary in a moving stream, the first wind tunnel. Mariotte's text, "Traite du mouvement des eaux," was published in 1686, a year before the incomparable "Principia Mathematica" of Sir Isaac Newton.

"In 1687 Newton published in his "Principia" the simple statement which delineates the viscous behavior of nearly all common fluids: "The resistance which arises from the lack of lubricity in the parts of a fluid--other things being equal--is proportional to the velocity by which the parts of the fluid are being separated from each other." Such fluids, water and air being prominent examples, are now called "Newtonian" in his honor. With the law of linear viscosity thus proposed, Newton contributed the first viscous-flow analysis by deriving the correct velocity distribution about a rotating cylinder.

"But the world was apparently not ready for viscous-flow theory. This was probably due to Newton himself, because of his more famous discovery, the differential calculus. Whereas those who preceded Newton were essentially limited to discussion of fluid-flow problems, those who followed him could use the calculus to attack such problems directly. It is natural that the first efforts were directed toward the idealized frictionless fluid. First to succeed was Daniel Bernoulli, who in 1738 demonstrated the proportionality between pressure gradient and acceleration in inviscid flow. Subsequently, the master of the calculus, Leonhard Euler, derived in 1755 the famous frictionless equation which now bears Bernoulli's name. Euler's magnificent derivation is essentially unchanged today in ideal-fluid theory, or hydrodynamics, as Bernoulli termed it. Paralleling Euler, Jean d'Alembert published in 1752 his famous paradox, showing that a body immersed in a frictionless flow would have zero drag. Shortly afterward, Lagrange (1736-1813), Laplace (1749-1827), and Gerstner (1756-1832) carried the new hydrodynamics to elegant heights of analysis.

"But theoretical results such as the d'Alembert paradox were too much for practical engineers to bear, with the tragic result that fluid mechanics was rent into two parts: hydrodynamics, under whose banner mathematicians soared to new frictionless summits, and hydraulics, which abandoned theory entirely and relied on experimental measurements. This schism continued unhealed for 150 years, to the beginning of the twentieth century. Indeed, the separation of fluid mechanics theory from experiment is not extinct even today, as witness the divergent views of the subject now held between aeronautical, chemical, civil, and mechanical engineers.

"After Euler and his colleagues, the next significant analytical advance was the addition of frictional-resistance terms to Euler's inviscid equations. This was done, with varying degrees of elegance, by Navier, in 1827, Cauchy in 1828, Poisson in 1829, St. Venant in 1843, and Stokes in 1845. The first four wrote their equations in terms of an unknown molecular function, whereas Stokes was the first to use the first coefficient of viscosity μ. Today these equations, which are fundamental to the subject, are

called the Navier-Stokes relations, and this text can do little to improve upon Stokes' analysis.

"Certainly the Navier-Stokes equations make this subject possible. But they are mathematically difficult, often unstable, and to date only about 70 particular solutions have been found. Only in the last 5 years have large-scale digital computers given hope for obtaining systematic (numerical) solutions. Hence the hydraulics workers of Stokes' time did not see great value in his work.

"Instead, the most important achievement in viscous-flow theory came in 1904, when Ludwig Prandtl demonstrated the existence of a thin boundary layer in fluid flow with small viscosity. The resulting viscous-inviscid matching procedure has made viscous flow amenable to approximate analysis, and the field may now be said to have reached a plateau of solid fundamentals. Prandtl's boundary-layer concept, while often not quantitative, makes it possible, as Howarth said, 'to think intelligently about almost any problem in real fluid flow.' Since Prandtl's 1904 paper, the subject has grown steadily until, like other disciplines, it is now on the verge of a paper explosion defying rational containment."

Excellent historical notes on fluid mechanics can be found in several texts on the subject: Rouse and Ince,[2] Bateman, et al.,[3] and Bell.[4] Other texts that were found useful by the author for the understanding of fluid dynamics include those by Schlichting[5] and Tennekens and Lumley.[6]

BASIC THEORY

The simplest kind of fluid, the kind one learns about in undergraduate texts, is called a perfect fluid; it has the properties of being incompressible and inviscid, and the flow of a perfect fluid will be steady and irrotational. (John von Neuman called this perfect fluid "dry water".) Since the fluid is incompressible, the density will be constant everywhere; since the flow is inviscid, there will be no frictional losses during flow and the flow can be described using an energy balance equation; since the flow is steady, the velocity field and the path of the particles will coincide and thus, the concept of streamlines can be introduced; finally, since the flow is irrotational the spacing of the streamlines must be equal. The energy balance equation that

described the flow of a perfect fluid is Bernoulli's equation:

$$\Delta P = \rho\ g_x\ \Delta x - \Delta(\ \tfrac{1}{2}\ \rho\ v^2\ ) \qquad \text{(III.1)}$$

where

P	is the pressure in the stream [Pa],
ρ	is the density of the fluid [kg/m^3],
v	is the velocity of the fluid [m/s],
x	is the distance along the flow path [m] and
g_x	is the external acceleration along the flow [m/s^2].

In fact, it is rare than any real fluid can be treated as perfect; accordingly, Bernoulli's equation cannot be used to solve our problem of finding the real flow through pipes. If there were any dissipative forces present e.g., viscosity, the scalar energy balance equation could not be used to determine the flow; the vector momentum balance equations should be used instead. This set of equations is the starting point for any serious discussion of hydrodynamics and is called the Navier-Stokes equation:

$$\partial_i P = \rho\ g_i - \rho\ v_j\ \partial_j v_i - \rho\ \partial_t v_i + \partial_j \tau_{ij} \qquad \text{(III.2)}$$

where

v_i	is the ith component of the local velocity vector [m/s],
g_i	is the ith component of the external acceleration vector [m/s^2],
τ_{ij}	is the shear stress tensor [Pa],
∂_i	is the spacial derivative operator [m^{-1}],
∂_t	is the temporal derivative operator [s^{-1}],

(Note that we have used indicial notation and that repeated indices are to be summed over the spacial components, i.e., from 1 to 3).

The shear stress tensor is a symmetric tensor of rank two that is proportional to the viscosity:

$$\tau_{ij} = \mu \left(\partial_j v_i + \partial_i v_j + \delta_{ij} \partial_k v_k \right) \qquad \text{(III.3)}$$

where

μ is the viscosity of the fluid [kg-m/s].

This definition is called Newton's law of friction to acknowledge Sir Isaac's contribution to the study of real fluids; fluids that obey this law are called Newtonian fluids. This equation is perhaps more familiar in the case of axi-symmetric viscous flow of incompressible Newtonian fluids, for which the shear stress tensor becomes,

$$\tau = \mu \frac{dv}{dr} \qquad \text{(III.4)}$$

where

$\frac{dv}{dr}$ is the velocity gradient (perpendicular to the flow) [s^{-1}].

A useful term related to the viscosity is the kinematic viscosity:

$$\nu = \frac{\mu}{\rho} \qquad \text{(III.5)}$$

where

ν is the kinematic viscosity [m^2/s].

The Navier-Stokes equation is a complex nonlinear vector equation; we can, however, use the conditions of interest to simplify it. Specifically, we are looking at the leakage of air through cracks in a building. The pressures involved are quite small compared to atmospheric pressure (10 Pa vs. 100,000 Pa) so we can ignore compressibility; likewise, the temperature differences involved are usually small compared with the absolute temperature (30 K vs 300 K). The only external force acting on the fluid is gravity but, since the typical drop across a single opening is small, we can ignore it.

While the viscosity can be a strong function of temperature or pressure, for our interests we can assume that it is a constant. Thus,

$$\partial_j \mu = 0 \qquad \text{(III.6.1)}$$

$$\partial_t \mu = 0 \qquad \text{(III.6.2)}$$

Since we have assumed that gravity is unimportant, we can neglect the external acceleration term:

$$g_i = 0 \qquad \text{(III.7)}$$

Furthermore, we can treat the fluid as incompressible; use of the continuity equation restricts the velocity field to be divergenceless:

$$\partial_i v_i = 0 \qquad \text{(III.8)}$$

The stress tensor then becomes,

$$\tau_{ij} = \mu \left(\partial_i v_j + \partial_j v_i \right) \qquad \text{(III.9)}$$

Combining all these assumptions together we can rewrite the Navier-Stokes equation for constant viscosity, incompressible flow as follows:

$$\frac{\nabla P}{\rho} = \nu \nabla^2 \underline{v} - \underline{v} \cdot \underline{\nabla v} - \partial_t \underline{v} \qquad \text{(III.10)}$$

As we shall see, it is useful to define a parameter that indicates the relative strength of the kinetic term to the viscous term; we shall use some simple dimensional analysis to form such a quantity. The first term on the right hand side is the viscous (Newtonian) term; it contains the information about the pressure drop due to fluid friction. The middle term is the inertial or kinetic term, it is the pressure due to the gradient in the kinetic energy of the field. The far right hand term is the explicit time dependence of the velocity and is only important if the pressure has explicit time dependence.

The character of the solutions depends critically on the relative size of the kinetic vs viscous terms. Accordingly, it would be advantageous to define a parameter that characterizes the solutions by the relative size of these terms. The explicit ratio of the kinetic to viscous terms yields,

$$\frac{\underline{v} \cdot \underline{\nabla} \underline{v}}{\nu \, \nabla^2 \underline{v}} \tag{III.11}$$

We wish our parameter to depend on the flow (equivalently, velocity or pressure) and the geometry of the pipe, not on gradients of the velocity field; accordingly, we will make these replacements:

$$\underline{v} \cdot \underline{\nabla} \underline{v} \rightarrow v \, \delta v \tag{III.12.1}$$

$$\underline{\nabla}^2 \underline{v} \rightarrow \frac{\delta v}{X} \tag{III.12.2}$$

where

X is the characteristic length perpendicular to the flow path [m].

The new quantity is called the Reynold's number (after Reynold's original work on flow through pipes):

$$R = \frac{v \, X}{\nu} \tag{III.13}$$

where

R is the Reynold's number.

The choice of definition of v and X are usually determined by the particular type of problem one is considering. For example, in pipe flow the length parameter is usually chosen to be the diameter and the velocity is chosen to be the average velocity through the pipe.

The Reynold's number determines the character of the flow; when the Reynold's number is small the flow is dominated by the frictional (viscous) forces and when the Reynold's number is large the flow is dominated by kinetic (inertial forces). If the Reynold's number is much smaller than unity,

$$R \ll 1 \tag{III.14}$$

the kinetic forces can be eliminated from the Navier-Stokes equation, which for steady flow becomes,

$$\underline{\nabla} P = \mu \nabla^2 \underline{v} \tag{III.15}$$

This (density-independent flow) is called "creeping flow" and can be solved for a wide variety of geometries. Unfortunately, the flow in real pipes is virtually never at such small Reynold's numbers.

The large Reynold's number regime is a bit more complicated. Even if the Reynold's number is large compared to unity, it is difficult to ignore the viscous term — a direct result of the fact that the velocity at the wall must approach zero and, thus, near the wall, the Reynold's number is no longer large. This problem could be handled by assuming that the viscosity is exactly zero, then using perturbation theory to find the effects of slowly increasing the viscosity; but in so doing, great care must be taken inasmuch as the viscosity term has the highest order of velocity derivative. Therefore, adding the viscous term will change the character of the solution; this type of problem is known as a singular-perturbation problem. Because of this the viscous effects near a solid boundary are always important in determining the flow at large Reynold's numbers. Indeed, the description of fluid flow at large Reynold's numbers is called "boundary layer" theory.

LAMINAR FLOW

When we considered creeping flow the problem became soluble because the velocity was so small that the kinetic term could be neglected. We can also make the kinetic term negligible if we hypothesize a solution

for the velocity of the form,

$$\underline{v} \cdot \underline{\nabla v} = 0 \qquad \text{(III.16)}$$

A solution of this form implies that (if it is nonzero) the velocity is orthogonal to its gradient i.e., the velocity gradient is perpendicular to the flow path.

In this type of solution there are laminae that move along the pipe at different speeds which depend on the distance from the wall — the further from the wall the faster the laminae move. Accordingly, this type of (boundary layer) flow is called laminar flow and it has a solution similar to the creeping flow solution but without the Reynold's number restrictions: creeping flow is the trivial case of laminar flow.

$$\frac{\underline{\nabla P}}{\rho} = \nu \nabla^2 \underline{v} - \partial_t \underline{v} \qquad \text{(III.17)}$$

If the cross-section of the pipe is not constant, there will be a change in the velocity of the fluid along the flow path in order to maintain continuity. This change in longitudinal velocity violates our assumption that the gradient of the flow is perpendicular to it. Therefore, in order to get laminar flow in the boundary layer regime we must also assume that the cross-section of the pipe does not vary. Specifically, the pitch times the Reynold's number must be small compared to unity:

$$R \sin\phi \ll 1 \qquad \text{(III.18)}$$

<u>where</u>

ϕ is the pitch angle (= 0 for constant cross section).

(cf. creeping flow condition)

If we assume that we are far enough upstream of the inlet the velocity will be a function of the radial coordinate(s) only:

$$\frac{\underline{\nabla}_x P}{\rho} = \nu \nabla_r^2 v - \partial_t v \qquad \text{(III.19)}$$

where

$\underline{\nabla}_x$ is the gradient parallel to the flow path and

$\underline{\nabla}_r$ is the gradient transverse to the flow path.

Before we attempt to solve this equation explicitly we can learn something about the general form of laminar flow by taking the divergence, and curl of this equation. If we take the divergence all of the terms containing the velocity disappear (due to our assumption of constant density):

$$\underline{\nabla}^2 P = 0 \qquad \text{(III.20)}$$

That is, the pressure field is laplacian, the solution of which is a pure boundary-value problem. Specifying the conditions at the boundary (e.g. specifying the pressure drop between the ends of the pipe) is sufficient to determine the pressure drop along the pipe; for pipes with constant cross-section the pressure will be linear down the length of the pipe. If we assume that the inlet and exhaust are kept at constant pressure (i.e. the pipe connects two pressure reservoirs), we can solve for the pressure gradient directly:

$$\partial_x P = \frac{\Delta P}{L} \qquad \text{(III.21)}$$

where

ΔP is the pressure drop between inlet and exhaust [Pa] and

L is the length of the pipe [m].

If we take the curl of the equation the pressure term disappears:

$$\partial_t \underline{\omega} = \nu \nabla^2 \underline{\omega} \qquad \text{(III.22)}$$

where

$\underline{\omega} = \underline{\nabla} \times \underline{v}$ is the vorticity [s^{-1}].

This can be recognized as a diffusion equation, describing the diffusion of vortices within the pipe. The kinematic viscosity plays the role of

a diffusion constant.

Steady Flow

Our Navier-Stokes equation contains a partial temporal derivative of the velocity; this derivative, however, will only be nontrivial if the pressure has an explicit time dependence. If the pressure varies slow enough the partial time derivative can be ignored. While the exact solution will depend on the geometry, e.g., circular pipe flow will involve Bessel functions a critical frequency can be calculated:

$$w_c = \frac{\nu}{r_o^2} \qquad \text{(III.23)}$$

where

w_c is the critical frequency [s^{-1}] and

r_o is the radius of the pipe [m].

Thus if the pressure varies slower than this critical frequency we can treat the pressure and flow as steady. Dropping the temporal derivative we can solve the Navier-Stokes equation, which has become identical to the creeping flow equation:

$$v(r) = \frac{\Delta P}{4 \nu L} (r_o^2 - r^2) \qquad \text{(III.24)}$$

where

L is the length of the pipe [m],

ΔP is the pressure drop over the length of the pipe [Pa] and

r_o is the radius of the pipe [m^2].

If we integrate this expression across a section of the pipe we can find the flow as a function of pressure:

$$Q = \frac{\pi r_o^4}{8 \nu L} \Delta P \qquad \text{(III.25)}$$

where

Q is the flow through the pipe [m^3/s].

This is the well known Hagen-Poiseuille flow equation. Finally, we can solve for the vorticity of the fluid:

$$\omega_\theta = \frac{r \Delta P}{2 \nu L} \qquad \text{(III.26)}$$

where

ω_θ is the critical frequency [s^{-1}].

Hydraulic Radius

We can generalize this equation to noncircular ducts by using the concept of the hydraulic radius. The hydraulic radius for noncircular ducts is equivalent to the actual radius for circular ones, in terms of its effect on the stress tensor. The following expression for the hydraulic radius is not exact but for most geometries gives reasonable accurate results:

$$r_o = \frac{2 A}{D} \qquad \text{(III.27)}$$

where

r_o is the hydraulic radius [m],

A is the cross-sectional area [m^2] and

D is the "wetted" perimeter [m].

Discharge Coefficient

The loss of momentum of the fluid is related to the shear stress of the fluid at the pipe wall. Conventionally, the stress tensor is normalized by the pressure head to yield a friction factor. We will adopt the most common form of the friction factor — the Darcy friction factor:

$$\lambda = \frac{8\tau_w}{\rho v^2} \qquad \text{(III.28)}$$

where

λ is the Darcy friction factor,

v is the average velocity in the pipe [m/s] and

τ_w is the stress tensor at the wall [Pa].

Using our results for laminar pipe flow we find that,

$$\tau_w = -\ 1/2\ r_o \frac{\Delta P}{L} \qquad \text{(III.29)}$$

which yields the friction factor:

$$\lambda = \frac{d_o}{L} \frac{\Delta P}{1/2\ \rho\ v^2} \qquad \text{(III.30)}$$

where

$d_o = 2r_o$ is the hydraulic diameter [m].

Solving for average velocity as a function of the friction factor yields,

$$v = \sqrt{\frac{2\ \Delta P\ d_o}{\rho\ L\ \lambda}} \qquad \text{(III.31)}$$

To find the flow all that is needed is to multiply be the cross sec-

tional area.

$$Q = A \left(\frac{d_o}{L \lambda} \right)^{1/2} \left(\frac{2 \Delta P}{\rho} \right)^{1/2} \qquad \text{(III.32)}$$

where

Q is the flow through the pipe [m^3/s] and

A is the cross-section [m^2].

We will define the discharge coefficient as follows:

$$Q = C_f \, A \sqrt{\frac{2 \Delta P}{\rho}} \qquad \text{(III.33)}$$

where

C_f is the discharge coefficient,

which leads to an expression for the discharge coefficient:

$$C_f = \sqrt{\frac{d}{L \lambda}} \qquad \text{(III.34)}$$

The specification of the flow is now reduced to finding the relationship between the friction factor and the Reynold's number. For the Hagen-Poiseuille case the relationship is,

$$\lambda = \frac{64}{R_d} = \frac{64}{\left[\frac{d_o \, v}{\nu} \right]} \qquad \text{(III.35)}$$

where

R_d is the Reynold's number using the diameter as the length scale.

Solving for the discharge coefficient and using the Hagen-Poiseuille relation to eliminate the velocity yields,

$$C_f = \frac{r_o^2}{16\ L\ \nu} \sqrt{\frac{2\ \Delta P}{\rho}} \qquad \text{(III.36)}$$

The appearance of the pressure (as well as the geometry of the pipe) in the expression for the discharge coefficient indicates that it will not be constant in the laminar regime. Therefore, the concept of a discharge coefficient, effective area, friction factor etc. may not seem that appropriate for laminar flow; however, as we shall see, these concepts are quite appropriate for turbulent and turbulent-like flow.

TRANSITION

Ostensibly, the problem of pipe flow in the boundary layer regime is solved; we have found a solution to the Navier-Stokes equation that has no Reynold's number restrictions placed on it. This is not, however, the only possible solution to the Navier-Stokes equation; we must, therefore, consider the possibility of instabilities arising in the laminar solution that might lead to a transition to some other solution. By selecting the laminar solution, we have eliminated the convective derivative term from the full Navier-Stokes equation, but when we consider the effect of infinitesimal perturbations of this solution we cannot ignore the convective part. Accordingly, we must use the full Navier-Stokes equation to derive the stability criterion for laminar flow.

This process can be conceptualized by adding a small (unknown) velocity field to the Hagen-Poiseuille solution and substituting this into the Navier-Stokes equation containing the convective term. The solution that remains after the laminar part has been subtracted is the stability equation. If this equation predicts that the perturbation decays over time then the solution is stable and if the perturbation grows over time then the solution is unstable. While the stability criterion can be stated in a paragraph, solving the stability equation is a formidable task. As a matter of fact, the stability equation for pipe flow has never been solved exactly.

Nevertheless, at some Reynold's number our laminar solution will become unstable; this indicates that the regime of transition has begun Transition is the most complex regime — more complex than either the laminar or turbulent regimes; no (adequate) theory of transition exists. Contrary to what one might expect the instabilities do not grow without bound, but rather they become finite instabilities (of a variety of types) and decay away; thus, transition is characterized by areas of wave, vortex, span-wise, etc. instabilities mixed in with areas of laminar flow. Transition is enhanced by discontinuities such as sharp inlets, but the transition takes place well downstream of the inlet. (The higher the Reynold's number the close transition gets to the inlet.) Finally, when the rate of creation exceeds the rate of decay of instabilities turbulence begins. Even after the onset of turbulence, there are pockets of laminar flow mixed with pockets of turbulent flow; as the regime of transition ends the flow becomes completely turbulent.

TURBULENT FLOW

Unlike transition, which is characterized by "spotty" behaviour, turbulent flow, like laminar flow, is a homogenous regime. But unlike laminar flow the velocity field is three dimensional and quite complex. If a stream of dye is injected into a pipe whose flow is in the laminar regime, there will be a well defined, visible, stream that can be easily followed (i.e. streamlines); if, however, the pipe in undergoing turbulent flow the stream will quickly appear to become diffuse and undefined. If one were to take an instant snap-shot of the turbulent flow, e.g., with spark photograph the dye stream would again be distinct, but repeated snap-shots would reveal that the stream was moving around with frequencies in the kilohertz range. We must now attempt to describe the "average" behavior of this fluid using the Navier-Stokes equation.

In the laminar case it was sufficient to deal with averaged quantities; the velocity field was confined to laminae and could be dealt with simply. The presence of the convective term effectively adds new variables to the Navier-Stokes equation. If we take the time average, i.e., average over the "random" velocities, of the Navier-stokes equation we

can see this:

$$\frac{\underline{\nabla} P}{\rho} = \nu \nabla^2 \underline{v} - \underline{v} \cdot \underline{\nabla} \underline{v} - \partial_t \underline{v} - \underline{\nabla} \cdot \left[\overline{\underline{v}\underline{v}} \right] \qquad \text{(III.37)}$$

where all the terms now represent their time averaged values and the term in brackets is the time average of the second order velocity tensor.

This effectively adds a term to the shear stress which is similar to a kinetic energy term:

$$\tau_{ij} = \mu \left(\partial_j v_i + \partial_i v_j \right) - \rho \left[\overline{v_j v_i} \right] \qquad \text{(III.38)}$$

The first term is the laminar term that we used previously; the second term is new and appears as a "turbulent shear" term. Of course, this only helps to see where the term comes from, it does nothing to help solve the equation since the turbulent shear tensor is completely unknown.

The presence of this term makes it impossible (as far as we know) to solve the turbulent flow problem exactly. Therefore, approximation techniques have been used to find the equation of state for specific cases. We will derive a simplistic model of turbulent flow and then go on to give some of the more complex ones from the literature which we use to extend our model accordingly.

In the main core of the flow in a pipe the velocity of the fluid is large and the flow is turbulent; however, the velocity must approach zero at the walls and, hence, the flow must have laminar behavior near the walls. We can use this laminar layer to calculate the shear stress and hence the friction factor, which leads ultimately to the discharge coefficient. As before, Newton's law of friction can be used to determine the shear stress at the walls:

$$\tau_w = \mu \left. \frac{dv}{dr} \right|_{r_o} \qquad \text{(III.39)}$$

Since we do not have the exact expression for the velocity, we can

approximate the derivative using finite differences:

$$\frac{dv}{dr} \rightarrow \frac{\delta v}{\delta r} \qquad \text{(III.40)}$$

where

δv is the change in velocity [m/s] and

δr is the radial distance for that change [m].

We now use the entire boundary layer for the finite differences; the change in velocity will just be equal to the average velocity.

$$\delta v \rightarrow v \qquad \text{(III.41)}$$

where

v is the mean velocity [m/s].

The thickness of the viscous boundary layer can be found by comparing the Reynold's number to the critical Reynold's number. At the critical Reynold's number the boundary layer is roughly equal to the radius; therefore, the thickness of the boundary layer will be equal to the radius times the Reynold's number ratio:

$$\delta r \rightarrow r_o \frac{R_c}{R} f_R \qquad \text{(III.42)}$$

where

f_R is a correction factor of order unity,

R_c is the critical Reynold's number and

R is the Reynold's number.

Thus (using our liberal replacements) the wall shear stress is,

$$\tau_w = \mu \frac{v}{r_o} \frac{R}{R_c} f_R \qquad \text{(III.43)}$$

Inserting this into the definition of the friction factor we find,

$$\lambda = \frac{16}{R_c} f_R \qquad \text{(III.44)}$$

and the discharge coefficient is,

$$C_f = \sqrt{\frac{r_o \; R_c}{8 \; L} f_R} \qquad \text{(III.45)}$$

This is a rather pleasant state of affairs — the friction factor and discharge coefficient are independent of the applied pressure (or velocity). However, we still require knowledge of the critical Reynold's number in order to make use of this formulae; unfortunately there is no theoretical way to find this out. Accordingly, we must turn to experiment to determine the critical value. The critical value will depend on the type of problem being solved; for the case of fully developed pipe flow Reynold's (in his original work) measured the critical Reynold's number as 2300 in typical situations. (In laboratory situations the Reynold's number can be as high as 10,000 before transition occurs.)

Because our approximation of a thin boundary layer whose thickness is inversely proportional to the Reynold's number is strictly true only at very high Reynold's number, we do not expect our model to be terribly precise at Reynold's numbers near transition. Several authors including Prandtl [7] Blasius, [8] and Techo [9] have used more rigorous methods to match the laminar layer near the wall to the the turbulent layer near the core (using a logarithmic overlap) and have used numerical data to improve the fit. Each author had a different functional form but all of the methods matched the experimental data to withing 3%. We give Prandtl's formula as an example:

$$\lambda = \left\{ \log_{10}(R_d^2 \lambda) - 0.8 \right\}^{-2} \qquad \text{(III.46)}$$

This can be solved numerically yielding theses values for the friction as a function of Reynold's number:

R_d	10^4	10^5	10^6	10^7	10^8
λ	0.0309	0.0180	0.0117	0.0081	0.0059

Although our model has an as yet unknown correction factor, it does predict that the friction factor should be Reynold's number independent. In order to find that correction factor, we will assume that the friction factor remains continuous at the laminar-turbulent transition; thus, we can equate the friction factor at the critical Reynold's number in both regimes:

$$\frac{64}{R} = \frac{16}{R_c} f_R \qquad (R=R_c) \qquad \text{(III.47)}$$

Therefore,

$$f_R = 4 \qquad \text{(III.48.1)}$$

and

$$\lambda = \frac{64}{R_c} \qquad \text{(III.48.2)}$$

in the turbulent regime.

Comparing this value to Prandtl's data we see that it corresponds to a Reynold's number of roughly 50,000 — a reasonable number for the flow we are considering. We now have a simplistic model of flow through smooth pipes that spans both laminar and turbulent regimes:

$$\lambda = \text{MAX}\left(\frac{64}{R}, \frac{64}{R_c} \right) \qquad \text{(III.49)}$$

Roughness

So far we have only treated smooth walled pipes; but in any real situation (especially, cracks in building walls) the walls of the pipe will have some roughness. Roughness will tend to break up the viscous boundary layer and ruin any near wall approximations. For laminar flow this will have little effect because the entire pipe is viscous boundary layer; in turbulent flow, however, the boundary layer can be quite thin — any roughness whose size is on the same scale as the boundary layer will cause a large deviation from the smooth solution. Prandtl modified his formula to include a roughness parameter:

$$\lambda = \left\{ \log_{10}\left\{ \frac{R_d^2 \lambda}{(1 + 0.1\ k{*}R_d \sqrt{\lambda})^2} \right\} - 0.8 \right\}^{-2} \qquad \text{(III.50)}$$

where

k is the roughness parameter.

The roughness parameter can be thought of as the ratio of the height of the roughness to the size of the pipe. $(0 \leq k \leq 1)$

In the limit that the roughness goes to zero this equation approaches the original Prandtl equation; however, the other limit is quite interesting as well. When the roughness becomes large (typically $k>1000/R$) the expression for the friction becomes independent of Reynold's number:

$$\lambda = \left\{ 1.2 - \log_{10} k^2 \right\}^{-2} \qquad \text{(III.51)}$$

This formula suggests a that a modification can be made to our (Reynold's number independent) expression for turbulent friction, that takes into account roughness.

$$\frac{64}{R_c} \rightarrow \frac{64}{R_c} + \frac{f_k}{(1.2 - \log_{10} k^2)^2} \qquad \text{(III.52)}$$

where the f_k is chosen to make the expression match the high roughness

value:

$$f_k = \frac{1-400}{9\ R_c} \qquad \text{(III.53)}$$

We can now combine this into the expression for the friction factor for the entire spectrum:

$$\lambda = \mathrm{MAX}\left(\frac{64}{R}, \frac{64}{R_c} + \frac{1 - 400/9R_c}{(\ 1.2 - \log_{10}k^2\ )^2} \right. \qquad \text{(III.54)}$$

ENTRY FLOW

In the preceding examples we have calculated the flow in pipes assuming that the flow was fully developed, .i.e. that the character of the flow did not change as a function of the distance along the pipe — long pipes. Near the entrance of a pipe this assumption will no longer be valid; but we would like to know what the value of the entrance length is and how much extra pressure drop is associated with entry.

Many authors have worked on this problem for laminar flow ;[1-3] all have found similar results. There is an excess pressure drop over the Hagen-Poiseuille pressure drop due to the entrance length of the pipe:

$$\delta P = K\ \tfrac{1}{2}\ \rho\ v^2 \qquad \text{(III.55)}$$

where

K	is the reduction factor
δP	is the excess pressure due to entrance [Pa] and
v	is the average velocity in the pipe.

The pressure reduction factor is a function of the entrance length relative to the length of the pipe; for long pipes the pressure reduction

factor approaches a constant

$$K \rightarrow 1.16 \qquad \text{(III.56)}$$

and for short pipes the reduction factor approaches zero.

The terms long and short refer, of course, to the entrance length of the pipe. Depending on the exact definition used for the entrance length and the approximations used in its calculation the expression may vary by as much as a factor of two. We relate the entrance length to the friction factor as follows:

$$L_e = \frac{4}{\lambda} d_o \qquad \text{(III.57)}$$

where

L_e is the entrance length [m].

We have seen that the developing boundary layer can cause a reduction in the apparent pressure drop across the pipe; there are, however, other effects which also cause pressure reductions. So far when we have refered to the pressure drop (ΔP) across the pipe we were refering to the actual static pressure difference between the inlet and exhaust of the pipe. However, what we will ultimately measure will be the pressure difference between a pressure reservoir connected to the inlet of the pipe and a pressure reservoir connected to the exhaust of the pipe. The distinction, while subtle, is, nevertheless real; there will be a pressure reduction associated with this, caused primarily by the presence of the exhaust jet.

Unlike the pressure reduction due to the entry length, this pressure reduction will not decrease to zero for short pipes — the total pressure reduction will be the sum of the two effects. Furthermore, other effects such as bend in the pipe can be approximated by pressure reduction factors that remain reasonably constant. Accordingly, we will approximate the pressure reduction factor by a constant value and, thus, we can express the discharge coefficient in terms of the entrance length and the total pressure reduction factor (instead of the friction

factor):

$$C_f = 1/2 \sqrt{\frac{L_e}{KL_e + L}} = 1/2 \left(K + \frac{L}{L_e} \right)^{-1/2} \qquad \text{(III.58)}$$

The above relations have been derived for the entry flow in the laminar regime only. Less work has been done for the turbulent case, but existing data seems to support the hypothesis that the formula for entrance length is correct as written.

When pipes are short (i.e. the entrance length is much longer than the length of the pipe) the above equation predicts that the discharge coefficient will be constant; thus the flow will be proportional to the square-root of the pressure regardless of the Reynold's number. As we shall see in the next chapter, this result is very important in the characterization of envelope leakage; since virtually all of the leaks in a building are short, there will be very little laminar behaviour present. If the Reynold's number remains below the critical value then as the length of the pipe increases the character of the flow will change from a square-root dependence on pressure to a linear dependence on pressure.

This has led many researchers to develop models in which the flow is proportional to the pressure drop raised to a power (between 1/2 and 1). For example, Kreith and Eisenstadt [4] have experimentally studied the relationship between the pressure drop and flow for short pipes, and they have chosen a power curve representation of the data. They use the expression,

$$Q = C_n \, \Delta P^n \qquad \text{(III.59)}$$

where

Q	is the flow through the pipe [m^3/s],
ΔP	is the total pressure drop across the pipe [Pa] and
C,n	are empirical constants determined by experiment ($.5 < n < 1$).

While this type of expression may be an easy one with which to fit the data, it is not a physically meaningful one; the coefficients C and n represent not physically interpretable quantities. Thus this method of data analysis sheds no light on the underlying processes of hydrodynamics.

Orifices

If the flow in short pipes moves from the linear (pressure) regime towards the square-root (pressure) regime, it is logical to assume that an infinitely short pipe, i.e., an orifice must be completely in the square root regime; in fact this is a reasonable accurate statement. Since an orifice has no length at all, there is no laminar boundary layer formed, and to a large degree viscosity can be ignored; viscosity, however, does play an important role in the wake downstream of the orifice and, hence there is a critical Reynold's number below which an orifice becomes a laminar jet. Experiments indicate that this Reynold's number is near 4 for a circular orifice vs. 2000 for a circular pipe — therefore, for all of our purposes we can assume that an orifice has square-root behavior.

If we neglect viscosity, the fluid becomes perfect and the Navier-Stokes equation reduces to Bernoulli's equation:

$$\Delta P = \tfrac{1}{2}\rho v^2 \qquad \text{(III.60)}$$

which predicts that the discharge coefficient is unity. In fact, the fluid cannot be treated as perfect because of the presence of the downstream jet. The jet causes a back pressure that retards the flow and decreases the discharge coefficient. Discharge coefficients for a wide variety of shapes have been measured, but the most important one is for a sharp edged circular orifice:

$$C_f \approx .7 \qquad \text{(III.61)}$$

where

C_f is the discharge coefficient for a circular orifice.

Our simple model would predict that the discharge coefficient for an orifice is,

$$C_f = 1/2 \; K^{-1/2} \tag{III.62}$$

which allows us to calculate the pressure reduction factor:

$$K \simeq 1/2 \tag{III.63}$$

Thus the orifice "sees" only about half the pressure drop between the two reservoirs.

PRESSURE REYNOLDS NUMBER

The Reynold's number as it is defined incorporates the velocity of the fluid in the pipe; but, in our case, this is the quantity we are trying to calculate from an known pressure distribution. We can make use of the fact that our model is independent of Reynold's number in the turbulent regime to redefine the Reynold's number to be a function of pressure and geometry rather than of velocity and geometry. We use the Hagen-Poiseuille solution to replace the velocity in the standard definition of the Reynold's number:

$$R_p = \frac{r_o^3 \, \Delta P}{4 \, \nu^2 \, L \, \rho} \tag{III.64}$$

This definition of the Reynold's number can be used to evaluate the entrance length (from the friction factor) in the laminar regime, as well as determine whether or not the flow through the pipe will be laminar or turbulent; it is not a useful quantity in the turbulent regime.

SIMPLE MODEL SUMMARY

In the various sections above, we have derived a simple of model of fluid flow along side the more complex (and more accurate) standard models. This model should serve us well for our problem of the flow through cracks in the building envelope. We review the results of our simple model below.

Let us begin by displaying the most important equation, the expression for the friction factor:

$$\lambda = \mathrm{MAX}\left(\frac{256\, \nu^2\, L\, \rho}{r_o^3\, \Delta P},\ 0.0278 + \frac{0.981}{(\ 1.2 - \log_{10} k^2\ )^2} \right) \qquad \text{(III.65)}$$

where

λ	is the Darcy friction factor,
ν	is the kinematic viscosity [m^2/s],
k	is the roughness parameter,
ρ	is the density of the fluid [kg/m^3],
r_o	is the hydraulic radius [m],
L	is the length of the pipe [m] and
ΔP	is the pressure drop across the pipe [Pa].

In the formula above we have replaced the critical Reynold's number by its value for circular pipes (i.e. R_c=2300); this is where the 0.0278 and 0.981 came from; additionally , we have used the definition of the (pressure) Reynold's number in the laminar part. (The first part is from laminar flow and the second is from turbulent flow.) The transition (between laminar and turbulent flow) is modelled as being sharp; and for a smooth pipe transition takes place at the critical Reynold's number (2300), but for rough pipe transition takes place sooner.

The flow can be related to the pressure drop and physical area via the discharge coefficient:

$$Q = C_f \, A \sqrt{\frac{2 \, \Delta P}{\rho}} \qquad \text{(III.66)}$$

where

Q	is the flow through the pipe [m^3/s],
C_f	is the discharge coefficient,
A	is the cross-section of the pipe [m^2],

The entrance length can be related to the Darcy friction factor:

$$L_e = \frac{4}{\lambda} \qquad \text{(III.67)}$$

This is reasonably accurate for both laminar and turbulent flow.

We can express the discharge coefficient in terms of the entrance length, the length of the pipe and the pressure reduction factor:

$$C_f = \tfrac{1}{2} \, (K + L/L_e)^{-1/2} \qquad \text{(III.68)}$$

where

K	is the pressure reduction factor

Tables of experimental values of the pressure reduction factor can be found in various engineering references, e.g., ASHRAE Handbook of Fundamentals for many complex geometries, but for simple (short) geometries K can be approximated by $1/2$.

For turbulent flow the friction factor is constant and hence, the discharge coefficient is constant; but for laminar flow the friction factor is inversely proportional to the velocity and the discharge coefficient becomes proportional to the square-root of the pressure.

SUMMARY AND DISCUSSION

We have derived a simple physical model of the flow of air through pipes, which relates the flow to the (square-root of the) pressure using a discharge coefficient. The physics is contained in the definition of the the discharge coefficient. PP This definition of discharge coefficient was chosen so that it would be independent of pressure for turbulent behaviour. Not only will the discharge coefficient be constant for turbulent flow, but, if the pipe is short the discharge coefficient will be constant — even if the Reynold's number is low. Furthermore, if the pipe is rough the Reynold's number at which laminar flow becomes turbulent decreases. In short, laminar flow will be likely only for long, smooth pipe under low pressure.

Since we are interested in determining the character of the flow through cracks in the building envelope, we need to know the conditions under which the flow will be laminar vs. turbulent.* We can use the qualitative discussion of the previous paragraph to estimate the largest crack that will exhibit purely laminar behavior. To find this critical crack size, we make the assumption that we are dealing with smooth pipe, whose length is at least equal to its entrance length and whose Reynold's number is below the critical Reynold's number:

$k \rightarrow 0$	Smooth pipe
$L > L_e$	Long pipe
$R < R_c$	Laminar regime

Thus the critical conditions for the appearance of laminar behaviour

---

* To be more accurate we wish to know when the discharge coefficient will be pressure dependent and when it will be constant. We will be more general and refer to laminar behavior when we mean that the flow is proportional to the pressure drop and turbulent when the flow is proportional to the square-root of the pressure drop.

are,

$$R = R_c = 2300 \qquad \text{(III.69.1)}$$

$$L = L_e = \frac{R_c}{8} r_o \qquad \text{(III.69.2)}$$

$$R_c = \frac{r_o^3 \Delta P}{4 \nu^2 L \rho} \qquad \text{(III.69.3)}$$

<u>where</u>

$r_o = r_c$

If we eliminate the length from these equation we get an expression that relates the critical radius to the pressure drop:

$$r_c = R_c \nu \sqrt{\frac{\rho}{2 \Delta P}} \qquad \text{(III.70)}$$

If we use 4 Pascals as being a typical pressure across the crack,

$$r_c \approx 13\text{mm} \qquad \text{(III.71)}$$

Using this value, the (critical) length of the crack comes out to be around 4 meter; clearly, this is much longer than any realistic crack in a building. If we restrict the length of the crack to be that of a typical narrow crack in a wall (i.e. 1 cm) we see that the condition on the hydraulic radius to assure laminar behavior is,

$$r_o \ll 2\text{mm} \ (\approx r_c) \qquad \text{(III.72)}$$

Thus the amount of laminar leakage in a real building will depend on the distribution of the leaks relative to 2 mm in size.

To summarize the last few paragraphs, the only cracks that will exhibit linear flow vs pressure leakage in conditions typical of the shell of a structure will be those cracks whose hydraulic radius is less than about 2 mm; those cracks whose hydraulic radius is much larger than this will exhibit square-root flow vs. pressure leakage (and thus,

constant discharge coefficient); and, cracks whose hydraulic radius is in the region near 2mm will show intermediate behavior. For cracks that are either rough, of inconstant cross section, or that have bends in them, the critical radius lessens.

Contained in these formulae is all the physics necessary to understand the flow through leaks in the envelope of a building. In the next chapter we shall apply this theory, combined with direct experimental measurement, to model the leakage of a building, taken as a whole.

REFERENCES

1. J. Boussinesq, Mem. Pres. Acad. Sci. Paris, 23:46 (1891)

2. L. Schiller, Z. Angew. Math. Mech, 2:96, (1922)

3. H. Langhaar, "Steady flow in the transition length of a straight tube," J. Appl. Mech. 9:A55 (1942)

4. R. Kreith, R. Eisenstadt, "Pressure Drop and Flow Characteristics of Short Capillary Tubes at Low Reynold's Numbers," Trans. ASME, p. 1070 (1957)

CHAPTER IV

WHOLE BUILDING LEAKAGE

In the preceding section we modeled the hydrodynamics of flow through a single crack, the micro-leakage structure; but to model infiltration we need to know the whole building leakage due to the summation of these leaks, the macro-leakage structure. The most straight forward method of determining the infiltration would be to sum the flows through each leak in the building envelope using weather induced pressures; this procedure requires knowledge about the discharge coefficient of each leak. Work based on this kind of model has been done by Alexander and Etheridge[1] in the United Kingdom. The principal drawback of such a model is that a large volume of leakage data must be acquired; specifically, the position, geometry, and discharge coefficient of each crack must either be measured or calculated. While this amount of effort might be acceptable in a pure research application, it is impractical for large-scale testing.

A more realistic approach would be to measure the combined effect of all of the cracks in a section of the envelope; this might be done by measuring the flow through this section in response to a constant pressure across it. If we were to subject a macroscopic section of the building envelope to a constant pressure drop, the flow from all of the leaks in that section will add arithmetically:

$$Q = \sum_i Q_i \qquad \text{(IV.1)}$$

$$= \sqrt{\frac{2\,\Delta P}{\rho}}\ \Sigma\, C_i\, A'_i$$

where

Q	is the total flow through the section [m^3/s],
Q_i	is the flow through the ith leak [m^3/s],
C_i	is the discharge coefficient of the ith leak,
A'_i	is the physical area of the ith leak [m^2],

We define the effective area of the section to be the sum:

$$A = \Sigma C_i A'_i$$

where

A is the effective area of the section [m^2].*

Since the effective area contains the discharge coefficients of all of the leaks, it need not be constant; if some of the discharge coefficients are pressure dependent, i.e., have appreciable laminar flow properties, the leakage area will be pressure dependent; similarly, if all of the discharge coefficients were constant, the leakage area would be constant.

A "section" is a very broad term that only serves to indicate that for some reason, we wish to treat that part of the envelope as a unit — as opposed to breaking it up into components. Conceptually, there are many ways of breaking up the building into sections: by function, e.g., windows, doors, walls, or by location, e.g., floor, walls, ceiling. If we were interested in multichamber techniques, it might be necessary to separate the leakage between each chamber, as well as from each chamber to the outside; however, the most important leakage value is the total leakage from the interior to the exterior of the structure. As outlined in the next chapter, infiltration would be proportional to this value. Accordingly, techniques should be developed for measuring the leakage of the entire envelope.

---

* Henceforth, we shall use the symbol A to represent the effective area; rather than the physical area as we did in the previous chapter.

EXPERIMENTAL TECHNIQUES

In the sections below two methods for measuring the total leakage function for a structure are discussed (the air flow vs. applied pressure curve). The first method, called fan (DC) pressurization, directly measures this function, but is limited in its pressure range. The second method, called AC pressurization*, (conceived and designed by the author) uses synchronous detection and lock-in techniques to improve the signal-to-noise ratio, and allows measurement of the leakage function at lower pressures. Once the flow vs. pressure function has been established, the total leakage area can be calculated as follows:

$$A_o = \frac{Q(\Delta P)}{\sqrt{\frac{2\,\Delta P}{\rho}}} \qquad \text{(IV.2)}$$

where

A_o is the total leakage area [m^2],

Q is the flow [m^3/s] as a function of

ΔP the applied pressure [Pa].

DC Pressurization

Until now, the standard method for finding the leakage function in a structure was fan pressurization or, "DC pressurization". In DC pressurization, the calculation of the leakage is straightforward. Because the applied pressure is constant and small compared to ambient pressure, the air inside the structure can be treated as incompressible. Ignoring various experimental errors (discussed below), the leakage can be obtained by applying the continuity equation:

---

* See Appendix B for the details.

$$Q(\Delta P) = Q_{fan}(\Delta P) \tag{IV.3}$$

where

ΔP is the pressure [Pa] across the envelope,

Q is the airflow [m^3/s] through the envelope at ΔP and

Q_{fan} is the air flow [m^3/s] through the fan

The flow through the fan must be equal to the net flow through the house; therefore, a measurement of the air flow through the fan vs. the pressure drop across the house gives a direct measurement of the whole house leakage function.

The procedure for fan pressurization[2] involves the use of a large-capacity fan to push the air into or out of the structure while measuring the associated pressure drop. The fan is mounted in the envelope of the structure (usually in place of a door or window) and the flow through the fan can be measured directly, e.g., using a pitot tube traverse or a vane anemometer, or it can be indirectly measured using the fan curve i.e., the characteristics of the fan are measured in the laboratory and a flows vs. RPM and pressure drop curve is derived. The pressure difference between the inside of the building and a point near (but out of the flow path) of the outside the fan is measured and the flow vs pressure function can be constructed. (An incline manometer is commonly used to measure the pressure drop.)

AC Pressurization

The tack taken in AC pressurization is profoundly different from that taken in DC pressurization. In AC pressurization, the volume of the building is modulated, by installing a piston and sleeve assembly in the building envelope, and the pressure response to the modulated volume is measured. The continuity equation is then used to calculate the flow through the structure. Of course, the continuity equation that is used is not as simple as the one used in DC pressurization, since it must include the effect of the compressibility of air as well as the effect

of the volume modulation:

$$Q(\Delta P) = -\frac{dV}{dt} - C' \frac{d(\Delta P)}{dt} \qquad \text{(IV.4)}$$

where

Q and ΔP	are air flow and pressure,
$d(\Delta P)/dt$	is the change in internal pressure [Pa/s] and
dV/dt	is the time change in volume of the structure [m^3/s],
C'	is the effective capacity of the structure [m^3/Pa].

For a full derivation of all the AC pressurization equations see the first part of Appendix B.

The effective capacity is primarily composed of two parts: 1) the compressibility of air ($V_o/\gamma P_a$) and 2) the flexing of the envelope. The flexing can be larger than the compressibility and, for high frequencies, cannot be ignored.

Given the change in volume and associated change in pressure, the continuity equation could be used to calculate the air flow through the structure; however, the quantity of interest is the steady-state flow associated with a steady-state pressure. In order to translate an oscillating flow into a steady state flow, we must introduce a model of leakage to relate the flow to the pressure difference across the envelope. We have used the following general model of whole building leakage:

$$Q(\Delta P) = L(\Delta P)\, \Delta P \qquad \text{(IV.5)}$$

where

L	is the leakage [$m^3/s/Pa$] function.

In Appendix B we made the simplification that the leakage function could be split into a large part — an even function of pressure, and a small part — an odd function of pressure; for the purpose of this discussion, however, we shall ignore this asymmetry.

If all the cracks that made up the leakage were long pipes undergoing laminar flow, we would expect the leakage function to be a constant; if, on the other hand, the cracks were short or undergoing turbulent flow we would expect the leakage function to be proportional to $\Delta P^{-1/2}$. Generally, the leakage function would be found somewhere in between but, in any case, we expect the leakage function to be a slowly varying function of pressure. (An exception to this might arise at very low pressures if the leakage were completely dominated by orifices.) As expected, DC measurements indicate that at higher pressures the air flow becomes proportional to the square root of the applied pressure.[3]

A priori, there is no reason why working at very low frequencies, i.e., DC pressurization, should be better or worse than working at higher frequencies, i.e., AC pressurization. Inspection of the sources of error for each measurement technique, however, would reveal their relative strengths and weaknesses. Since we are measuring two independent quantities — pressure and flow, — ostensibly there are two independent sources of error; we will discuss these errors separately below.

Errors in Pressure Measurement

In both AC and DC pressurization the measurement of the inside-outside pressure difference is necessary. The pressure signal we wish to measure is the response due to the equipment (oscillating plug or fan) and not any signal due to the weather; any wind-induced signal, for example, is noise.

Because the wind is the source of the noise, care must be given to the power spectrum of the wind when signal-to-noise is important. Mayne and Cook[4] have plotted the data of Van der Hoven,[5] as displayed in figure 1. The power spectrum is bimodal, having a major peak near several days (with a minor peak at about 2 hours), called the macrometeorological peak; the other peak is at about 1 minute called the micrometeorological peak. The macrometeorological peak is caused by major weather patterns such as storm fronts, etc; the

micrometeorological peak is caused by turbulence in the wind that can be enhanced by terrain features. The power spectrum declines at frequencies much higher than the micrometeorological peak; but, just as the power spectrum of the wind begins to decline, the power spectrum of structure-generated noise becomes important.

The presence of the structure in the wind stream will cause small scale turbulence that creates high-frequency pressure noise around the envelope of the structure. Eaton and Mayne[6] have measured the power spectrum of both the on-site wind and the pressures on different sections of houses; figure 2 shows three different power spectra: one for the wind as measured at 10m on-site, one for the windward surface pressure and one for the roof pressure. The windward wall pressure is shifted noticeably towards high frequencies (relative to the wind) indicating that building induced turbulence is important; the roof pressure is shifted even further to high frequencies due to the prominence of such effects as vortex shedding and separation. Figure 3 gives two other typical (pressure) power spectra for one of Eaton and Mayne's experimental houses. Figure 3a is for a leeward or side pressure and figure 3b is for the internal pressure. The internal pressure is generally dependent on the relative leakiness of the faces of the structure and the pressure on them; therefore, the power spectrum may be anywhere from exactly the same as one of the faces (for the case of one very leaky face) or the appropriate average of the pressures from all the sides. In the latter we would expect the amplitude to be generally reduced because of the averaging process. Note that both spectra have a peak near the micrometeorological peak at one minute as well as a peak at about ten seconds.

DC Pressurization: In DC pressurization the pressure measurement is made by taking the difference between the internal pressure (which is assumed not to vary within the structure) and the external pressure near the site of the fan, i.e., at one particular point on the structure. The reading is averaged for a few seconds — effectively eliminating any

---

The designations on figs. 2 and 3 are from the original work.

noise at frequencies above 0.1 Hz. The measurement, however, is still sensitive to all noise below that frequency. Thus the size of the noise would be given by that fraction of the power spectrum less than this frequency. If the averaging time were increased to ten minutes, all of the micrometeorological disturbances (as well as the structure-induced noise) would be eliminated; this would not, however, eliminate the macrometeorological contribution, i.e., the measurement would still be affected by prevailing winds. Accordingly, the magnitude of the wind induced interference will depend on the average wind pressures exerted during the complete measurement period; — typically in the 1-10 Pascal range.

AC Pressurization: Several different techniques were used to improve the quality of the pressure signal for AC pressurization relative to DC pressurization. The internal pressure was measured by using a physical filter which filtered out all the high-frequency components of the pressure on the reference side of a differential pressure sensor, thus allowing the differential reading to contain only the high-frequency components. (The cut-off frequency has a period of approximately five minutes.) Hence, there was no interference due to the macrometeorological peak or to changes in barometric pressure. Furthermore, since the internal pressure is related to the average of the external pressures, the size of the noise was further reduced.

The primary technique used to improve the signal-to-noise ratio, however, has been synchronous detection. In this approach the period of the (volume) drive was measured to the nearest millisecond; the pressure signal was then fourier analyzed at this frequency with a band bass width of approximately .05 Hz. Therefore, the only part of the noise spectrum that could have affected our measurement was the part within .05 Hz of the fundamental frequency. Thus, we were able to measure the fourier component of the pressure down to 0.1 Pascals cleanly. (It may have possible to measure the pressure even lower, but other factors prevented taking the experiment to lower pressures.)

Errors in Flow Measurement

As noted, the other independent quantity measured is the flow; in DC pressurization one measures the flow directly, while in AC pressurization one measures volume displacement and calculates the flow from this value and the continuity equation.

DC Pressurization: There are several methods used to measured the flow in DC pressurization: pitot tube traverse, vane anemometer, precalibrated fan law using RPM and pressure etc. All of these techniques, however, share a common failing — when the velocity in the duct gets low enough the character of the flow changes and the measurement becomes imprecise. A common arrangement is to have an 18 inch diameter duct leading up to a 3000 cfm fan; the fan is so chosen in order to assure that large (leaky) houses can be pressurized. With this size fan, the flow profile begins to lose its flat shape at about 400 cfm and, consequently, most methods for measuring the flow will fail. A possible solution is to use smaller duct and increase the velocity; however, while this would work for tight houses, it would keep loose houses from being measured, thus necessitating several fans of different sizes.

AC Pressurization: In AC pressurization where the modulation of the volume and the continuity equation are used to find the flow, the equivalent source of error is in the measurement of the volume modulation. There are three factors that make up the volume modulation: the cross-section of the piston, the stroke, and the frequency. Because the cross-section is easily measured and stays constant at all times, there is negligible error from it. The stroke length, like the cross section, is an easily measured parameter.* The period of the drive was measured to the nearest millisecond and could cause no more than ±0.1 percent error in the determination of the frequency; the major error in the frequency was the cycle to cycle variation, which was found to be less than ±5 percent deviation from the mean at all times.

Other Systematic Errors

In each experiment there is the possibility of other types of systematic errors. For example, for DC pressurization (if the calibration curve is used) or for AC pressurization, the pressure is used to help determine the flow through the structure; hence, the errors are not truly independent, but we shall ignore the cross-correlation.

DC: When the fan is placed in the envelope of the structure, an otherwise solid area, i.e., the door is replaced by a hole, i.e., the fan opening,. If there is a (wind induced) pressure drop between this face of the structure and the inside there will be a flow through the fan that is not accounted for. This error will be quite large until the fan induced pressure becomes much greater than the wind induced pressure; regardless of the signal conditioning of the pressure signal, any steady pressure difference will cause an error in the flow determination.

AC: In AC pressurization where the penetration of the envelope is filled with a piston rather than left open, the problem becomes one of the integrity of the sliding seals rather than the leak from the entire opening. In our experiment, we used several axial rows of teflon seals to minimize both the leakage and the sliding friction. (The seal leakage area was crudely measured to be 20 cm^2.)

One further complication arises in applying the AC technique that does not arise in the DC technique: in the AC technique we apply a sinusoidal volume modulation that causes a (pseudo) sinusoidal pressure oscillation. Thus, the leakage function we calculate is a leakage function that has been averaged over the pressure range; the assumption of slowly-varying leakage function allows to replace the leakage function L by its value at the root-mean square pressure:

$$L(\Delta P) \rightarrow L(\Delta P_{rms}) \qquad \text{(IV.6)}$$

This assumptions allows us to equate our AC leakage results with steady state pressures.

Within the pressure range of interest, the AC technique has superior analyzing power for determining of the leakage of a building. The synchronous detection analysis combined with the use of a physical filter achieve a far greater signal-to-noise ratio than is possible with any DC technique. Because there is no attempt to directly measure the flow through the envelope, the AC technique is insensitive to the errors associated with low-velocity flow measurement. Finally, the AC technique avoids incurring the large systematic errors introduced when a hole is placed in the building envelope.

DISCUSSION OF RESULTS

While a great deal of data is available for DC pressurization, this technique cannot answer any of the fundamental questions regarding the leakage function of a structure at low (0-10 Pa) pressures. Therefore, our discussion will be based on the low-pressure leakage data obtained by means of AC pressurization, all of which is contained within this paper. Accordingly, the conclusions drawn may not be true in the general case, but they are useful, nevertheless, as an indication of the underlying result.

To summarize the results displayed in Appendix B, the leakage function appears to be a monotonically decreasing function of pressure that approaches zero. The low end of the function does not appear to approach a constant within the range of the experiment, indicating that laminar flow is not the dominant flow type for a residence.

If linear flow were not dominant, could we assume that turbulent flow would be? This question cannot be resolved by the data in the form presented in Appendix B; in order to see the role played by turbulent-like flow, we replot the data (along with some additional low pressure data not displayed in the Appendix) showing the effective leakage area vs. applied pressure (see figure 4.). If turbulent flow were completely dominant, we would expect the leakage area to be independent of pressure.

As can be seen from figure 4, the leakage area does have some pressure dependence, but the pressure dependence of the effective area is much weaker than was the pressure dependence of the leakage function. This weaker dependence indicates that the concept of a constant effective leakage area is "closer" to the truth than that of of a constant (linear) leakage — hardly surprising since (as we calculated in the previous chapter) the only leaks we would expect to find in a structure having linear leakage would be those in the sub-millimeter (radius) range. Our results indicate that only a small portion of the leakage can be attributed to these "laminar cracks". It is this conclusion, perhaps, that is most subject to the criticism that only a single structure had been tested. In a tighter structure where more attention has been given to detail and the larger leaks have been sealed, we might expect a larger proportion of the leakage to be laminar. Nevertheless, in all but the most pathological cases we would expect that the leakage will be dominated by turbulent-like flow. Inasmuch as our ultimate goal is to develop a simple physical model of infiltration, we chose to describe leakage in terms of a constant leakage area; that is, a single parameter — the effective leakage area — would describe the flow response of a macroscopic section to an applied pressure.

A problem that immediately arises with this theory is how to evaluate the leakage area when, in fact, it is pressure dependent. The assumption of a constant leakage area would not cause an error in the calculation of flow if the pressure across the section were constant and the leakage area were evaluated at that pressure. In a real situation, however, the pressure will not be constant, but rather will vary between two limits (usually -10 Pa to +10 Pa). To minimize any, error associated with our choice of model, we will choose to evaluate the leakage at a pressure that is typical of the pressure felt by the structure. Because the leakage area is multiplied by the square-root of the pressure, the average condition will be the average of the square-root of the pressure over the range. We have chosen the value of four pascals

as the reference pressure at which we evaluate the leakage area.

LOCALIZATION OF LEAKAGE

In both the AC and DC techniques described above, only a single leakage value is obtained for the structure as a whole. While this is the simplest measurement to make, in some cases it may not yield enough information. Localizing the leakage is desirable for a variety of reasons: to determine the leakage of various large sections (e.g. floor, walls, ceiling) in order to assist model calculations; to determine the component leakage (e.g. windows, doors, wall outlets) to gauge the generalized sources of leaks; and to determine the specific leakage sites (e.g. under kitchen sink, weatherstripping of living room walls) to suggest retrofits. All of these classification schemes have been used.

Several researchers, especially in Canada,[7] have sealed off large areas with sheets of plastic to find the floor, wall and ceiling leakage. In many instances over half the leakage area of a residence could be attributed to the leakage through the ceiling. This leakage can usually be attributed to the various ceiling penetrations, e.g., exhaust vents, recessed lighting, etc..

By selectively sealing components, air leakage can be apportioned to each one. While this type of analysis is important for finding the general leakage behavior of structural parts, results may tend to vary greatly from structure to structure and climate to climate; furthermore, specifics will strongly depend on the type of construction, the age of the structure, upkeep, and construction quality. However, Texas Power and Light Company[8] surveyed 50 houses, selectively sealing all components and found the percentage leakage associated with each one. While the results tabulated below represent only a limited number of house types, they are in general agreement with other, similar measurements made on individual houses.

AIR LEAKAGE PER COMPONENT*			
Component	% Leakage	Component	% Leakage
Soleplate	25	Wall Outlets	20
Duct System	14	Windows	12
Range Vent	5	Fireplace	5
Recessed Lights	5	Exterior Doors	5
Dryer Vent	3	Sliding Doors	2
Bath Vent	1	Other	3

The conclusion of this study was that most of the leakage in these houses could be eliminated by caulking and weather-stripping.

A third method locates, but does not quantify the leaks in a structure. If the structure is placed under pressure there will be air leaking out of the cracks; if a small source of smoke is placed near suspected leaks the smoke can be seen exiting. This "smoke-stick" method is a very simple way of finding leakage sites during a fan pressurization test. From the localization of leakage sites, decisions regarding retrofit measures can be made.

A superior, but more expensive, method of finding leaks can be employed if there were a substantial inside-outside temperature difference. Instead of using a smoke-stick to find the leaks, a scanning infrared camera is used. If the house were being depressurized (assuming the outside is colder) the air coming in through the leaks would cool the part of envelope immediately surrounding it. Since this can easily been seen with an infrared camera from any point within that room, an entire house can be inspected in a few minutes, and, unlike the smoke-stick method, one does not have to be in the immediate vicinity of the leak to find it.

---

* In the actual experiment, three different strokes were used; furthermore, a small amount of slop in the connecting rod was found and compensated for.

FUTURE DIRECTIONS

AC pressurization appears to be a powerful technique for the evaluation of envelope leakage at low pressures. Many new experiments were suggested (and most are being pursued) by the original AC measurement.

Experimental Apparatus

Our original experimental apparatus used to measured AC pressurization consisted of a motor driven plug that oscillated with a crank motion. Because it was an unbalanced massive arrangement, it could operate only at limited frequencies (20 rad/sec max. at the small displacement). Future experiments could use a smaller displacement and a balanced arrangement that would allow higher frequencies. The original experiment mounted the oscillating plug in the building envelope; this procedure could cause technical problems, and reduces the portability of the apparatus. Future experiments could use a sealed back-volume instead of the "outside" and thus be more portable than the original.

A new mechanism is currently being constructed that would make use of both these improvements. It consists of an opposed two-cylinder engine, driven by a motor; the pistons are 1/2 meter in diameter and have a 5 cm stroke. The back of the pistons are connected to a sealed volume which is alternately compressed and expanded; with a 1 hp motor we hope this can be driven at up to 10 Hz.

---

* The results in this table are in terms of air flow at a fixed pressure, rather than leakage area. Hopefully, if the data were converted to leakage area there would not be substantial changes.

Data Analysis

Rather than use the general, but elaborate, analysis used so far, the alternate analysis (given in Appendix B) could be used to find the leakage. That is, if we make the assumption that the leakage can be described by a power law,*

$$Q(\Delta P) = C_n \Delta P^n \tag{IV.7}$$

we can find the coefficient, C_n, for a given n using the continuity equation:

$$C_n \Delta P^n + \frac{dV}{dt} + C' \frac{d\Delta P}{dt} \tag{IV.8}$$

If we multiply through by the (time dependent) pressure drop and integrate over a cycle, the last term will vanish and we can solve for the coefficient without regard to the capacity of the structure:

$$C_n = \frac{< \Delta P \frac{dV}{dt} >}{< |\Delta P|^{n+1} >} \tag{IV.9}$$

where

< > indicates an average over one cycle of the volume modulation.

Our earlier assumption of constant leakage area is equivalent to setting the exponent in the equation to be 1/2 and expecting the coefficient to remain independent of the size of the drive; from this coefficient we can calculate the effective leakage area directly. If we were to fix the exponent to be 1/2, then we can directly calculate the (possibly

* This should be interpreted to mean that the sign of the pressure carries through to the flow, but otherwise the sign of the pressure is ignored when taking the nth power.

pressure-dependent) leakage area (on-line):

$$A = \sqrt{\frac{\rho}{2}} \frac{< \Delta P \frac{dV}{dt} >}{< |\Delta P|^{3/2} >} \qquad \text{(IV.10)}$$

This analysis technique suggests that the data analysis can be done with real-time analog circuitry, rather than the microprocessor technology that was used in the original work.

Multichamber Pressurization

Because AC pressurization is able to measure the leakage at low pressures, it might be possible to determine the intra-building leakage. If there are several chambers inside a structure it might be necessary to find the multichamber infiltration; in order to do this, the multichamber leakage must be determined; that is, the leakage between each chamber must be found, in addition to finding the leakage between each chamber and the outside. If the volume modulation device is placed in one chamber and then the pressure response is measured in all of the chambers and this process is repeated for each chamber it may be possible to determine the n^2 leakage areas. In a large building, the pressure signal from one chamber to another may be severely attenuated and careful signal processing will have to be done in order to retrieve significant data.

CONCLUSIONS

The most important conclusions to be drawn from this chapter are that AC pressurization is a powerful tool for probing the low pressure leakage function of a building, and that the effective leakage area is the best way to characterize the leakage of a typical section of the building envelope under normal pressure conditions.

REFERENCES

1. D.K. Alexander and D.W. Etheridge, "The British Gas Multicell Model for Calculating Ventilation," ASHRAE Trans. 86-II (1980)

2. A. Blomsterberg, D. Harrje, "Approaches to Evaluation of Air Infiltration Energy Losses in Buildings", ASHRAE Trans. Vol 85, Part I (1979)

3. D.T. Grimsrud, M.H. Sherman, R.C. Diamond, R.C. Sonderegger, "Air Leakage, Surface Pressures and Infiltration rates in Houses", LBL Report #8828 (1979) , 2nd Int. CIB Symp. on Energy Conservation in the Built Environment.

4. J.R. Mayne, N.J. Cook, "On design procedures for wind loading," Build. Res. Estab. Current Paper, CP 25 (1978)

5. I. Van der Hoven "Power spectrum of horizontal wind speed in the frequency range from 0.0007 to 900 cycles per hour," Journ. Meteorology, 14:160 (1957)

6. K.J. Eaton, J.R. Mayne, "The measurement of wind pressures on two-storey houses at Aylesbury," Build. Research. Estab. CP 70 (1974)

7. Tamura, G.T., "The Calculation of House Infiltration Rates," ASHRAE TRANSACTIONS, 85, 1:58-71, 1979.

8. G.E. Caffey, "Residential Air Infiltration," Texas Power and Light Co., (1977)

FIGURE CAPTIONS

FIG. IV:1 Spectral frequency of wind.

FIG. IV:2 Power Spectrum of wind at 10m, windward surface pressure and roof surface pressure of experimental building.

FIG. IV:3 Power spectrum of pressures on experimental building: a) (top) is typical of side or leeward wall b) (bottom) is for internal pressure

FIG. IV:4 Low pressure plot of effective leakage area vs. applied pressure.

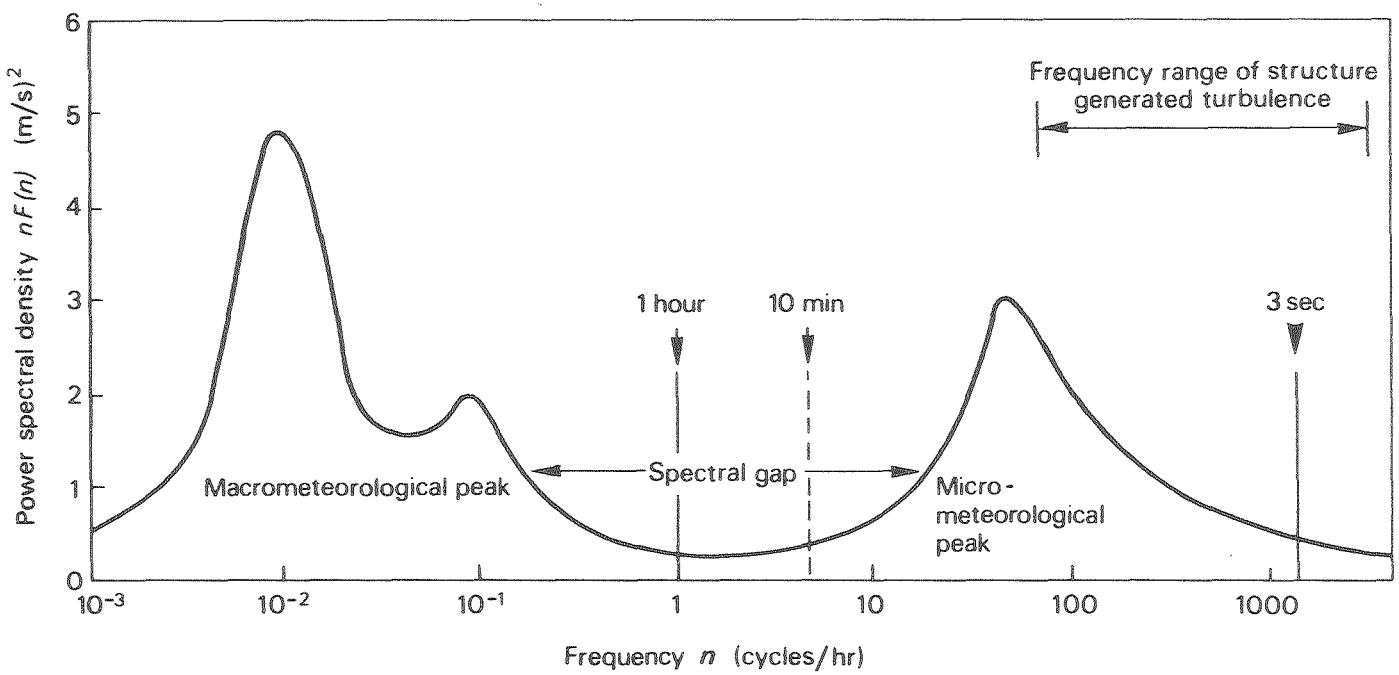

XBL 807-10668

FIG. IV:1 Spectral frequency of wind.

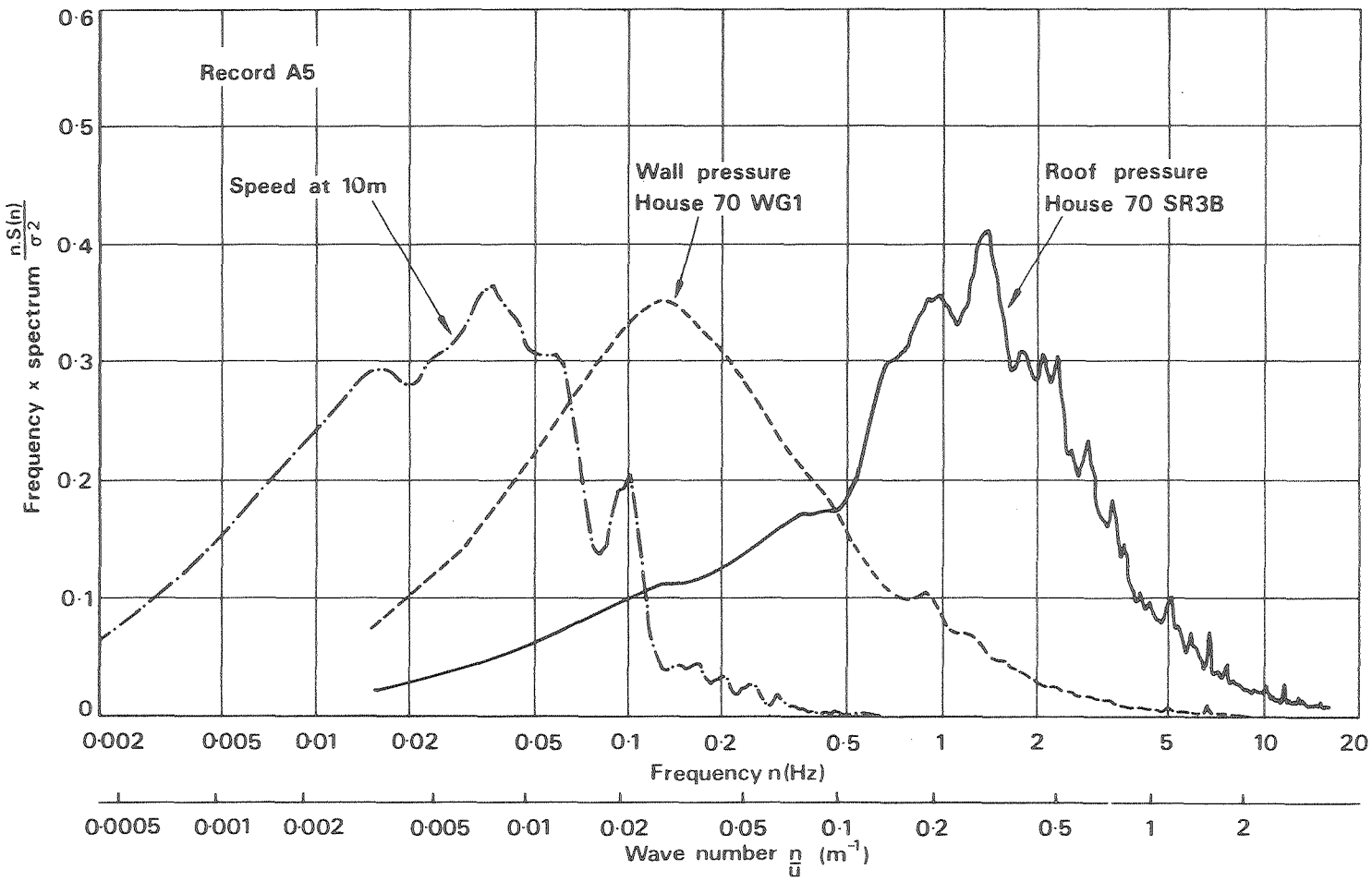

XBL 807-10667

FIG. IV:2 Power Spectrum of wind at 10m, windward surface pressure and roof surface pressure of experimental building.

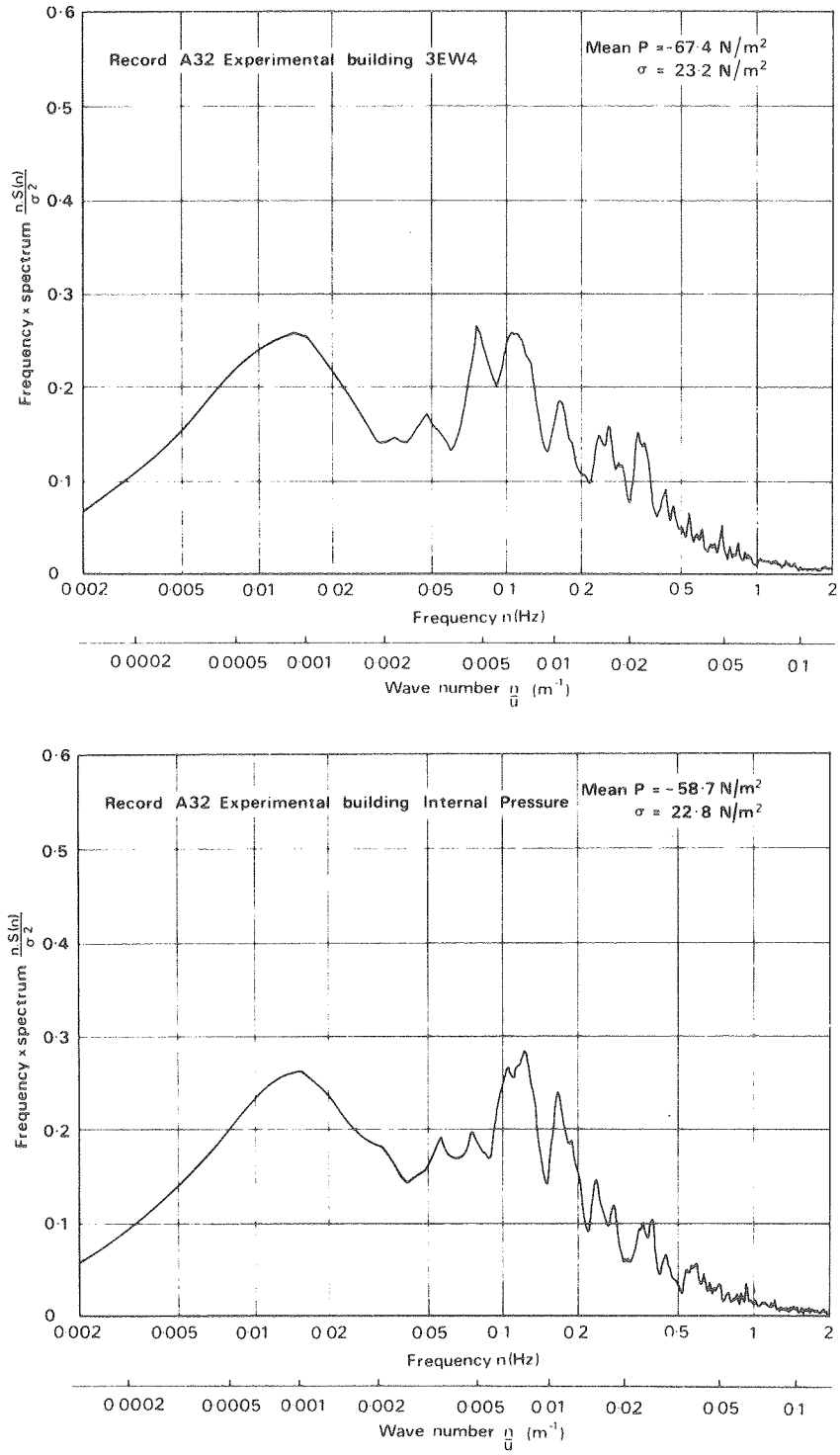

XBL 807-10666

FIG. IV:3 Power spectrum of pressures on experimental building.

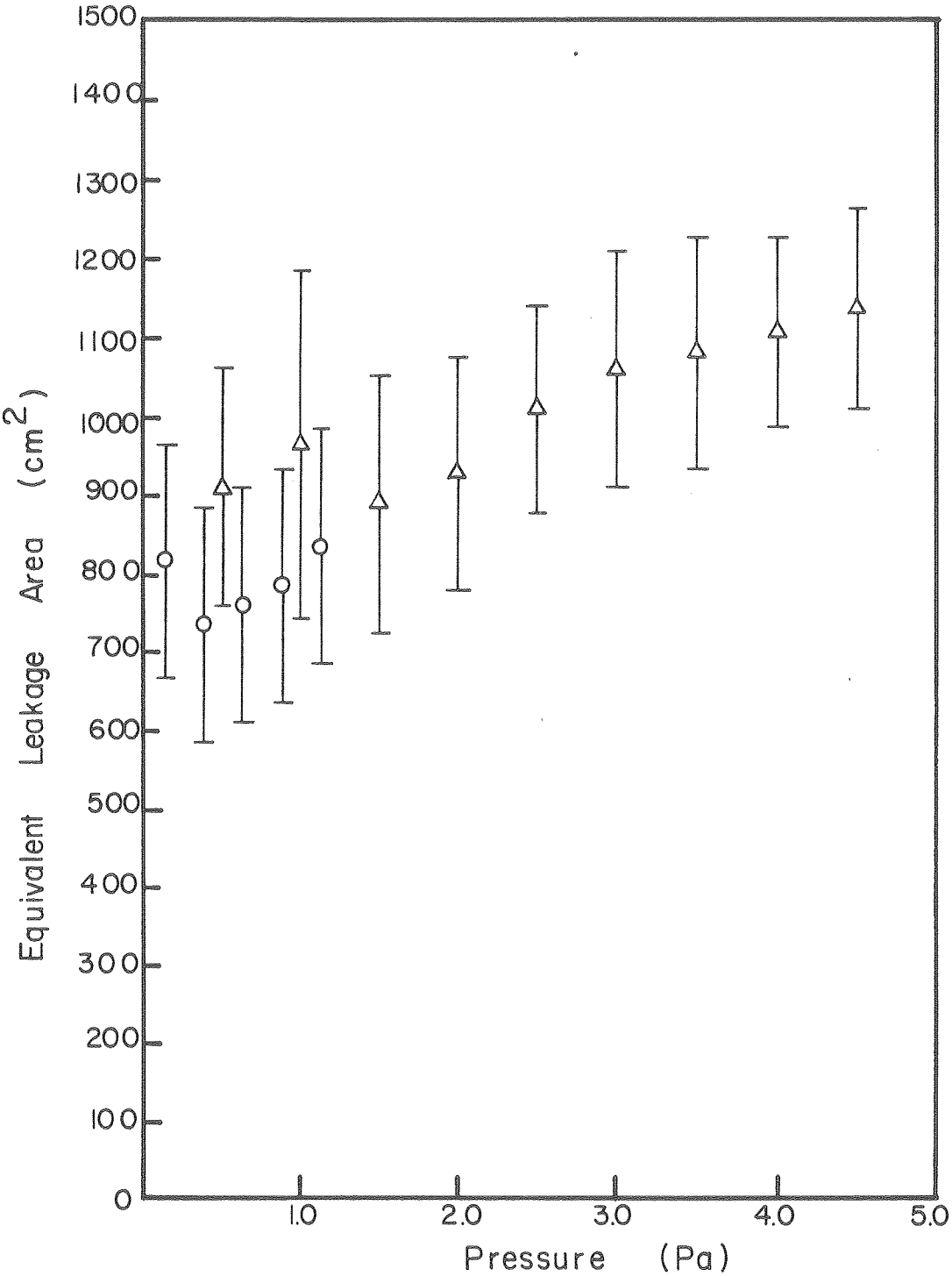

XBL 7912-13745

FIG. IV:4 Low pressure plot of effective leakage area vs. applied pressure.

CHAPTER V

MODELING

Because infiltration is a primary source of energy loss in residences, understanding the infiltration process is critical to any residential conservation program. Yet we are far more capable of calculating losses due to conduction than losses due to infiltration. Several explanations for this disparity can be cited. First, conduction losses are more easily calculated because the heat transfer is proportional to the temperature difference and does not depend strongly on any other driving force. Infiltration, on the other hand, depends on the interior-exterior pressure difference but is not simply proportional to it. Furthermore, the driving pressure is caused by uncorrelated physical effects (wind speed and temperature difference). Second, conduction losses can be characterized by means of one parameter, thermal resistance, whereas infiltration, until now, has had no equivalent quantity.

Many attempts at infiltration modeling have been made in the past; but the results of such models have been very disappointing. Virtually all of the previous models have been either inaccurate or site-specific; the only exception is a class of detailed models requireing such a large amount of information that they are impractical to use as predictive tools. Listed below are the types of models currently in use:

- Constant Rate: The constant-rate model is the simplest model of all; it assumes that the infiltration rate (i.e., the number of volumes per unit time) is a constant, independent of all other factors (e.g., weather, leakage, occupancy, size, etc.). It is this model that most large computer programs currently use for calculating of building performance. Understandably, a strong appeal of this model is precisely because the only information required to calculate infiltration is infiltration. In the absence of a better model, designers and engineers have simply been specifying the infiltration rate in their designs without having any idea whether their guesses approach reality. It's also true that in the past the only need for calculating infiltration was to size equipment (e.g., heating plant, air-handling systems etc.) and this "zeroth" order approach was

sufficient. Now that energy conservation and, with it, indoor air quality have become important issues, this type of model is clearly inadequate.

- Air-Change Method: This model represents an attempt to estimate the total infiltration by modifying the constant-rate method on a room-to-room basis. Each room is assumed to have a constant infiltration rate that is based on the number of existing exterior doors and windows; studies made on small buildings yield the values for this rate. Again, no attempt is made to measure or estimate either the leakiness of the envelope or the driving pressures across it.

- Crack Method: The crack method, the first real attempt to estimate the leakage of the building envelope, assumes that the infiltration will be proportional to the "crackage" and some pressure raised to an arbitrary power:

$$Q = C \Delta P^n \qquad (V.1)$$

where

Q	is the infiltration,
C	is the crackage,
ΔP	is a "design pressure drop" and
n	is the exponent.

The exponent is usually assumed to be equal to 0.65 and the pressure drop is a single number calculated by estimating the pressure due to the difference in buoyancy between inside and outside air, and adding to that value the pressure caused by the wind. The crackage is calculated by finding the length of crack associated with each door and window in the envelope, multiplying it by a tabulated quantity dependent on the type of penetration (e.g., double-hung window, wall-frame leaks around masonry, etc.). Although this method does attempt to use weather information to estimate the infiltration, unfortunately, since it uses only design pressures, it cannot be used to estimate instantaneous infiltration, or even long-term

average infiltration — only design infiltration. Furthermore, the estimation of crackage does not take into account installation of fenestration, etc. It has been found that installation practices and aging can each change the leakage behavior by a factor of two.

The above two methods have been used by designers and, until recently, have been the ASHRAE standard methods used to size equipment as well as to estimate infiltration. A review of the ASHRAE models has been prepared by J. Jansen[1]

- Linear Regression Techniques: Because they do not consider the instantaneous pressures across the envelope, the previous models are completely unable to predict instantaneous infiltration. Realizing that weather is the dominant driving force for infiltration, researchers attempted in a statistical sense; to fit the infiltration to the weather variables that is, the infiltration was assumed to be linearly dependent on the temperature and wind speed:

$$Q = a + b\,\Delta T + c\,v \qquad (V.2)$$

where

Q	is the infiltration,
ΔT	is the inside-outside temperature difference,
v	is the wind speed and
a,b,c	are regression constants.

In order to use this model, a great deal of data (infiltration, temperatures, and wind speed) are taken at a particular site and the constants a,b,c are fit to it; once the constants have been found, the infiltration can be calculated from the weather variables using the above equation. Such regression equations have been found to be quite accurate for the site at which the data was taken;.[2-4] however, if the same constants are tried at another site or if the weather variables are outside the range of the initial data, the results are completely unreliable. Furthermore, since the regression constants have no physical meaning, it is impossible to

formulate a method that converts one set of regression constants for one particular site into those for another site.

Because only the weather variables appear specifically, the effect of envelope leakage is not evident. While it can be assumed that the leakier the structure, the more the infiltration, a linear regression fit does not predict how the infiltration of the structure will change if the leakage of the envelope is decreased.

- Detailed Models: Models are now being developed that perform very detailed calculations to find the instantaneous infiltration. Basically, this type of model calculates the pressure distribution everywhere (maintaining self-consistency) and from that pressure distribution it calculates the flow through each leak. This computation requires intimate knowledge of the location and characteristics of each leak, (e.g. crack geometries and distribution, precise siting and terrain information etc.) as well as the information necessary to calculate the pressure drops. While such detailed models can be made quite general and still be very accurate; they do require, however, that a large body of information about the structure be acquired.

In some detailed models[5] the pressure drop across the envelope is explicitly measured and combined with leakage characteristics of the envelope to find the infiltration. While this model can be very accurate in predicting infiltration, it does require constant monitoring of the pressures and thus it is clearly impractical for large-scale measurements.

Generally speaking, the large body of information required to determine infiltration makes these, detailed models unsuitable for most applications. In a computer design program, it would be not only unreasonable but impossible for a designer or engineer to specify the location and size of every crack. For field testing, it would take an unreasonable length of time to locate and characterize each leak — assuming it were possible. Detailed techniques, then, are most suited to intensive research applications.

Clearly, none of these model types is adequate for predicting infiltration in the general case. What is needed is a simple, physical model of infiltration that allows infiltration to be calculated from a few easily measurable quantities, and that does not need to be modified for different climates or structure types.

This report introduces an infiltration model that sacrifices accuracy for versatility and simplicity. Rather than predicting accurately the weather-induced infiltration of a particular structure, the model is designed to calculate the infiltration of a general structure. Furthermore, the model predicts the impact of retrofits or other changes in the building envelope on the basis of performance changes effected in a few measurable parameters:

1) The leakage area(s) of the structure.
   The leakage area is the parameter that describes the tightness of the structure (obtained by pressurization). Most retrofits will affect the leakage area or the leakage distribution.

2) The geometry of the structure.
   The height and other geometric quantities are usually known or can be directly measured.

3) The inside-outside temperature difference.
   The temperature difference gives the magnitude of the stack effect. It is also necessary for calculating the energy load due to infiltration.

4) The terrain class of the structure.
   The terrain class of the structure is determined by the density of other buildings and obstructions that influence the dependence of wind speed on height near the structure. Knowing the terrain class of the structure allows the use of off-site weather data for calculating wind-induced pressures.

5) The wind speed.

The wind speed is required to calculate the wind-induced infiltration for comparison with the stack effect.

Using standard wind formulae (see Table C.1) the wind speed used by the model can be calculated from a wind speed measured on any weather tower in the area. Thus, on-site weather collection is not necessary. The only requirement is that the measured wind data is for the "same wind", i.e., there can be no mountains or other major disturbances in terrain between the site and the wind tower.

THEORY

For this model, we assume that the structure is a single, well-mixed zone; we use typical shielding values for a simple rectangular structure and neglect terms that depend on the sign of the temperature difference. Most importantly, we split the problem into two distinct parts: the wind-regime, where the dynamic wind pressure dominates the infiltration, and the stack regime, where the temperature difference dominates the infiltration. Infiltration in the two regimes is expressed as follows:

$$Q_{wind} = f_w^* A_o v' \qquad (V.3.1)$$

$$Q_{stack} = f_s^* A_o \sqrt{\Delta T} \qquad (V.3.2)$$

where

Q_{wind} is the infiltration in the wind-regime [m^3/sec],

Q_{stack} is the infiltration in the stack regime [m^3/sec],

f_s^* is the reduced stack parameter [m/s/$\sqrt{K}$],

f_w^* is the reduced wind parameter,

v' is the (weather tower) wind speed [m/sec] and

ΔT is the inside-outside temperature difference [^oK].

Derivations for reduced parameters and a complete delineation of the assumptions are given in Appendix C and the results are given below.

The reduced wind parameter is given by the following expression:

$$f_w^* = C' \left[(1 - R)^{1/3} \right] \left[\frac{\alpha \left(\frac{H}{10}\right)^{\gamma}}{\alpha' \left(\frac{H'}{10}\right)^{\gamma'}} \right] \qquad (V.4)$$

where

C'	is the generalized shielding coefficient,
R	is the vertical leakage fraction
α, γ	are terrain parameters,
H	is height of the structure [m] and
H'	is the height of the wind measurement [m].

The reduced wind parameter contains three terms: the generalized shielding parameter, the R factor, and the terrain factor. The first term describes the shielding around the structure; we have used wind tunnel data[6] to find the generalized shielding coefficient for the case where there are no significant obstructions in the vicinity of the structure and have broadened the concept to allow for five different classes of shielding. Shielding class I is the unobstructed case and the values of the other classes reflect the fact that increasing the amount of obstructions near the structure will lower the pressures acting on that structure. Although shielding values in each class are potentially measurable quantities, lacking direct experimental evidence, we have simply used equally-spaced (pressure) intervals as the separation between classes and have used suitably qualitative descriptions to define them. Work remains to be done to give these shielding classes proper experimental corroboration.

The second term in the reduced wind parameter expression accounts for the fact that the amount of leakage area available to the wind is reduced as the leakage area is shifted from the walls to the floor and ceiling. That is, for a given total leakage area, as R is increased

there is less leakage area exposed on the walls; thus, since there is no direct wind effect on the floor and ceiling (due to our assumption of good shielding) the amount of air flow due to wind must decrease. Furthermore, in the limit of R=1 there will be no infiltration due to the wind.

The third term in the reduced wind parameter expression accounts for the fact that the wind measured on a weather tower will not be the same as the effective wind speed at the structure. To compensate for this effect we use standard wind engineering formulae[7] to translate the wind in one terrain and at one height to the same wind in another terrain and at another height. The primed quantities in the reduced wind parameter expression refer to the variables at the wind-measurement site, and the unprimed ones refer to the variables at the structure.

At first sight, terrain and shielding appear to be the same thing; the difference, however, is that of scale. Shielding refers to wind obstructions within a few typical dimensions of the structure and is, therefore, a local manifestation. Terrain effects refer to the general roughness of the surrounding countryside and are, therefore, global effects. (Tables containing the shielding and terrain parameters for different classes can be found at the end of Appendix C.)

The reduced stack parameter is given by the following expression:

$$f_s^* = \frac{(1 + R/2)}{3} \left[\frac{\sqrt{8\,\beta^o}\,\sqrt{1 - \beta^o}}{\sqrt{\beta^o} + \sqrt{1 - \beta^o}} \right] \sqrt{\frac{gH}{T}} \qquad (V.5)$$

where

g	is the acceleration of gravity [9.8 m/s^2],
H	is height of the structure [m],
T	is the inside temperature [295K] and
f_s	is the (dimensionless) stack parameter.
β^o	is the (dimensionless) height of the neutral level.

The neutral level, β^o, is the height above the floor divided by the height from floor to ceiling at which the pressure inside exactly equals the pressure outside (due to the stack effect). Although this variable is experimentally determinable,[8] it is quite difficult to conduct this experiment. A byproduct of the calculation that leads to the stack equation above is a relation between the neutral level and the difference in the ceiling/floor leakage:

$$X = \frac{\frac{4}{3}(1-R)\left[(\beta^o)^{3/2} - (1-\beta^o)^{3/2}\right] + R\left[\sqrt{\beta^o} - \sqrt{1-\beta^o}\right]}{\sqrt{\beta^o} + \sqrt{1-\beta^o}} \qquad (V.6)$$

where

$X = \frac{A_{ceiling} - A_{floor}}{A_o}$ is the ceiling-floor leakage difference.

Unfortunately, this equation gives X in terms of β^o rather than the other way around. Numerical means, however, can be used estimate the value of the neutral level for a given value of X. Rather than requiring this laborious step each time, we have developed an approximation formula from this determining equation for the reduced stack parameter:

$$f_s^* = \frac{(1 + R/2)}{3}\left[1 - \frac{X^2}{(2-R)^2}\right]^{3/2}\sqrt{\frac{gH}{T}} \qquad (V.7)$$

This formula is correct up to the fourth order in X and has the correct limit as X approaches unity.

Superposition Law for Infiltration

We now have expressions that allow us to calculate the stack-induced infiltration and the wind-induced infiltration, the only problem that remains is that of combining them. In general, the interaction of such independent phenomena will be quite complicated but, in our simplified approach, we look only at the way in which each affects the differential

pressure. Since both the stack effect and the wind effect influence the pressure distribution, we assume that their superposition can be treated by simply adding their pressure effects. Based on our assumption a square-root of dependence of flow-on pressure, it is reasonable to assume that stack-induced and wind-induced infiltration add in quadrature.

$$Q = \sqrt{Q_{stack}^2 + Q_{wind}^2} \qquad (V.8)$$

where

Q is the combined infiltration [m^3/s].

In a previous work[13] the authors demonstrated that whenever the wind effect or stack effect dominates, the first-order cross term vanishes, making this type of combinatorial rule possible (i.e., there is no term of the form $Q_{stack} \times Q_{wind}$ in the above expression). Accurate prediction of the infiltration in the intermediate region requires detailed knowledge of both the weather and the structural parameters; hence, our simple model will be the least accurate in the region where the wind and stack infiltrations are equal.

RESULTS

Fifteen different sites were selected from the literature to represent wide variability in climate, house construction, and measured infiltration rates.[9-11] In all cases, leakage data obtained by fan pressurization was available, permitting us to calculate the effective leakage area. (Note that in Fig. 1. the effective leakage area varies by a factor of 16 from tightest to loosest.) The terrain class and the fraction of leakage in the floor and ceiling were estimated from the qualitative description of each site.

Appendix D contains tables providing data for each of the 15 sites; also included is the method of calculating effective leakage area. Figure 1 presents a bar graph showing the effective leakage area of each

site. For most of the sites, the data consists of several short-term infiltration measurements made on a single day. Most infiltration measurements were made using a tracer gas decay technique[4] which measured infiltration over a one-hour period with 5%-10% accuracy. For each measured infiltration point, a predicted infiltration was calculated from the weather variables and house parameters. Figures 2 and 3 contain the plots of predicted vs measured infiltration. Figure 4 displays the deviation of the predicted infiltration (by the percentage difference from the measurement) vs. the leakage area (cm^2) for that site.

DISCUSSION

Considering the simplicity of the model and the fact that there are no adjustable parameters,* the agreement is good. However, there are a few sites that do not show particularly good agreement; some overpredict and some underpredict. In order to explain these discrepancies, we examined other factors that may affect the infiltration.

The biggest single factor affecting the accuracy of our model is the assumption that directional effects are unimportant. Directional effects could become important if the leakage of the walls varies from wall to wall, or if the shielding varies from face to face — either of which is possible. Directional effects could be especially important for the data contained herein because all of the weather and infiltration data were short-term — decreasing the likelihood that the wind direction was random.

---

* We use "adjustable" to imply that there is no physical meaning associated with that parameter (e.g., regression coefficients). While physical parameters (e.g., R) may be estimated, they are not adjusted to improve the fit.

Aside from the directional dependence, nonuniformity of wall leakage area will cause a relative decrease in the actual wind-induced infiltration. For example, if one wall of a structure is much leakier than the rest, it will act like a wind trap; when the wind blows on that wall, the internal pressure will rise to mitigate the air flow through that face. Thus the wind-driven infiltration ought to be lower for nonuniform leakage than for uniform leakage. It is generally true that any directional effects will lower the infiltration — on the average (i.e., for some directions the infiltration may be increased by nonuniform leakage, but if wind direction is averaged the infiltration will be lowered).

Most likely, shielding will be the least uniform when it is the greatest, suggesting that directional effects should be more pronounced in more highly shielded situations. If we look at all of the Shielding Class 5 structures (2,8,13) we see a definite pattern of overprediction (19%,43%,19% respectively). While in no way conclusive, this may indicate that directional effects are significant for these structures.

Our model has also assumed that the floor and ceiling are unaffected by the wind. This assumption is violated whenever a leak through the floor or ceiling leads directly into the wind stream, such as occurs with a vent, chimney or flue. If the wind is blowing over the top of a flue, the infiltration will be greatly increased over what it would be otherwise. However, this effect is very directionally dependent because of the turbulence caused by the wind interacting with the roof structure. The effect will be largest when the flue has a large leakage area; thus we expect to see a large effect in structures that have undampered fireplace chimneys. Two of the test structures had undampered chimneys (10,14) and both showed significant underprediction (-16%, -22% respectively).

While the accuracy of the model is sufficient for a wide variety of applications, the shortcomings described above suggest ways in which accuracy can be improved. Not only can we include new parameters to account for local shielding, but we can extend the model to account for stack flows through vents and flues and for active systems (e.g.,

furnace fans), all of which may interact with natural ventilation.

Graphical Method

Some of the direct calculations (especially of the stack parameter) are difficult to do on a hand calculator in the field. We, therefore, have developed a graphical method of obtaining the neutral level, the stack parameter, and the infiltration from the data. Aside from the ease of operation, the graphical approach allows one to see the effects of different quantities directly — in a far clearer way than the bare equations provide.

Figure 4 presents a graph of the stack parameter (which is the reduced stack parameter without the $\sqrt{gH/T}$ term) vs the neutral level for several different values of the vertical leakage fraction, R. Note that the solid portion of each curve represents the physically allowed region; that is, for a given value of R, the neutral level can have only a limited range of values — it is for the case of R=1 alone that the neutral level can take on its full range from 0 to 1.

The neutral level is not the parameter that is usually measured, however; it is the ceiling-floor leakage difference, X, that is most often known. Accordingly, Figure 6 contains a plot of X versus neutral level, again for several values of R. These two curves can be parametrically combined to eliminate the neutral level yielding the relationship between the stack parameter and the ceiling-floor leakage difference; Figure 7 shows this function.

The fact that the reduced parameters do not depend on weather variables implies that there are just two (simple) degrees of freedom in the infiltration expression; that is, the only two variables that are time dependent in the superposition of infiltration are the wind and the temperature difference. Thus, we can use a graph of the wind vs temperature difference to find the total infiltration. Figure 8 is such a graph and the following paragraph describes how it is used.

Having found the stack parameter, we can find the reduced stack parameter by multiplying by $\sqrt{gH/T}$. From the terrain parameters and the shielding class, we can find the reduced wind parameter as well. These parameters are then combined with the weather variables (temperature difference and measured wind speed) to find a point on the graph. This point corresponds to a particular ratio of infiltration to total leakage area, as can be read from the curved lines of Figure 8. Finally, the ratio is multiplied by the total leakage area to find the infiltration. Since only the weather variables change over time, this method can be used repeatedly on a single site with a minimum of calculation.

FUTURE DIRECTIONS

The discussion of results indicated several areas in which the model might be improved Furthermore, some effects influencing certain structures might not have been apparent in our 15 sites -- for example, directional effects and unevenly distributed leakage, multichamber effects, vents, occupancy effects and linear leakage Accordingly, we will attempt to address some of these issues here.

Directional Effects

If, within a given period of observation, the wind direction is suitably random, the orientation of the building or unevenly distributed leakage will not affect infiltration. If, however, the wind comes from a restricted range of directions, the orientation of the structure and its leakage distribution can affect the infiltration. Similarly, directional differences in shielding will cause the infiltration to be directionally dependent. Conceptually, this situation can be handled by adding an additional factor to the reduced wind parameter; this factor would be a function of the wind direction and would contain information regarding the leakage distribution from wall to wall, as well as the effects of localized shielding. Furthermore, to preserve the current formalism, the angle average of this function would be unity. (Conceivably, this function could be subsumed into the generalized shielding coefficient.) Little more can be said about directional effects until more data has been taken. Theoretical work remains to be done on the effect of localized leakage from wall to wall and experimental work remains to be done on localized shielding of one wall as opposed to another.

Vents

In our analysis of infiltration we assumed that all of the significant air flow took place directly through the shell of the envelope; in most cases this is true, but in a large proportion of structures a

substantial amount of air flows through vents a significant fraction of the time. We define a vent to be any pathway that leads from the inside of the structure to the outside (e.g. chimney, exhaust vent, etc.). Vents may either be powered (by a fan or heat source) or unpowered, examples, of powered vents are furnace flues and exhaust vents with fans; unpowered vents would be chimneys or flues with no heat sources, or exhaust vents with no fan in operation.

Since powered vents have their own pressure source that is causing air flow, it is clear that they must be treated separately from the rest of the infiltration. Less obvious is the fact that unpowered vents must also be treated separately because vents generally "see" a different pressure across them than does the part of the envelope they pierce. For example, most flues and exhaust vents go through the ceiling of the structure and stick out above the roof; they are specifically designed to protrude into the free-stream wind and, hence, will experience a very different pressure from that of a (well-shielded) ceiling. (An unpowered vent that does not protrude away from the envelope (e.g., dryer vent) can be considered as a "hole" not a "vent" and thus treated in the standard model.

The flow through these vents is calculated by ignoring the presence of the wind and stack infiltrations and treating each vent independently. If the vent is powered by a fan, we can assume that the flow through the vent will simply be the fan rating. The problem becomes far more difficult if the vent is powered by a heat source (e.g., fireplace or furnace flue). Modera and Sherman[12] have derived a model of the flue flow using the leakage area of the flue, the leakage area of the structure, and the waste heat of the appliance. We derive the following cubic equation for the flow up the flue:

$$\left(1+\frac{A_{vent}^2}{A_o^2}\right) Q_{vent}^3 + \left(2+\frac{A_{vent}^2}{A_o^2}\right) Q_o\, Q_{vent}^2 + Q_o^2\, Q_{vent} = 2A_{vent}^2\, gh'\, Q_o \qquad (V.9)$$

where

Q_{vent} is the flow rate up the vent [m^3/s],

h' is the stack height (above the neutral level)[m],

A_o is the leakage area of the house (excluding vent) [m^2] and

A_{vent} is the leakage area of the vent [m^2].

Q_o is a function of the waste heat that goes up the stack:

$$Q_o = \frac{\Phi}{\rho \; C_p \; T} \qquad (V.10)$$

where

C_P is the specific heat of air [1000 joules/kg-K] and

Φ is the waste heat [watts].

Because this expression ignores the effect of the outside weather on the stack flow, we must evaluate the weather-driven case as well. As suggested earlier, a possible method for combining these two flows would be in quadrature.

If the vent is unpowered, the driving force, as in the standard model, is the weather, but we cannot use the same expressions. In this case, the pressure across the vent can be given by the following expression:

$$\Delta P = \tfrac{1}{2} \; \rho \; v^2 + \rho g h' \; \frac{\Delta T}{T} \qquad (V.11)$$

where

v is the velocity at the top of the stack [m/s],

h' is the height of the stack (above the neutral level)[m],

which leads to an expression for the flow through the vent:

$$Q_{vent} = A_{vent}\, v \sqrt{\left| 1 + \frac{2gh'}{v^2} \frac{\Delta T}{T} \right|} \qquad (V.12)$$

Unlike the standard infiltration model, this (unpowered) vent flow model is dependent on the sign of the temperature difference; in the winter the effects of the stack and wind terms are in the same direction, but in the summer the stack and wind effects act oppositely and, if the wind in low enough and the outside temperature high enough, the flow in the stack will reverse.

Because the stack can be assumed to stick up into the free-stream wind we can approximate the velocity by the velocity at roof height. The second term is strictly true only if it is warmer inside than out and if the stack can be assumed to be at indoor temperature. If the stack is at outside temperature, then h′ should be interpreted as being the difference between the neutral level and the bottom of the stack.

Once the individual flows from each of the vents have been calculated, it remains to combine them with each other and the stack and wind infiltration to find the total infiltration. We must separate the vent flow into balanced and unbalanced flows: vent flow is balanced if there is vent flow of the opposite direction that compensates for it; that is, if there is an exhaust vent it will be balanced only if there is an intake vent of the same air flow Balanced flow does not affect the interior pressure as does unbalanced flow which has no compensating airflow. Balanced flow will add simply to the total infiltration while unbalanced flow (like the stack and wind flows) will add in quadrature:

$$Q_{total} = Q_{balanced} + \sqrt{Q^2_{unbalanced} + Q^2_{wind} + Q^2_{stack}} \qquad (V.13)$$

The balanced and unbalanced flows can be expressed as follows:

$$Q_{balanced} = \mathrm{MIN}(\ \Sigma\ Q^{+}_{vent},\ \Sigma Q^{-}_{vent}\ ) \qquad (V.14.1)$$

$$Q_{unbalanced} = \mathrm{MAX}(\ \Sigma\ Q^{+}_{vent},\ \Sigma Q^{-}_{vent}\ ) - Q_{balanced} \qquad (V.14.2)$$

where

Q^{+}_{vent} is the vent infiltration [m^3/s] and

Q^{-}_{vent} is the vent exfiltration [m^3/s].

Generally speaking, vent infiltration will seldom be a factor, except when air-to-air heat exchangers are used. These heat exchangers run two streams of air -- one inside to out, the other outside to in -- and the heat from one is transferred to the other, supplying "preconditioned" fresh air to the structure This process is a perfect example of balanced vent flow; the two air streams balance each other and increase infiltration without changing the internal pressure.

Very little work has been done on the effect of vents on the total infiltration. The simple model of vents presented here may be adequate for determining the total infiltration, but only experimental tests can validate it.

Occupancy Effects

Occupancy effects are one of the hardest problems to deal with in constructing an infiltration model. Most other problems can be modeled, albeit with simplified models, but occupancy effects require a socio-physiological model of human comfort and behavior, which we are unable to present. Certain general features of occupancy effects can be enumerated; however: Door openings and closings can be modeled as a discrete amount of flow; window openings can be treated as an increase in the wall leakage area and, if the windows are distributed on different sides of the structure, they can be handled by the standard model. Fortunately, occupancy effects matter the most when infiltration matters the least — that is, occupants are most likely to open windows when the outside temperature is in the comfort range. Hence, the need for modeling infiltration at these times is minimal.

Multichamber Effects

In a large structure like an office building or an apartment building, the assumption of a single well-mixed interior zone breaks down. In this case it is not sufficient to calculate the total amount of outside air that infiltrates the structure; what is important is to be able to calculate how much fresh air gets into each chamber individually, and even how much air is exchanged between the chambers. In these structures, then, a multichamber model is needed.

Much work remains to be done before an acceptable multi-chamber model can be developed. As yet there exists no accurate method to measure the actual infiltration in the multichamber case, nor is there a method to measure the leakage between the chambers. Until these experimental problems have been solved, the existence of a multi-chamber model remains a moot point.

Linear Leakage

From the leakage measurements of the previous chapter we concluded that leakage can be best described by its square-root dependence on pressure that leads to the definition of the effective leakage area. This assumption appears to be borne out reasonably well by the data collected in this section. In some situations, however, square-root leakage dependence is insufficient and leakage must be described by a linear model. Because such a drastic change in the leakage model would require a complete reworking of the infiltration model, we have rederived the infiltration model in Appendix E under the assumption of linear leakage, but no attempt has been made to apply this model to any real situation. It remains to be seen whether such a model will ever be required, or whether the current infiltration model will be sufficient for all real cases.

REFERENCES

1. J.E. Jansen, "Calculating Infiltration: An Examination of Handbook Models," ASHRAE Trans.86:II (1980)

2. D.R. Bahnfleth, D.T. Moseley, and W.S. Harris, "Measurement of Infiltration in Two Residences," ASHRAE Trans., 63, 439-452, (1957).

3. J.B. Dick, and D.A. Thomas, "Ventilation Research in Occupied Houses," J. Inst. Heat. Vent. Eng., 19, 306-332, 1951.

4. N. Malik, "Field Studies of Dependence of Air Infiltration on Outside Temperature and Wind," Energy and Buildings, 1, 281-292, 1978.

5. D.T. Grimsrud, M.H. Sherman, R.C. Diamond, P.E. Condon, and A.H. Rosenfeld, "Infiltration-Pressurization Correlations: Detailed Measurements on a California House," ASHRAE Trans., 85, 1:851-865, (1979). LBL Report No. 7824 (1978)

6. R.E. Akins, J.A. Peterka, and J.E. Cermak, "Average Pressure Coefficients for Rectangular Buildings," Proceedings of the Fifth Int. Conf. Wind Engineering, Boulder, Colorado, July 1979.

7. European Convention for Constructional Steelwork, "Recommendations for the Calculation of Wind Effects on Buildings and Structures", Technical General Secretariat, Brussels, Belgium September 1978.

8. M.H. Sherman, D.T. Grimsrud, R.C. Diamond, "Infiltration-Pressurization Correlation: Surface Pressures and Terrain Effects," ASHRAE Trans. 85-II, (1979) Lawrence Berkeley Lab. Report No. 8785 (1979)

9. D.T. Grimsrud, M.H. Sherman, A.K. Blomsterberg, and A.H. Rosenfeld, "Infiltration and Air Leakage Comparisons: Conventional and Energy Efficient Housing Designs," Presented at the International

Conference on Energy Use Management, Los Angeles, October 1979. Lawrence Berkeley Laboratory Report LBL-9157 (1979)

10. Johns-Manville Research and Development Center, "Demonstration of Energy Conservation through Reduction of Air Infiltration in Electrically Heated Houses," RP 1351-1, (1979).

11. G.T. Tamura, "The Calculation of House Infiltration Rates," ASHRAE Trans, 85, Part 1 p. 58-71, (1979).

12. M.P. Modera and M.H. Sherman, "The Calculation of Air Flow through Fossil Fueled Fired Flues," Unpublished.

FIGURE CAPTIONS

FIG. V:1 The effective leakage area for each of the 15 measured sites.

FIG. V:2 The correlation of infiltration measured using a tracer gas technique and using the model presented in this report. Dashed lines represent raw measurement error limits. Only data under $150m^3/hr$ is shown.

FIG. V:3 The correlation of infiltration measured using a tracer gas technique and using the model presented in this report. Dashed lines represent raw measurement error limits. Only data over $100m^3/hr$ is shown.

FIG. V:4 The percentage disagreement between tracer measurements and predictive technique vs leakage area for each site. Solid points are individual measurements; open points with error bars represent site average. Composite for all sites is shown at right.

FIG. V:5 Plot the stack parameter versus neutral level.

FIG. V:6 Plot the neutral level versus the ceiling/floor leakage difference.

FIG. V:7 Plot the stack parameters versus the ceiling/floor leakage difference.

FIG. V:8 A graphical method for calculating infiltration from weather data.

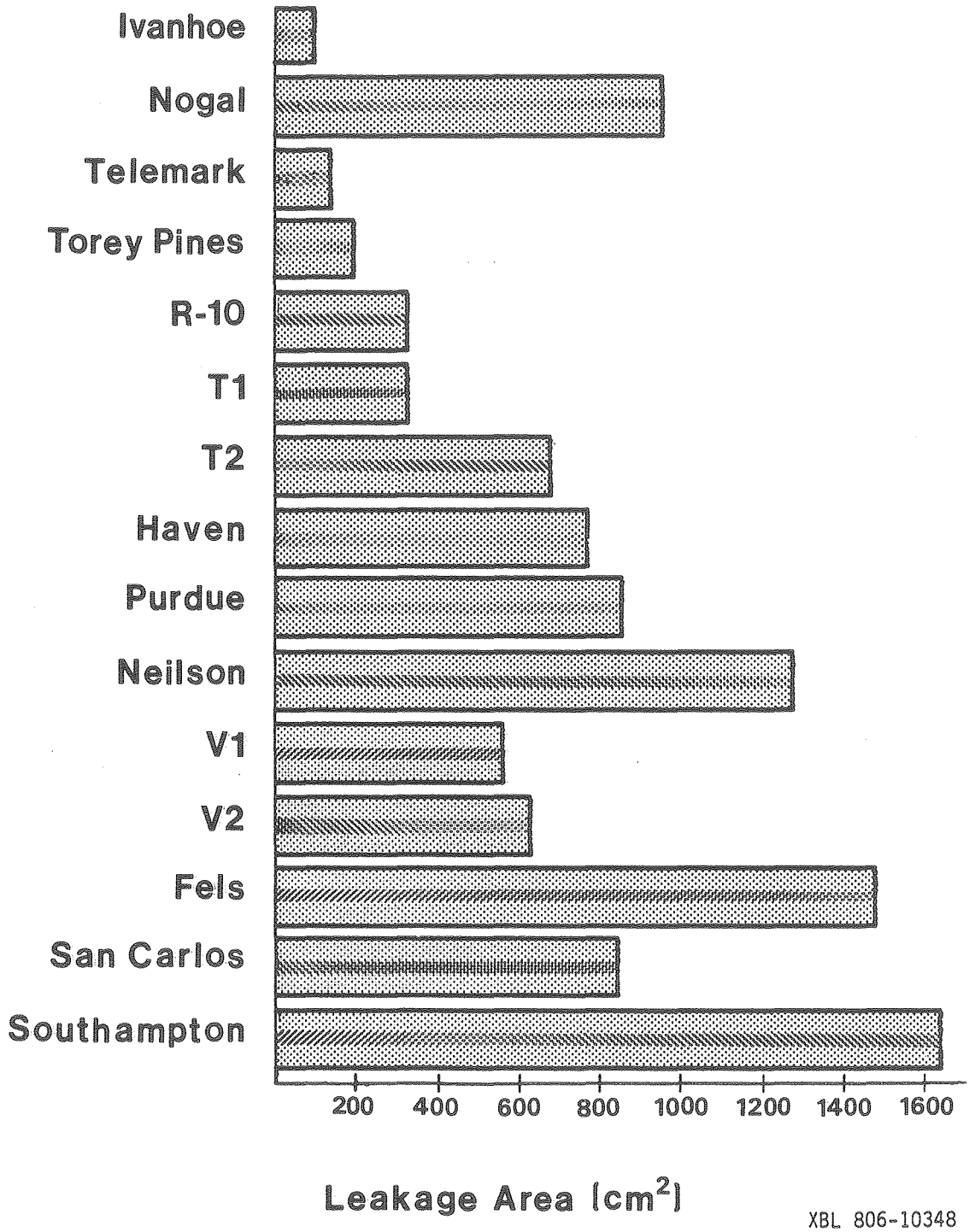

FIG. V:1 The effective leakage area of each of the 15 measured sites.

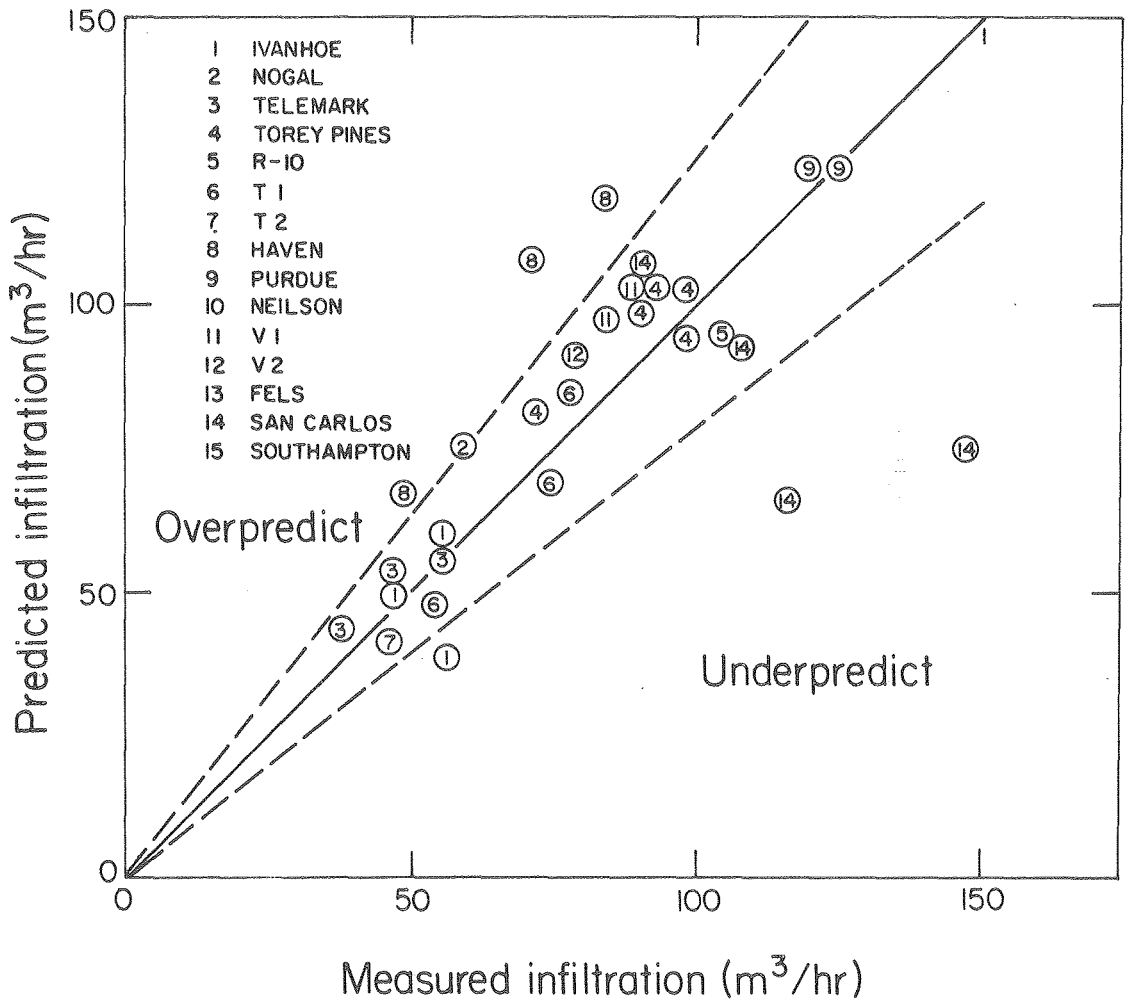

XBL 805-907

FIG. V:2 The correlation of infiltration measured using a tracer gas technique and using the model presented in this report.

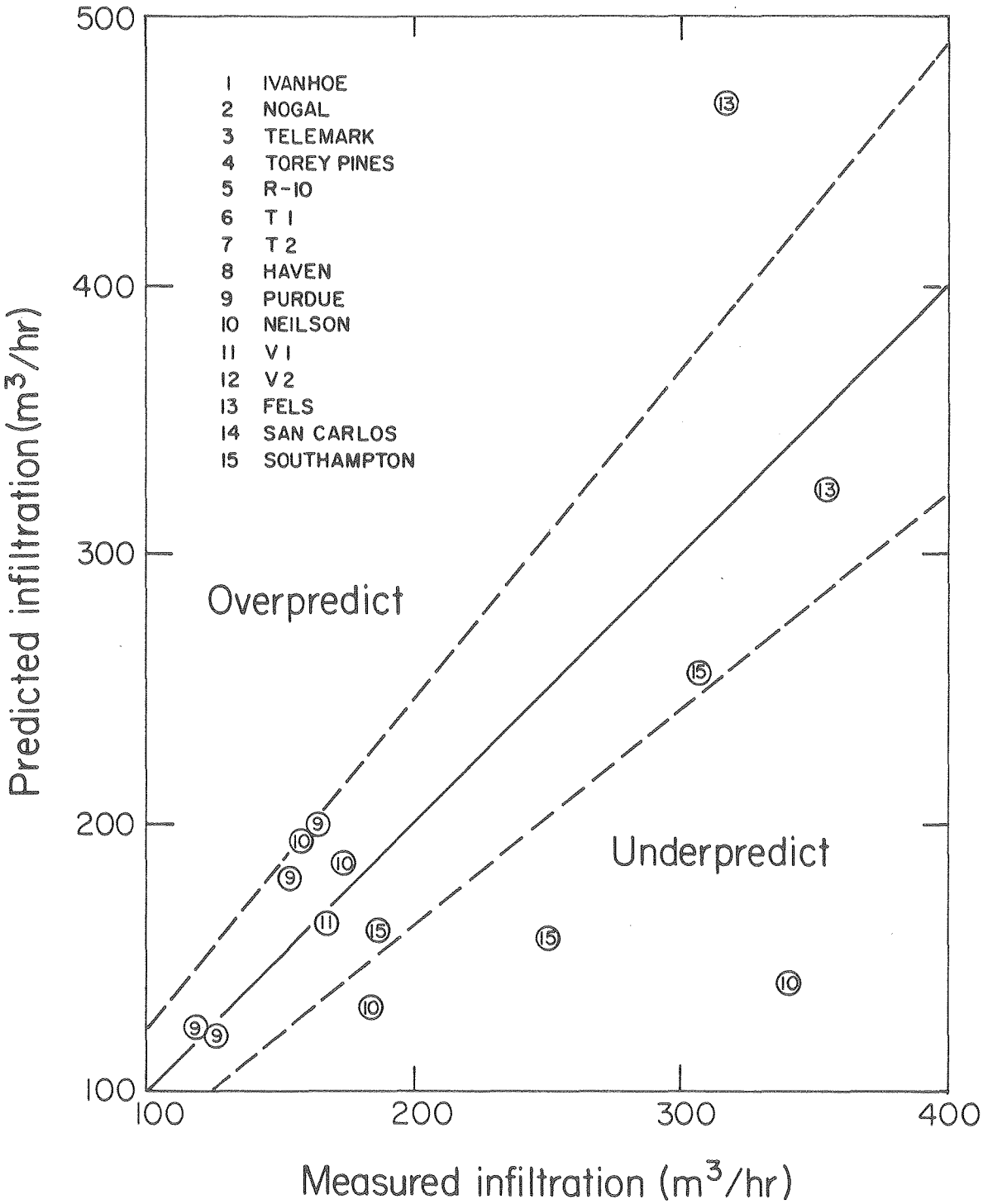

XBL 805-908

FIG. V:3 The correlation of infiltration measured using a tracer gas technique and using the model presented in this report.

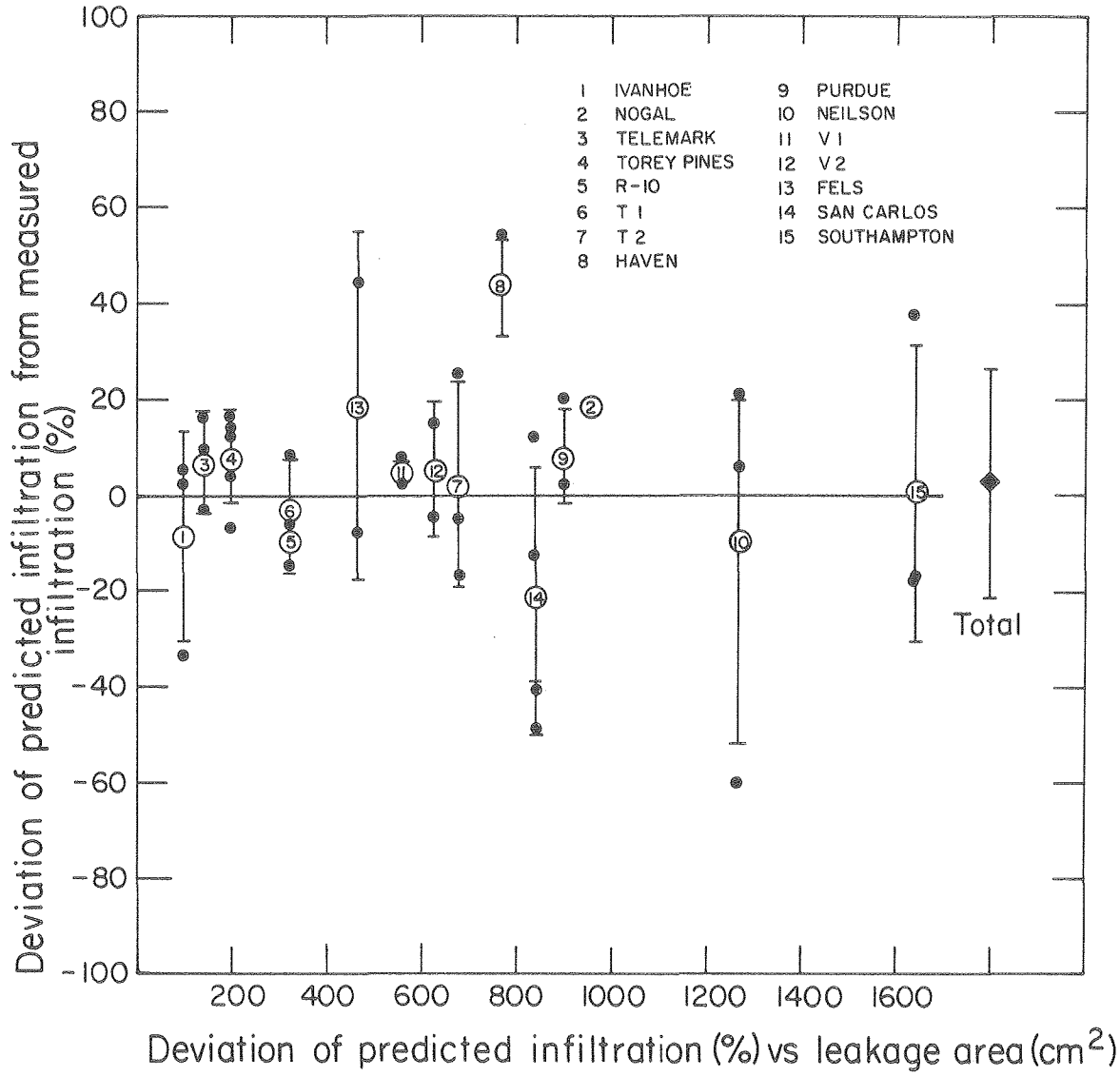

XBL 805-909

FIG. V:4 The percentage disagreement between tracer measurements and predictive technique vs leakage area for each site.

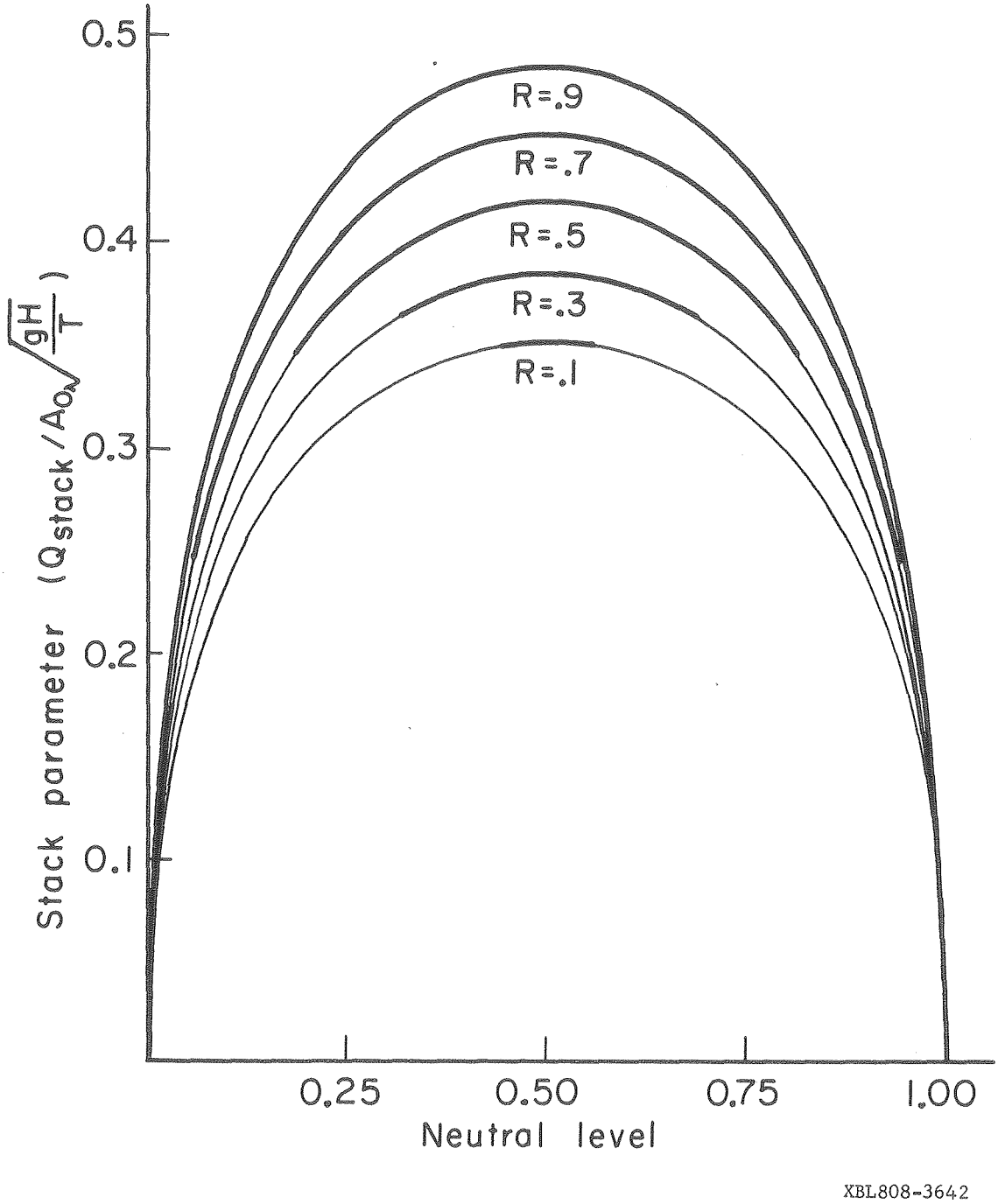

FIG. V:5 A graph of the stack parameter versus neutral level.

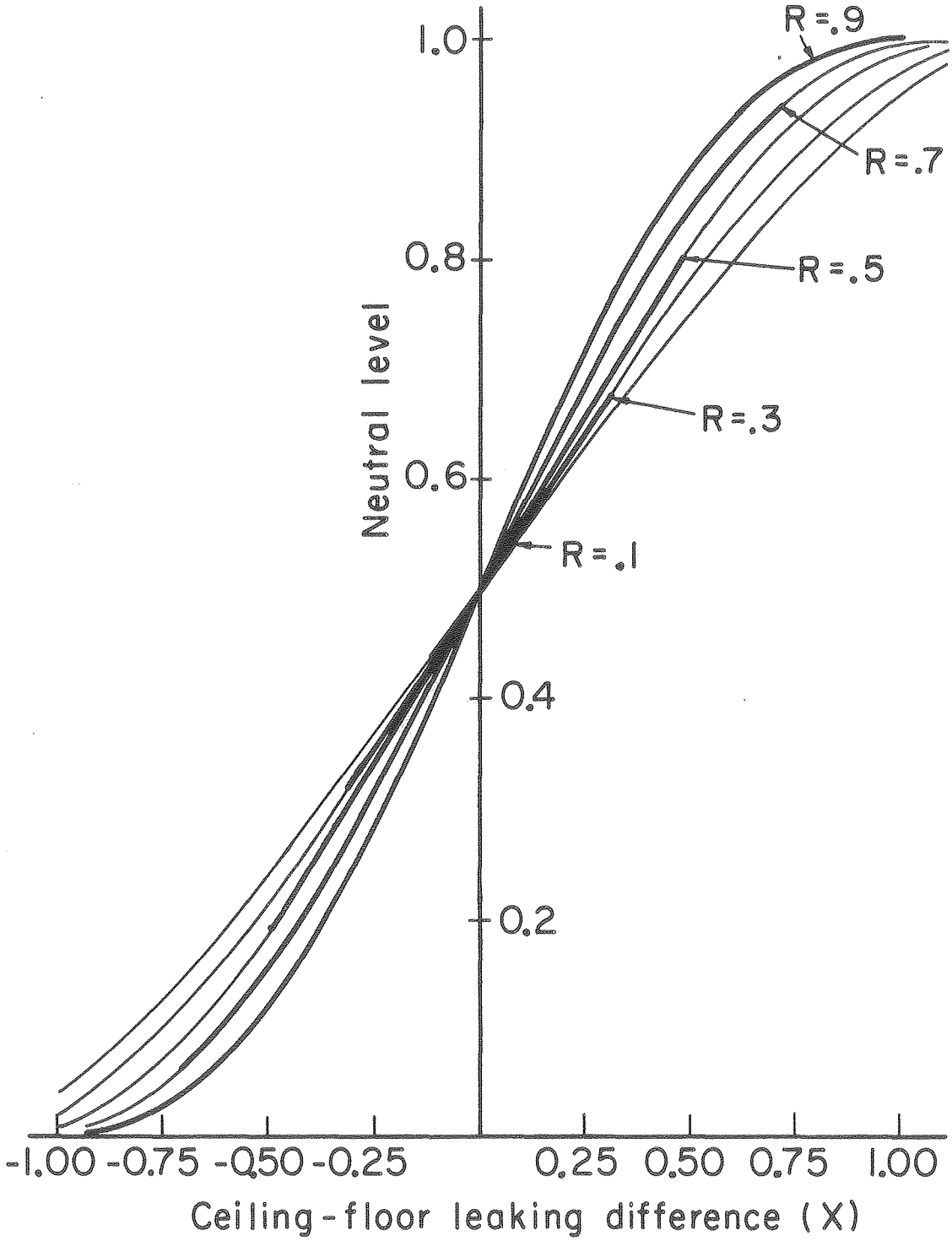

XBL808-3640

FIG. V:6 A graph of the neutral level versus the ceiling floor leakage difference.

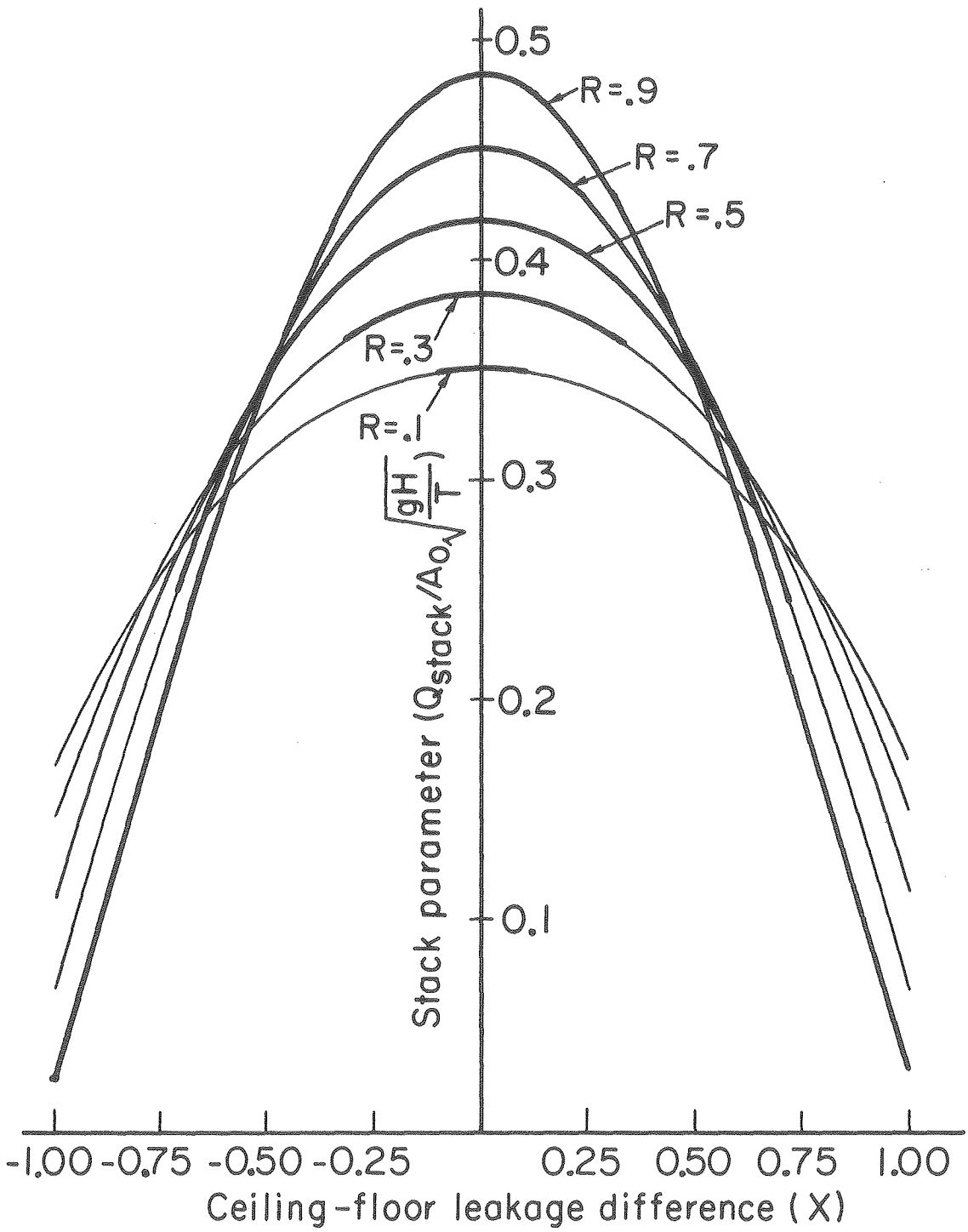

XBL808-3641

FIG. V:7 A graph of the stack parameters versus the ceiling floor leakage difference.

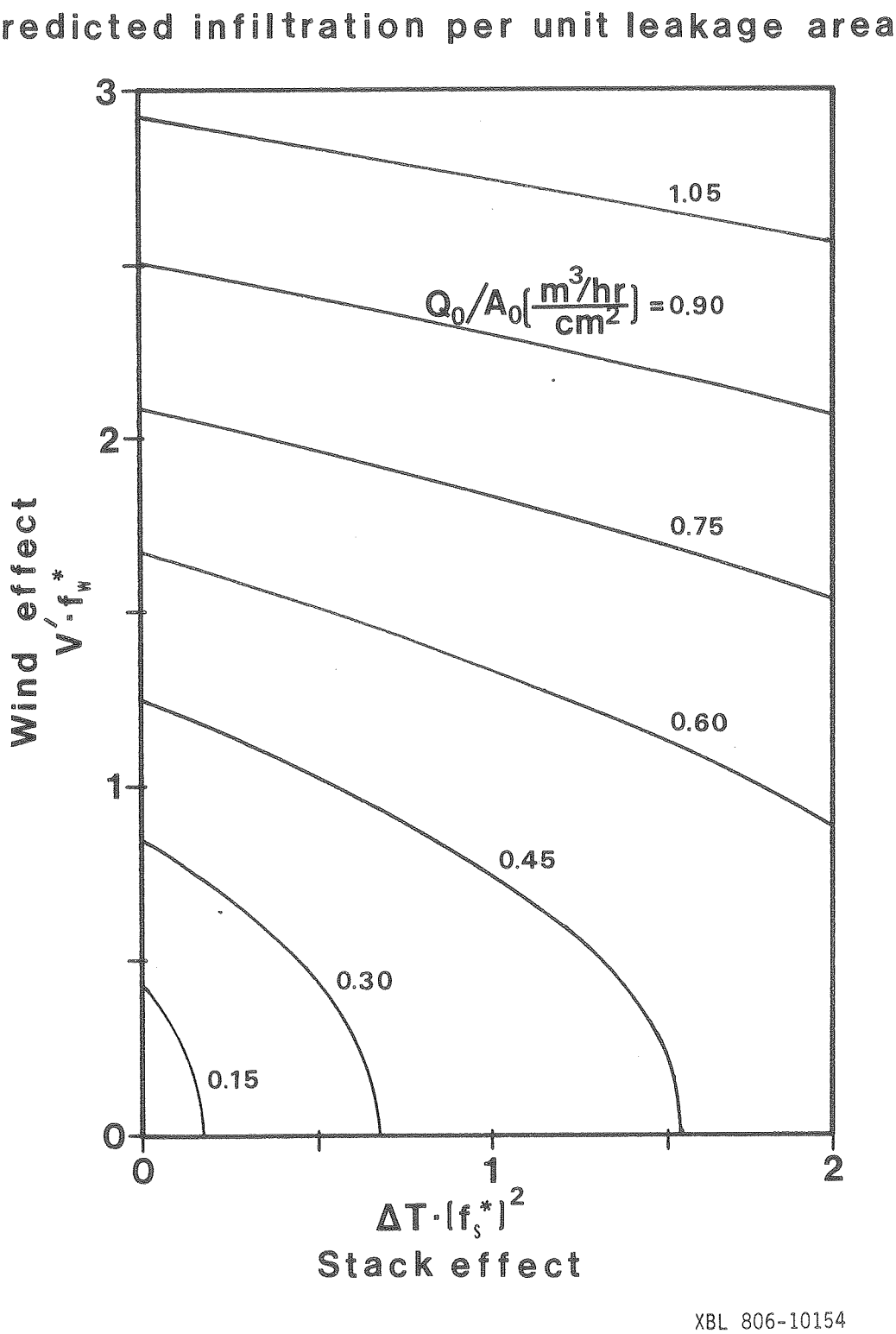

FIG. V:8 A graphical method for calculating infiltration from weather data.

CHAPTER VI
CONCLUSIONS

The focus of this work has been to develop a simple physical model of weather-driven infiltration in buildings. Such a model is needed to estimate energy loads both for structures, in the design stages and those in place. In already constructed buildings, we are also interested in being able to estimate the effect of retrofits in terms of their impact on infiltration. Not only is the prediction of infiltration necessary for calculating energy loads but also for assesing indoor air quality. For purposes of assesing indoor air quality, it is necessary to know both the minimum infiltration rate (to evaluate the effects of short-term health hazards from such chemicals as carbon monoxide) and the average infiltration rate (to evaluate the effects of long-term health hazards generated by substances such as radon).

Neither of these purposes require a highly accurate estimate of the infiltration, but both demand that the effect of changes in the weather and the leakage character of the envelope be accurately reflected in the estimate. Furthermore, the model must be versatile enough and general enough to adequately predict infiltration in the wide variety of construction styles and climatic conditions that exist within the country. Finally, to be fully useful such a model should be usable by on-site workers; therefore, it must be simple enough to be put on a hand-calculator, for example and, ideally, the back of an envelope.

The model presented in the preceding chapters meets most, if not all, of these requirements: it is general (requires leakage area(s), geometry of site and weather variables only); it is versatile (since it calculates instantaneous infiltration, it can be used for both long-term and short-term predictions as well as design load limits); and it is simple (it can be done on a hand calculator or graphically). The question of its accuracy can best be answered by examining the predicted vs measured infiltration data presented in Appendix D. Assuming that data to be representative, the overall accuracy of the model is roughly ±25% — remarkably good considering that the uncertainties associated with the field measurements (leakage area, wind speed, temperature difference) combined with the direct infiltration measurement comprise most

of this difference.

In effect our model makes the measurement of infiltration interchangeable with a measurement of leakage area. That is, a single measurement of the leakage area can be combined with the weather variables and our model to predict the infiltration at any time. Similarly, a single measurement of infiltration and the weather variables can be combined in our model to estimate the leakage area of the the structure, which in turn can be used to find the future infiltration. Thus, even though the concept of leakage area in essential to our model of infiltration, it is possible to use the model without ever directly measuring the leakage.

In the process of developing this model, a considerable amount of intermediate modeling and instrumentation design was necessary. Much of this work is both interesting and useful in its own right and will be summarized briefly below.

A careful (multichamber) derivation of the continuity equation reveals the sources of many problems experienced by other investigations working in the area of infiltration measurement, and suggests effective techniques. What becomes evident, for example, is that different types of measurement techniques are required for different circumstances — the simple tracer decay method for measuring infiltration while very popular, is not the best choice in most situations.

In the course of our experimentation, we developed a Continuous Infiltration Monitoring System (CIMS) which is useful for accurately measuring the infiltration on a continuous basis. Furthermore, because it calculates the effective volume of the structure, it is useful for evaluating internal mixing problems. This system is currently in use in several applications: ventilation and indoor air quality measurements[1,2] as well as passive solar applications. A simplified version of this system (using stepwise constant flow) is being used as part of a technique developed at LBL called "Electric Co-heating"[3] which provides for instantaneous monitoring of heat load due to infiltration

The other major innovation that we are developing in infiltration measurement is a system for Average Infiltration Monitoring (AIM). This system is a portable, inexpensive method of measuring the average infiltration in a structure for periods up to several weeks. This measurement technique is ideally suited to answer one of the simplest, yet still unanswered questions about infiltration — what are average infiltration rates in the U.S. housing stock.

Perhaps the most exciting and unexpected discovery to come from this research was the technique of "AC pressurization". AC pressurization allows precise measurement of the leakage function (or, equivalently, the leakage area) of a structure down to very low pressures (<1 Pa) with a degree of accuracy never attained before by whole building leakage measurements. From a research standpoint this technique open a whole new realm of investigation specific to the important parameters of the leakage characteristics of the building envelope; specifically, accurate leakage measurements combined with a model of fluid flow through pipes (See Chapter III) can yield substantial information about the size and distribution of leaks.

AC pressurization has already yielded benefits in that it has confirmed the hypothesis that low pressure leakage is not dominated by steady laminar flow but, rather, can be treated as having a square-root dependence on pressure. This finding allows the meaningful definition of the leakage area as the parameter that quantifies leakage.

RESEARCH DIRECTIONS

The work contained in this paper is in no sense complete; there remains much to do in the study of infiltration. Large scale field testing is needed both to validate measurement techniques (e.g. AIM) and infiltration models, as well as to catalog leakage areas and infiltration rates in the existing housing stock. Further developmental research is needed on projects such as AC pressurization and multichamber infiltration, before such techniques can be used for extensive field measurements.

Model Validation and Extension

The model, as it stands, needs wide-scale field validation to expose its strengths and its weaknesses. All of the validation involved the use of short-term data; even though short-term validation is a stronger test than long-term validation, long-term tests should be done to separate that part of the disagreement which is random from that part which is systematic. Structures of different leakage areas and exposures should be tested; the relative importance of stack vs. wind driven infiltration should be measured.

The shielding values used in our model were condensed from wind-tunnel data on model structures. In a wind tunnel the effect of terrain on the vertical wind profile can be reproduced (this is called a boundary-layer wind-tunnel) but, the effect of obstacles in the near-field around the structure cannot. Thus, wind-tunnel studies can only yield the shielding coefficients for a structure that has no local obstructions around it — this is our shielding class I. To account for the effects of local obstructions we developed a qualitative classification scheme analogous to the classification scheme used to describe terrain effects. As yet there is no direct experimental evidence linking our qualitative classification scheme to any physically measurable parameters (e.g. blockage per unit solid angle, etc.); accordingly, effort should be expended to define shielding coefficients that contain more physical information. In addition, the effect of unevenly distributed leakage and the directional dependence of the wind should be investigated, as should the effect of vents and chimneys on the internal pressure of the structure.

In order to answer the questions posed in these paragraphs we have constructed a Mobile Infiltration Test Unit (MITU). This unit is an 8′x16′ trailer that has been fully instrumented to measure and record the following quantities: continuous infiltration (using CIMS), the surface pressures around the structure, the wind speed at 10m and the temperature profile both inside and outside the structure. Furthermore, the envelope of MITU has been made very tight so that there are virtually no leaks, except in replaceable leakage panels that cover the

shell. These panels are precalibrated with a certain leakage area and can be changed in just a few minutes. This feature allows us to vary both the absolute amount of leakage and the relative distribution from wall to wall or from top to bottom.

The MITU trailer is portable and can be towed to virtually any climatic region we chose. The trailer is light enough to be rotated by hand if we wish to change the orientation of MITU with respect to a prevailing wind.

Multichamber Models

Throughout this work the multichamber problem has been mentioned repeatedly; it is one of the most difficult but potentially important aspects of infiltration. Any time the building of interest must be broken up into multiple interconnected sub-volumes (instead of being treated as a single well-mixed volume) a multichamber analysis is necessary. In single-family residences or low-rise commercial buildings the multichamber effect is usually not important but in multifamily or high-rise commercial buildings, multichamber effects can dominate.

To extend the model presented here to include multichamber effects requires that direct techniques for measuring multichamber infiltration and techniques for measuring multichamber leakage also be developed. Multichamber leakage measurements would yield the effective leakage area between each chamber and every other chamber (including the outside). Because of fan capacity limitations and low signal-to-noise ratio, it is almost impossible to measure such multichamber leakage using conventional DC pressurization techniques. It may be possible, however, to make such measurements using AC pressurization techniques.

Even if the experimental hurdles of measuring these two quantities are surmounted, there still remains to develop a model that can use the leakage data to calculate airflows from one chamber to another. This type of model is a network model that is quite similar to some of the detailed models used in the U.K. Obviously, such a model will be more complicated than the single-chamber model we have presented.

REFERENCES

1. C.D Hollowell, J.V. Berk, M.L. Boegel, R.R. Miksch, W.W. Nazaroff, G.W. Traynor, "Building Ventilation and Indoor Air Quality," Lawrence Berkeley Laboratory Report LBL-10391 (1980)

2. J.V. Berk, C.D. Hollowell, C.D. Lin, J.H. Pepper, "Design of a Mobile Laboratory for Ventilation Studies and Indoor Air Pollution Monitoring," Lawrence Berkeley Laboratory Report LBL-7817 (1978)

3. R.C. Sonderegger, P.E. Condon, M.P. Modera, "In-situ Measurements of Residential Energy Performance Using Electric Co-heating," ASHRAE Trans. 85-II (1980); Lawrence Berkeley Laboratory Report LBL-10117 (1980).

APPENDIX A

EQUATIONS GOVERNING INFILTRATION MEASUREMENTS

In this Appendix the equations governing infiltration, as measured by tracer-gas techniques, will be derived for the most general case. Such a general derivation has the advantage of explicitly stating the assumptions as they occur and allowing the possibility of changing those assumptions. The ramifications of violating some of these assumptions are also considered.

DERIVATION

We are treating the problem of the dilution of a tracer gas as an analygon to air infiltration. That is, we dope the air with a tracer gas and measure the airflow by following the concentration of tracer gas over time.

Consider the Universe to be divided into several mutually interconnecting volumes: one infinite volume, and N finite ones. We designate the infinite volume as chamber 0 and the finite ones as chambers 1 through N. The finite volumes may represent different rooms in a structure, and the infinite volume the "outside".

The fundamental equation that governs the movement of the gas is the continuity equation:

$$\nabla \cdot \bar{J} + \frac{d\tilde{n}}{dt} = \tilde{f} \qquad \text{(A.1)}$$

where

$\bar{J}$	is the flux vector of the tracer gas [moles/s/m^2]
∇	is the gradient operator [m^{-1}],
$\tilde{n}$	is the density of tracer gas [moles/m^3] and
$\tilde{f}$	is the tracer injection density [moles/s/m^3].

We now integrate this over the volume of a particular chamber:

$$\int_{V_j} \nabla\cdot\bar{J}\, d^3x_j + \int_{V_j} \frac{d\tilde{n}}{dt}\, d^3x_j = \int_{V_j} \tilde{f}\, d^3x_j \qquad j=0\cdots N \qquad (A.2)$$

where

V_j is the volume of the jth chamber [m^3].

Using Green's theorem on the first term yields

$$\int_{V_j} \nabla\cdot\bar{J}\, d^3x_j = \sum_{k=0}^{N} \int_{S_{jk}} \bar{J}\cdot d^2\underline{s}_{jk} \qquad j=0\cdots N \qquad (A.3)$$

where

S_{jk} is the surface between the jth chamber and the kth chamber [m^2].

This surface integral has two parts to it: the flow of tracer from chamber j to chamber k and the flow of tracer from chamber k to chamber j:

$$\int_{S_{jk}} \bar{J}\cdot d^2\underline{s}_{jk} = q_{jk} - q_{kj} \qquad (A.4)$$

where

q_{jk} is the tracer flow from the jth chamber to the kth chamber [moles/s].

The remaining two terms integrate easily:

$$\int_{V_j} \frac{d\tilde{n}}{dt}\, d^3x_j = \dot{n}_j \qquad (A.5.1)$$

$$\int_{V_j} \tilde{f}\, d^3x_j = f_j \qquad (A.5.2)$$

where

$\dot{n}_j$ is the jth chamber tracer exfiltration [moles/s] and

f_j is the flow injected into the jth chamber [moles/s].

Combining these results yields a fully integrated expression for the conservation of tracer in each room:

$$\dot{n}_j + \sum_{k=0}^{N} \left(q_{jk} - q_{kj} \right) = f_j \tag{A.6}$$

This expression describes the flow of tracer from one chamber to another; we are, however, attempting to use a tracer gas to approximate the flow of air from one chamber to another. Accordingly, we must define the connection between the flow of tracer from one chamber to another and the flow of air from one chamber to another. We assume that the flow of air is proportional to the flow of tracer and that the constant of proportionality is the concentration:

$$C_j = \frac{\tilde{n}_j}{\tilde{n}_o} \tag{A.7}$$

where

C_j is the average concentration in the jth chamber and

$\tilde{n}_j$ is the density of tracer in the jth chamber [moles/m^3] and

$\tilde{n}_o$ is the density of an ideal gas [moles/m^3].

Simultaneously, we will change from units of moles to units of volume (m^3) to agree with conventional presentations:

$$F_j = \frac{f_j}{\tilde{n}_o} \tag{A.8}$$

and

$$\dot{n}_j = \tilde{n}_o \, V_j \, \dot{C}_j \tag{A.9}$$

where

F_j is the volumetric injection rate [m^3/s] and

V_j is the volume of the jth chamber [m^3].

Our model for the air flow then becomes,

$$Q_{jk} = -\frac{q_{kj}\ C_k}{\tilde{n}_o} \qquad (A.10)$$

where

Q_{jk} is the negative of the air flow to j from k [m^3/hr].

Putting these all together we can rewrite the continuity expression cancelling the density of an ideal gas:

$$V_j\ \dot{C}_j + \sum_{k=0}^{N} \left\{ Q_{jk}\ C_k - Q_{kj}\ C_j \right\} = F_j \qquad j=0 \cdots N \qquad (A.11)$$

Rewriting the sum to factor out constant terms yields:

$$V_j\ \dot{C}_j + \sum_{k=0}^{N} Q_{jk}\ C_k - C_j \sum_{k=0}^{N} Q_{kj} = F_j \qquad j=0 \cdots N \qquad (A.12)$$

So far we have not defined the diagonal term Q_{jj}; however, the expression above suggests a convenient definition for it:

$$Q_{jj} = \sum_{k=0}^{N} - Q_{kj} \qquad j=0 \cdots N \qquad (A.13)$$

Thus the diagonal term represents the total exfiltration from that chamber. Using this definition,

$$V_j\ \dot{C}_j + \sum_{k=0}^{N} Q_{jk}\ C_k = F_j \qquad j=0 \cdots N \qquad (A.14)$$

In general the concentration of tracer gas will be zero in (the infinite volume of) chamber 0. Hence the sum in the above equation need not start at zero but can start at one:

$$V_j\ \dot{C}_j + \sum_{k=1}^{N} Q_{jk}\ C_k = F_j \qquad j=1 \cdots N \qquad (A.15)$$

Note that this elimination of a chamber is equivalent to defining the concentration of the outside to be the origin of the concentration

measurements and is only valid if the outside concentration is constant.

Because the volume of the zeroth chamber is infinite, the equation for j=0 (i.e. the outside) contains no information. Therefore, we must invoke the continuity equation for air to make up the missing information.

If we assume that air is an incompressible fluid, the total air flowing into a chamber must be equal to the air flowing out of the chamber:

$$\sum_{k=0}^{N} Q_{kj} = 0 \qquad j=0 \cdots N \tag{A.16.1}$$

as well as

$$\sum_{k=0}^{N} Q_{jk} = 0 \qquad j=0 \cdots N \tag{A.16.2}$$

Therefore, if we restrict the range of chambers so as to exclude the outside, we can recover the information from the sum of the other terms:

$$- Q_{0j} = \sum_{k=1}^{N} Q_{kj} \qquad j=1 \cdots N \tag{A.17.1}$$

$$- Q_{j0} = \sum_{k=1}^{N} Q_{jk} \qquad j=1 \cdots N \tag{A.17.2}$$

and finally,

$$- Q_{00} = \sum_{k=1}^{N} \sum_{j=1}^{N} Q_{jk} \tag{A.17.3}$$

Thus all information about the air flow is retained.

Matrix Notation

The appearance of the tracer continuity equation suggests that it can be put in the form of a matrix equation; however, the term involving the volume is not in the correct form. We must, therefore, define a

volume matrix to put the equation in the correct form:

$$V_{kj} = V_k \, \delta_{kj} \tag{A.18}$$

where

δ_{kj} is the Kronecker delta function.*

Now the continuity equation becomes,

$$\bar{\bar{V}} \cdot \frac{d\bar{C}}{dt} + \bar{\bar{Q}} \cdot \bar{C} = \bar{F} \tag{A.19}$$

where

$\bar{\bar{V}}$, $\bar{\bar{Q}}$ are two-dimensional matrices and

$\bar{C}$, $\bar{F}$ are vectors (one-dimensional matrices).

This notation offers great simplicity in expression, and we will use it whenever possible.

MIXING

Built into the preceding derivation are several assumptions which could easily be violated in any real situation. In general, these violations come under the heading of mixing problems. Virtually all of the mixing problems come from violations of two of the assumptions in the preceding derivation:

1) The measured concentration is equal to the average concentration. This is equivalent to assuming that the volume participating in air exchange with other chambers and the outside is equal to the physical volume of the chamber.

---

* The Kronecker delta is equal to 1 if k=j, and is equal to zero if k≠j.

2) The gas flow is proportional to the average concentration. This is equivalent to assuming that each chamber is well mixed or, equivalently, that the concentration of tracer gas is the same everywhere in a chamber.

If there are parts of a chamber that participate in air exchange with other chambers but have significantly different concentrations from the rest of the chamber, then more chambers must be added to the analysis to accurately measure the air flows. For example, one might consider a house to be a single-chamber but, if some of the rooms are much leakier than the body of the house, the concentration in those rooms will be much lower and, in a multichamber analysis, they must be considered as separate chambers.

The volume of a chamber that does participate in air exchange is not easy to quantify. If there are regions of a chamber that do not communicate at all with that chamber, the effective volume will be smaller than the physical volume of the chamber. For example, closets and cabinets may not communicate with the rest of a room; stratification may create a layer of air near the ceiling that does not mix with the rest of the air, etc. It is even possible for the effective volume of the chamber to be larger than the physical volume; if, for example, it communicates with an otherwise unconditioned space (e.g. basement, attic), some of the volume of the unconditioned space could participate in the exchange. Therefore, we should interpret the volume that appears in the expressions to be the effective volume and not the physical volume. A measurement of the effective volume should be made to minimize errors.

A final problem comes from the fact that the tracer gas is usually injected into a limited number of places in each chamber. Thus, while the average concentration in the chamber goes up instantaneously, the measured increase in concentration will be delayed; furthermore, the effect on tracer flow out of that chamber will be delayed as well. We can model this effect by defining an effective flow that incorporates this delay in it:

$$F_j^{eff}(t) = \int_0^{\infty} g(t' \; ; \; t_j^m, \; t_j^d) \; F(t - t') \; dt' \tag{A.20}$$

where

F^{eff} is the effective flow [m^3/hr],

g is the mixing function,

t^m is the rise time [hr] and

t^d is the delay time [hr]

In this equation there are actually two mixing times: one of them is a simple delay, the other is a smoothing time. Even after the delay time, the effective flow will not jump discontinuously up to its final value but, rather, will approach it asymptotically; thus, this second time constant controls the rise time of the effective flow.

Figure 1 shows a typical response of the room concentration to a step function in flow. If there were perfect mixing, the increase in concentration would follow the flow (i.e. it would be a step function); however, when the mixing is not perfect, the rise in concentration lags behind the flow. The rise-time of the concentration is another characteristic of the mixing time, and may be called the circulation time. Figure 1 also shows the approximate (normalized) mixing function for the measured site.

Another effect caused by the localized injection of tracer gas is that the injected gas may leave the chamber in which it is injected without mixing. This effect is called "short-circuiting" because of the way the flow bypasses the chamber that it starts in. Short-circuiting occurs when flow injected into one chamber does not mix with the air in that chamber but, rather, flows directly into another chamber and adds to the concentration in that chamber. For example, if a small air current were to blow some of the injected tracer into an adjacent room, or if there were a leak in the tracer distribution system that allowed the gas to appear in one chamber when it was attributed to another, we would describe these occurrences as short-circuiting.

Since the effect of short-circuiting is to increase the concentration in one chamber caused by flow in another, it will appear as an off-diagonal element in both the infiltration matrix and the volume matrix. Additional off-diagonal elements appearing in the infiltration matrix are difficult to detect; however, since there are no off-diagonal elements in the volume matrix without short-circuiting, the appearance of any off-diagonal elements in the volume matrix can be attributed to short-circuiting. This fact can be used to find the amount of short-circuiting and, if the volume matrix is measured, correct for it. Because short-circuiting of a measured flow rate is equivalent to injecting a different flow without short-circuiting, we can define an apparent flow rate from the physical flow and a quantity called the short-circuiting matrix:

$$\overline{F}' = \overline{\overline{S}} \cdot \overline{F} \tag{A.21}$$

where

$\overline{F}'$ is the apparent flow [m^3/s],

$\overline{\overline{S}}$ is the short-circuiting matrix and

$\overline{F}$ is the physically injected flow.

If we assume that the mixing function discussed in the previous paragraphs has already been taken into account, we can rewrite the continuity equation in terms of the apparent flow:

$$\overline{\overline{V}} \frac{d\overline{C}}{dt} + \overline{\overline{Q}}\ \overline{C} = \overline{F}' \tag{A.22}$$

Because the S matrix is as yet undetermined, the apparent flow is unknown; however, we can use the effective volume matrix to find the values of the short-circuiting matrix. To do this, we multiply the equation from the left by the inverse of the S matrix (assuming, of course, that the S matrix is not singular). Substituting in the definition of the apparent flow matrix yields,

$$\bar{\bar{S}}^{-1} \cdot \bar{\bar{V}} \frac{d\bar{C}}{dt} + \bar{\bar{S}}^{-1} \cdot \bar{\bar{Q}}\ \bar{C} = \bar{F} \tag{A.23}$$

We can now define the apparent volume matrix and the apparent infiltration matrix in terms of these quantities:

$$\bar{\bar{V}}' = \bar{\bar{S}}^{-1} \cdot \bar{\bar{V}} \tag{A.24.1}$$

$$\bar{\bar{V}} = \bar{\bar{S}} \cdot \bar{\bar{V}}' \tag{A.24.2}$$

$$\bar{\bar{Q}}' = \bar{\bar{S}}^{-1} \cdot \bar{\bar{Q}} \tag{A.25.1}$$

$$\bar{\bar{Q}} = \bar{\bar{S}} \cdot \bar{\bar{V}}' \tag{A.25.2}$$

which yields

$$\bar{\bar{V}}'\ \frac{d\bar{C}}{dt} + \bar{\bar{Q}}'\ \bar{C} = \bar{F} \tag{A.26}$$

<u>where</u>

$\bar{\bar{V}}'$ is the apparent volume matrix [m^3] and

$\bar{\bar{Q}}'$ is the apparent infiltration matrix [m^3/s].

In a real experiment, then, it is the apparent volume and infiltration matrices that are measured, not the physical one; it is, however, the physical matrices that are of interest. Accordingly, we must be able to find the S matrix in order to calculate the physical quantities. We can use the fact that the off-diagonal elements of the physical volume matrix are zero to determine something about the short-circuiting matrix

$$\left(\bar{\bar{S}} \cdot \bar{\bar{V}} \right)_{ij} = 0 \qquad i \neq j \tag{A.27}$$

which is, in fact, a set of N^2-N equations in N^2 unknowns:

$$\sum_{i=1}^{N} S_{ki} V'_{ij} = 0 \qquad k \neq j \tag{A.28.1}$$

This set of equations alone is not sufficient to determine the S matrix. To find missing N equations, we must make use of the fact that the total amount of tracer injected is the same regardless of any short-circuiting (i.e. the S matrix is normalized):

$$\sum_{k=1}^{N} S_{jk} = 1 \qquad j=1 \cdots N \tag{A.29}$$

This choice of normalization implicitly assumes that none of the injected tracer gas short-circuits to the outside. If it does, independent information regarding the effective volume of each chamber must be supplied. The diagonal elements of the physical volume matrix are equal to the effective volume of each chamber:

$$\left(\bar{\bar{S}} \cdot \bar{\bar{V}}' \right)_{jj} = V_j \tag{A.30}$$

Thus the missing N equations can be found from the (measured) apparent volume matrix and the (measured) effective volumes of each chamber.

Mixing problems of any sort (e.g. effective volume, mixing function or short-circuiting) can affect the direct determination of the infiltration, but the degree of trouble that mixing problems can cause is directly determined by the technique used to measure infiltration. For example, the effective volume/physical volume question has no effect on a constant concentration experiment, the mixing function has no bearing on a constant flow experiment, and short-circuiting plays no part in a single-chamber experiment.

APPENDIX B

AC PRESSURIZATION

The concept of AC pressurization was first presented by the author (see reference 1).[1] The only similar work was done by Card, et al[2] but that work was not successful. In this Appendix we shall derive the basic equations necessary for the analysis of our AC pressurization technique and then go on to describe the experimental technique and the results derived there from.

In the first part of this appendix, we shall derive the relations governing the interactions among a changing volume, the leakage through the envelope, and the change in internal pressure, which are necessary to interpret the data collected by the AC technique.

AIR FLOW

We begin the derivation by assuming the gas within the structure to be ideal, that is,

$$PV = nRT \tag{B.1}$$

where

P	is the absolute pressure [Pa],
V	is the structure volume [m^3],
n	is the number of moles of gas,
R	is the ideal gas constant (8.32 joules/mole-^oK) and
T	is the absolute temperature [^oK].

Conservation of energy for an ideal gas yields,

$$RT\ dn = P\ dV + C_v dT \tag{B.2}$$

where

C_v is the heat capacity of air at constant volume [joules/mole-^oK].

Using Eq. B1 to eliminate dT,

$$RT\ dn = PdV + \frac{1}{\gamma} VdP \qquad (B.3)$$

where

γ is the ratio of the heat capacities of air (1.4).

The leakage of air through the envelope is related to the time derivative of the number of moles of gas in the structure. We can use these definitions to eliminate the number of moles of gas from the expression for the air flow.

$$Q = -\frac{V}{n}\frac{dn}{dt} \qquad (B.4.1)$$

$$= -\frac{RT}{P}\frac{dn}{dt} \qquad (B.4.2)$$

$$= -\frac{dV}{dt} - \frac{1}{\gamma}\frac{V}{P}\frac{dP}{dt} \qquad (B.4.3)$$

where

Q is the air leakage out of the envelope [m^3/hr].

To conform to common usage in the field, we have used the convention that the air flow, Q, is positive when it flows out of the structure to correspond; however, the term dn/dt is positive when air flows into the structure, hence the minus signs in Eq. B4.

If the induced change in the volume of the structure is small, then the change in internal pressure will be small compared to atmospheric pressure. In this case the volume and pressure in the above expression

may be replaced by their steady-state values:

$$Q + \frac{dV}{dt} + \frac{V_o}{\gamma P_a}\frac{dP}{dt} = 0 \qquad (B.5)$$

where

V_o is the normal structure volume [m^3] and

P_a is the normal internal pressure (1 atm.)

AIR LEAKAGE

The continuity equation, Eq. B5, can be used to find the air flow through the envelope caused by given pressure and volume changes, however, the quantity of interest is not the flow itself but the leakage function. The leakage function relates the flow through the structure envelope to the instantaneous pressure across it. DC measurements suggest that at high pressures the leakage may be described by a power law expression where the exponent of the pressure is between one-half and one. At low-pressures we expect the leakage to be linear in the pressure drop across the shell because the flow must be laminar.

Linear Leakage Model

The simplest of all leakage models is the linear leakage model, which assumes that the flow through the envelope is proportional to the applied pressure:

$$Q = L_o \Delta P \qquad (B.6)$$

L_o is the leakage constant and it is the parameter of interest. Under the linear leakage assumption, the continuity equation can be solved

exactly. We can use Eq. B6 above to eliminate the pressure from Eq. B5.

$$Q + \frac{dV}{dt} + k_o \frac{dQ}{dt} = 0 \qquad (B.7.1)$$

(Note that $\frac{dP}{dt} = \frac{d(\Delta P)}{dt}$.) Equivalently,

$$\Delta P + \frac{1}{L_o}\frac{dV}{dt} + k_o \frac{d(\Delta P)}{dt} = 0 \qquad (B.7.2)$$

where

$$k_o = \frac{1}{L_o}\left(\frac{V_o}{\gamma P_a}\right) \qquad (B.7.3)$$

The time constant, k_o, is a direct measure of the leakage function of the house. Equation B7 is a first-order linear differential equation with constant coefficients. It can be solved for a sinusoidal driving function.

$$V = V_d \sin(wt) \qquad (B.8)$$

where

V_d is the displacement volume [m^3] (half of peak to peak)

w is the fundamental frequency of the drive [hr^{-1}].

Solving the differential equation, Eq. B7, leads to a solution of the form,

$$Q = Q_o \sin(wt+\theta_o) \qquad (B.9.1)$$

or,

$$\Delta P = \Delta P_{AC} \sin(wt + \theta_o) \qquad (B.9.2)$$

where

ΔP_{AC} is the amplitude of the (AC pressure) response [Pa],

$Q_o = L_o \Delta P_{AC}$ is the amplitude of the (air flow) response [m^3/hr]

θ_o is the phase shift between the response and the drive.

Solving the differential equation also leads to expressions for Q_o and θ_o in terms of the drive, time constant, and fundamental frequency:

$$\tan\theta_o = \frac{1}{wk_o} \tag{B.10.1}$$

$$Q_o = - wV_d \sin\theta_o \tag{B.10.2}$$

$$= \frac{wV_d}{\sqrt{1 + w^2 k_o^2}} \tag{B.10.3}$$

$$\Delta P_{AC} = \frac{wV_d/L_o}{\sqrt{1 + w^2 k_o^2}} \tag{B.10.4}$$

$$\cos\theta_o = - \frac{\Delta P_{AC} V_o}{\gamma P_a V_d} \tag{B.10.5}$$

From Eq. B10.5 we can calculate the phase angle from the measured pressure and the displacement. From Eq. B10.1 we can calculate the time constant from the phase angle. Using the definition of the time constant (Eq. B7.3) we can find the leakage constant.

$$L_o = - \frac{wV_d}{\Delta P_{AC}} \sin\theta_o \tag{B.11.1}$$

$$= w \sqrt{\left(\frac{V_d}{\Delta P_{AC}}\right)^2 - \left(\frac{V_o}{\gamma P_a}\right)^2} \tag{B.11.2}$$

Q_o is the size of the air flow through the structure in response to a sinusoidal drive. Assuming perfect mixing, all of the air flow will contribute to an increase in infiltration. Since the air flowing in will be equal to the air flowing out we need only find the total amount

of air that flows out during a half cycle and divide that by the cycle time to find the induced infiltration.

$$Q^I = \frac{\int_0^{\pi} Q_o \sin\beta \, d\beta}{\int_0^{2\pi} d\beta} \tag{B.12.1}$$

$$Q^I = \frac{Q_o}{\pi} \tag{B.12.2}$$

$$Q^I = -\frac{wV_d}{\pi} \sin\theta_o \tag{B.12.3}$$

where

Q^I is the infiltration induced by the drive [m^3/hr] and

$$\beta = wt + \theta_o \tag{B.12.4}$$

Non-Linear Leakage

Our linear leakage model does not account for any nonlinearities (i.e. if the leakage is not strictly proportional to the applied pressure, our model, as it stands, fails). Therefore, we must relax the assumption of linearity and allow for the possibility of nonlinearities in the model. (Such a relaxation is motivated by the fact that turbulent flow will be proportional to the square root of the applied pressure.)

The presence of nonlinear terms in a differential equation always causes harmonic generation; that is, if a sinusoidal drive of frequency w is used, there will be a pressure response at frequency w as well as at all of the higher multiples of w, (i.e. 2w, 3w, ...), as well as a possible constant term. For experimental reasons, direct measurement of these higher harmonics is quite difficult and, therefore, we will derive a leakage function without requiring the measurement of the higher

harmonics.

To allow for the nonlinearities, we generalize the concept of the leakage constant to that of a leakage function that depends on pressure:

$$Q(\Delta P) = L(\Delta P)\ \Delta P \tag{B.13}$$

Physically, the leakage function must be slowly varying and monotonically decreasing. Furthermore, we expect that at very high pressures it must decrease as the square root of the pressure.

In general, the air flow due to a positive pressure on the structure will be nearly equal in magnitude to the air flow due to the same negative pressure on the structure. It is mathematically convenient to treat the leakage function as an even function of the pressure; but since there may well be a small asymmetry between the air flows, we must add a small asymmetric term to the symmetric leakage function.

$$Q(\Delta P) = L(\Delta P)\ (1 + \alpha\ \Delta P)\ \ \Delta P \tag{B.14}$$

<u>where</u>

$L(\Delta P)$ is an even function [m^3/hr-Pa] of pressure and

α is the asymmetry parameter [Pa^{-1}].

The presence of this asymmetric term has the interesting feature of changing the average internal DC pressure when there is a sinusoidal volume change in the structure. This DC offset arises because the leakage is larger on pressurization than on depressurization; thus, to assure that the air flow in is equal to the air flow out, the average internal pressure must drop a little.

To obtain this DC offset for our equations, we must use the fact that under AC pressurization the average flow through the envelope is

zero. Averaging the continuity equation, B5, over one cycle yields:

$$- \langle Q(\Delta P)\rangle = \langle \frac{dV}{dt} \rangle + \frac{V_o}{\gamma P_a} \langle \frac{dP}{dt} \rangle \qquad (B.15.1)$$

$$= 0 \qquad (B.15.2)$$

$$= \langle L(\Delta P)\Delta P \ (1 + \alpha(\Delta P)\rangle \qquad (B.15.3)$$

The brackets <...> around a quantity indicate that that quantity is to be averaged over a cycle.

Since we have assumed that the leakage function is slowly varying, we can replace it by its average value during the oscillation. The error introduced by doing this will be small as long as the leakage function does not change radically in the working range of pressure. Since the leakage function is slowly varying and the pressure is oscillatory, we assume the average leakage function to be approximated by the leakage function at the root mean-square pressure.

$$< L(\Delta P) > \approx L\left(\sqrt{< \Delta P^2 >}\right) \qquad (B.16)$$

Since we have assumed that the leakage function for the AC tests can be approximated by its value at the root mean pressure, there is an equivalent steady-state pressure at which the leakage will have the same value, namely the root mean square pressure. Therefore, we define the equivalent DC pressure as,

$$\Delta P_{DC} = \sqrt{< \Delta P^2 >} \qquad (B.17)$$

<u>where</u>

ΔP_{DC} is the equivalent applied pressure. [Pa]

$< \Delta P^2 >$ is the mean square pressure [Pa^2].

Substituting for the leakage function in Eq. B15.3, we can obtain a

relation for the asymmetry:

$$L(\Delta P_{DC})\ (< \Delta P > + \alpha < \Delta P^2 >) = 0 \qquad (B.18)$$

Since the leakage function is never zero, it can be divided out and the equation can be solved for α:

$$\alpha = - \frac{< \Delta P >}{< \Delta P^2 >} \qquad (B.19)$$

where

$< \Delta P >$ is the average DC pressure offset [Pa.]

This last expression allows the calculation of the asymmetry constant, α, from the DC pressure offset, $< \Delta P >$, and the mean square pressure, $< \Delta P^2 >$. Conversely, once the asymmetry constant has been measured, it allows the calculation of the DC offset from a measurement of the mean square pressure.

We can find the root mean pressure in terms of the component of the pressure at the fundamental frequency. In general, the pressure can be expanded in terms of harmonics of the fundamental frequency, w.

$$\Delta P = < \Delta P > + \Delta P_{AC} \sin(wt + \theta) + \Delta P_2 \sin(2wt + \phi_2) \cdots \qquad (B.20)$$

where

$< \Delta P >$ is the average pressure difference [Pa],

ΔP_{AC} is the component at the fundamental frequency [Pa],

θ is the phase shift between the drive and response and

ΔP_n is the component at the nth harmonic.

ϕ_n is the phase angle of the nth harmonic

To calculate the average mean square pressure, we must square the above expression and then average over one cycle. When we do the averaging, all of the cross terms will drop out leaving only the squared terms of

each fourier component.

$$< \Delta P^2 > = < \Delta P >^2 + \tfrac{1}{2}\Delta P_{AC}{}^2 + \Sigma(\text{higher harmonics})^2 \qquad (B.21.1)$$

If we assume that higher harmonics are negligible compared to the other two terms, we can approximate the mean square pressure by,

$$< \Delta P^2 > \approx \tfrac{1}{2}\ \Delta P_{AC}{}^2\ (1 + \tfrac{1}{2}\alpha^2\ \Delta P_{AC}{}^2) \qquad (B.21.2)$$

where we have used the definition of α recursively.

Therefore,

$$\Delta P_{DC} = \Delta P_{AC} \sqrt{\tfrac{1}{2}\ (1 + \tfrac{1}{2}\alpha^2\ \Delta P_{AC}{}^2)} \qquad (B.22)$$

Once the asymmetry and equivalent DC pressure have been found, we must derive a relation between the leakage function and the experimental parameters. In the linear case we derived a formula for the leakage by solving the linear differential equation for a sinusoidal driving function. In the nonlinear case, we cannot solve the equation exactly, nor could we do so if we had an explicit form for the leakage function. We can, however, derive a similar expression for the leakage function by fourier analyzing the continuity equation at the frequency of the drive.

Since we know that the largest part of the pressure response will be at the fundamental frequency of the drive, we can extract more information by using a fourier analysis at that frequency. The analysis is the equivalent of multiplying our continuity equation by sin(wt) and cos(wt) alternately and then averaging over one cycle.

$$- < Q(\Delta P)\sin wt > = < \frac{dV}{dt} \sin wt > + \frac{V_o}{\gamma P_a} < \frac{d(\Delta P)}{dt} \sin wt > \qquad (B.23.1)$$

$$= wV_d < \cos wt \sin wt > + \frac{V_o}{\gamma P_a} w\ \Delta P_{AC} < \cos(wt + \theta)\sin wt > \qquad (B.23.2)$$

$$= - w \frac{V_o}{\gamma P_a} \Delta P_{AC} \frac{\sin\theta}{2} \qquad (B.23.3)$$

The definition of Q can be used to expand the left hand side of the equation, using the same approximation for the leakage function.

$$- < Q(\Delta P)\sin wt > \; = L(\Delta P_{DC}) \; (< \Delta P \sin wt > + \alpha < \Delta P \sin wt >) \qquad (B.24.1)$$

$$= L(\Delta P_{DC}) \; \Delta P_{AC} (<\sin wt \; \sin(wt+\theta)> + 2\alpha < \Delta P ><\sin wt \; \sin(wt+\theta)>) \qquad (B.24.2)$$

$$= L(\Delta P_{DC}) \; \Delta P_{AC} \; (1/2 + \alpha < \Delta P >) \cos\theta \qquad (B.24.3)$$

Using Eq. B19,

$$- < Q(\Delta P)\sin wt > = 1/2 \, L(\Delta P_{DC}) \; \Delta P_{AC} \cos\theta \; (1 - 2 \alpha^2 < \Delta P^2 >) \qquad (B.24.4)$$

We can combine the two expressions for Q to get,

$$\tan\theta = - \frac{1}{k_o w} \frac{L(\Delta P_{DC})}{L_o} \; (1 - 2 \alpha^2 < \Delta P^2 >) \qquad (B.25.1)$$

$$\tan\theta = - \frac{L(\Delta P_{DC}) \gamma P_a}{w V_o} \; (1 - 2 \alpha^2 < \Delta P^2 >) \qquad (B.25.2)$$

This gives us an expression for the leakage in terms of the phase angle.

$$L(\Delta P_{DC}) = - \frac{w}{1 - 2 \alpha^2 < \Delta P^2 >} \left(\frac{V_o}{\gamma P_a}\right) \tan\theta \qquad (B.26)$$

In a manner similar to the one above, the averaging can be done with cos(wt) instead of sin(wt).

$$< Q(\Delta P)\cos wt > \; = < \frac{dV}{dt} \cos wt > + \frac{V_o}{\gamma P_a} < \frac{d(\Delta P)}{dt} \cos wt > \qquad (B.27.1)$$

$$= \tfrac{1}{2} w V_d + \frac{V_o}{\gamma P_a} \tfrac{1}{2} w \Delta P_{AC} \cos\theta \qquad (B.27.2)$$

$$< Q(\Delta P)\cos wt > = L(\Delta P_{DC}) \; (< \Delta P \cos wt > + \alpha < \Delta P \cos wt > \qquad (B.27.3)$$

$$= L(\Delta P_{DC}) \; \tfrac{1}{2} \; \Delta P_{AC} \sin\theta \; (1 - 2\,\alpha^2 < \Delta P^2 >) \qquad (B.27.4)$$

The last two equations can be combined with the definition of k_o to yield another expression for the phase angle.

$$\cos\theta = - \frac{\Delta P_{AC} \; V_o}{\gamma P_a \; V_d} \qquad (B.28)$$

This is the same expression for the phase angle as the one from the linear case; however, the measured pressure response for a given frequency and displacement (ΔP_{AC}) will have a different value from that of the linear case; therefore, the value of the phase angle will also be different. We can now eliminate the phase angle from Eq. B27 to yield an expression for the leakage:

$$L(\Delta P_{DC}) = \frac{w}{(1 - \alpha^2 \, \Delta P_{AC}{}^2)} \sqrt{\left[\frac{V_d}{\Delta P_{AC}}\right]^2 - \left[\frac{V_o}{\gamma P_a}\right]^2} \qquad (B.29.1)$$

$$L(\Delta P_{DC}) = \frac{\dfrac{w V_d}{\Delta P_{AC}}}{(1 - \alpha^2 \, \Delta P_{AC}{}^2)} \sin\theta \qquad (B.29.2)$$

With the exception of the asymmetry term, Eq. B29 looks very similar to Eq. B11; however, the interpretation of the two equations in slightly different. Eq B11 is an estimate of leakage <u>constant</u>, which should be the same at any applied pressure. Eq. B29 is an estimate of the average leakage <u>function</u> at a particular applied pressure. The applied pressure is a known function of the pressure response at the fundamental frequency from a sinusoidal drive.

FLEXING

When an AC pressure is applied to the shell of the structure, there may be a small amount of flexing. The amount of flexing need not be very large in order to effect a significant change in the pressure response; it need only change the volume of the structure by an amount that is significant compared to the displacement volume ($\simeq .2\ m^3$). Because such flexing will decrease the pressure response, making the leakage appear to be larger than it actually is, it is necessary to be able to account for its effects.

The resonant frequency of most structures is approximately 15 Hz.[3] Since the frequency range we are working in is much lower than this (typically .1-1 Hz), we can assume that the additional volume created by the flexing will be in phase with the applied pressure.

"Linear flexing" is the term applied to the stretching or expanding of the envelope under an applied pressure and generally takes place in walls and windows. The change in volume of the structure is treated as being proportional to the applied pressure. Therefore, we define the flexing constant as the constant of proportionality between the applied pressure and volume change.

$$\delta V = \lambda \Delta P \tag{B.30}$$

where

δV is the volume [m^3] change due to the flexing and

λ is the flexing constant [m^3/Pa]

The volume that belongs in the continuity equation is the sum of this volume and the drive volume.

$$V' = V + \delta V \tag{B.31.1}$$

$$= V_d \sin wt + \lambda \Delta P \tag{B.31.2}$$

where

V' is the effective (volume) drive [m^3].

If we now substitute this result in the continuity equation,

$$Q + \frac{dV}{dt} + \lambda \frac{dP}{dt} + \frac{V_o}{\gamma P_a} \frac{dP}{dt} = 0 \qquad (B.32.1)$$

which can be rewritten as,

$$- Q(\Delta P) = \frac{dV}{dt} + (\lambda + \frac{V_o}{\gamma P_a} \frac{d(\Delta P)}{dt} \qquad (B.32.2)$$

The effect of the flexing has been to increase the capacity term, $(V_o/\gamma P_a)$ by adding the constant flexing term, λ. Because we are working far below the frequency at which the capacity term is important, we will ignore the capacity term for the purpose of calculating the correction term. We define the apparent leakage as leakage that would occur if the capacity term were ineligible (i.e. the apparent leakage is the ratio of the drive term to the pressure response),

$$L_a = \frac{wV_d}{\Delta P_{AC}} \qquad (B.33)$$

where

L_a is the apparent leakage [m^3/hr-Pa]

The apparent leakage is the leakage calculated by assuming that the capacity of the structure is negligible, which is equivalent to assuming that the phase angle is always -90°. The actual leakage takes into account the effect of the flexing and the compressibility of air.

$$L(\Delta P_{DC}) = w \sqrt{\left[\frac{V_d}{\Delta P_{AC}}\right]^2 - \left[\lambda + \frac{V_o}{\gamma P_a}\right]^2} \qquad (B.34.1)$$

$$= L_a \sqrt{1 - \left[\frac{w}{L_a}\left(\lambda + \frac{V_o}{\gamma P_a}\right)\right]^2} \qquad (B.34.2)$$

Squaring this expression and solving for the apparent leakage puts this equation into a form that demonstrates its dependence on the capacity:

$$L_a^2 = L^2 + w^2\left[\lambda + \frac{V_o}{\gamma P_a}\right]^2 \qquad (B.35)$$

As expected, this last equation shows that the apparent leakage is larger than the actual leakage. Furthermore, it shows that the disparity grows rapidly with increasing frequency.

If we are using the linear equations, we expect the leakage to be constant; however, if we are using the nonlinear equations, we expect the leakage to be slowly decreasing with increasing pressure. In either case, a well established trend is present: in the presence of flexing there will be an increase in the apparent leakage. If we look for an upturn in a set of data for a particular displacement, we should be able to use Eq. B35 to extract an upper bound on the value of λ. Once found, the flexing parameter can be used to correct all of the data points appropriately.

ALTERNATE DERIVATION

If we are willing to put certain constraints on our model of leakage, we can simplify the derivation considerably. We assume the following:

1) The asymmetry of the leakage is unimportant. This allows us to assume that the magnitude of the flow through the structure is independent of the sign of the pressure drop across it.

2) The flexing and real capacity terms are uninteresting. If we are not interested in finding these quantities experimentally, we can manipulate the equations to eliminate them, thus reducing the amount of data and the experimental uncertainty.

3) The leakage can be expressed in the form of a power law. By assuming an explicit functional form for the leakage, unknown parameters may be solved for exactly.

Thus the leakage is,

$$Q(\Delta P) = L\,\Delta P\,\left|\,\Delta P\,\right|^{n-1} \tag{B.36}$$

where

L is the leakage coefficient

n is the leakage exponent ($1/2 \leq n \leq 1$)

Inserting this definition into the continuity equation yields,

$$L\,\Delta P\,\left|\,\Delta P\,\right|^{n-1} + \frac{dV}{dt} + \frac{V_o}{\gamma P_a}\frac{dP}{dt} = 0 \tag{B.37}$$

Multiplying the equation by the instantaneous pressure and averaging over one cycle we find,

$$L < \left|\,\Delta P\,\right|^{n+1} > + < \Delta P\,\frac{dV}{dt} > + \frac{V_o}{\gamma P_a} < \Delta P\,\frac{dP}{dt} > = 0 \tag{B.38}$$

Since the pressure is periodic,

$$< \Delta P\,\frac{dP}{dt} > = 0 \tag{B.39}$$

which yields an expression for L:

$$L = -\frac{< \Delta P\,\frac{dV}{dt} >}{< \left|\,\Delta P\,\right|^{n+1} >} \tag{B.40}$$

This expression can be used to calculate the leakage for a particular value of n from the measured volume drive and pressure response. The advantage of this form is that it uses real-time variables in simple

arithmetic combinations rather than a fourier analysis.

If we assume that the leakage is proportional to the square-root of the pressure, we can use this expression to find the leakage area:

$$A = \sqrt{\frac{\rho}{2}}\, L(\ n = 1/2\ ) \tag{B.41.1}$$

$$A = \sqrt{\frac{\rho}{2}} \left\{ - \frac{< \Delta P \frac{dV}{dt} >}{< \left| \Delta P \right|^{n+1} >} \right\} \tag{B.41.2}$$

where

A is the effective leakage area [m^2].

EXPERIMENTAL DETAILS

In this part of the Appendix we shall discuss the apparatus, method, and results of our AC pressurization experiments. The equipment described herein was designed to validate the concept of AC pressurization and, accordingly, was sized to assure sufficient overlap with the DC data.

Procedure and Analysis

To conduct our leakage tests, we used a research house that has been extensively studied.[4] The house was tested in both "loose" and "tight" configurations. In the loose configuration, the structure is in its normal operating condition: all vents open, all dampers and windows shut. In the tight configuration, all vents were sealed and the heating system (registers, return duct, and furnace closet) was also sealed. In neither configuration was any weather-induced noise noted above the other random errors.

To measure leakage at very low pressures by means of AC pressurization, we change the volume of the structure and measure the resultant pressure response. By measuring only at that pressure response, which is at the same frequency as the volume drive (i.e. synchronous detection), we avoid the noise associated with DC measurements and, because a much greater signal-to-noise resolution is thus obtained, we can work at applied pressures that are smaller than the random weather-induced pressures.

The volume is changed by installing a large piston and guide assembly in place of an existing exterior door (See Fig. 1). The piston is moved in the guide by a motor/flywheel assembly that allows adjustable displacement and frequency control. The piston rides on sliding teflon seals to prevent leakage and reduce drag. The pressure is monitored using a differential pressure sensor with 0.1 Pa resolution and a full-scale reading of 70 Pa. Our leakage measurements were made at frequencies between 6 and 60 rpm.

If the structure is rigid, we can use the measured volume drive and pressure response to calculate the airflow through the envelope during AC pressurization. If there were no leakage at all, then the change in pressure would be precisely determined, given the volume of the structure and the displacement of the piston; therefore, any deviation from this predicted pressure can be attributed to leakage through the envelope. The continuity equation allows us to calculate exactly how much air leaks out for a given drive and thus to calculate the air flow for a given (constant) external pressure.

In general, building structures are not rigid and, when the pressure inside the structure changes, the envelope flexes to counteract the change in pressure. By assuming that the flexing is proportional to the differential pressure across the shell, we can correct for this effect.

Equipment: The source of the pressure signal is a large cross-section ($\simeq 1m^2$) rectangular piston which moves in and out of the shell through a suitably sized guide. (cf Fig. 1a) The guide is installed in an exterior door of the test structure. As the piston moves outward through the guide, the volume of the house is increased; as it moves

inward the volume is decreased. The guide is made of plywood and has teflon seals all around it to minimize both friction and air leakage through the guide.

The piston is connected via a connecting rod to a light flywheel. The diameter of the flywheel is about 0.5m; there are nine different holes in the flywheel to allow for different displacements of the piston during a drive stroke. The maximum displacement peak-to-peak is about $0.3m^3$. The flywheel is driven through a gearbox by a variable speed 3/4 hp motor, having a frequency range from 2 to 250 rpm.

The pressure response of the envelope is measured with a differential pressure sensor whose range is ± 70 Pa. The reference end of the pressure transducer must be at a constant pressure in order to measure the pressure response of the system; if it were connected to the outside, a large amount of noise due to wind would be introduced into the data.

Rather than use the outside as our reference pressure, we used the time-averaged interior pressure. To do this time averaging, we built a physical low-pass filter that responds to slow-pressure drifts but does not respond to high-frequency fluctuations (i.e. noise from wind or unevenness of piston travel are ignored). The filter consists of a volume and a resistance: the volume is a large brass cylinder of about 3 liters and the resistance is a micrometering valve. (cf Fig. 1b)

Since the resistance is variable, we can adjust the time constant of the filter to any desirable level. The time constant was chosen to be about 5 minutes so that wind fluctuations and our pressure signal would be filtered out but the normal changes in atmospheric pressure would not. The volume is insulated with about 2cm of polystyrene insulation to minimize pressures induced by temperature fluctuations. This provides a reliably steady pressure with which to reference our measurements.

Procedure: Two sets of test runs were used to measure the leakage. The first set of runs was done with the test house in a relatively tight configuration: the fireplace and kitchen vents were sealed with plastic to prevent leakage and, since the ductwork does not go through the

conditioned space, all of the registers as well as the closet containing the furnace were sealed with tape. The second set of runs was done with the house in a loose configuration, more typical of normal operation: the fireplace was unsealed but the damper left closed, and the kitchen vents and registers were untaped and left in their normal operating state.

For each set of runs, the DC pressurization was measured by fan pressurization. Both pressurization and depressurization were measured. Then three different AC pressurization runs were conducted within each set, each run having a different displacement volume for the drive. In every run the frequency was varied from a minimum of about 3 rpm to a maximum of about 1 rps. Data was collected continuously by the microprocessor and processed every minute during a (40-minute) run.

The parameters α and λ were calculated separately. To measure the asymmetry parameter, α, the drive was left on for several minutes at the same frequency, allowing the physical filter on the pressure sensor to come to full equilibrium with the average pressure inside the structure. Once equilibrium was established, the volume drive was shut off and the DC pressure offset was noted. This procedure was carried out at several representative pressures and the results averaged.

Although the flexing parameter, λ, becomes dominant at higher frequencies, its value is needed to correct the apparent leakage for envelope flexing at low frequencies. Accordingly, we measured the response at frequencies higher than that of any of the runs and fit the data to Eq. B35 to find λ. Data was taken at frequencies from 0.1 Hz to 3 Hz using the smallest of the displacements.

<u>Data Acquisition and Analysis:</u> Only two quantities are measured during the course of the leakage experiment: the time-dependent pressure and the frequency. The stroke of the piston is an experimental parameter that may be adjusted; the quantities V_o, P_a and γ are known.

The pressure is recorded by a strip-chart recorder and by a microprocessor. The frequency is monitored by the microprocessor which incorporates an infrared diode system that records each revolution of the flywheel. Digital filtering of the incoming data is used to remove noise and reduce aliasing.

Data at very high frequencies can be used to determine the flexing constant and data at high-pressures can be used to determine the asymmetry constant. Once these two parameters are known, the average leakage can be calculated for every measured data point.

During the infiltration experiments, the data was collected on a separate chart recorder for later analysis. The leakage was calculated using Eq. B38 for each of the one-minute data points. All of the data points in a 1/2 Pa range were then averaged together using their standard deviations to weight the averages.

Error Analysis: An estimate of the error was made for each point on the air flow vs applied pressure curves. For DC measurements the error comes principally from two sources: the uncertainties involved in the calibration of the flow through the fan, and the uncertainty in the measurement of the pressure drop across the structure.

The error analysis for the AC measurements is a little more involved. Using the formula for the leakage function, we can estimate the error in the leakage from the measurement error in the variables. At low pressures the error in the leakage is dominated by the uncertainty in the displacement and in the measured pressure. At high frequencies the error is dominated by the uncertainty in the flexing parameter.

All of the points that fell within a half pascal range were averaged together to get a composite leakage function. The averaging was done using the standard deviation of each point to weight the average. This composite leakage function and the asymmetry parameter were combined with the pressure to give the air flow vs applied pressure curves in Fig. 4-7.

Results

Fig. 2 and 3 are plots of the data points for the AC pressurization data in both configurations, also drawn is the average leakage curve calculated from a weighted average of the data points. Fig. 4 and 5 are graphs of the predicted air flow vs applied pressure for the house in the loose and tight configurations. Each graph indicates the points from the AC pressurization run as well as the points from the DC pressurization run, and each point has the error bars associated with each measurement. Fig. 7 is a plot of both the loose and tight configurations for the full range of DC leakage points. The low-pressure range is duplicated on Fig. 4 and 5.

All AC tests were done with a variety of different piston displacements and frequencies. There appeared to be a systematic difference between sets of data at different displacements, but this difference was within the error bars and did not affect the interpretation of the data.

As reflected by the nonzero value of the asymmetry constant, there is some difference between the leakage curves for pressurization and depressurization. An explanation for this asymmetry might be that the windows in the test structure are the sliding aluminum type which, upon pressurization are pushed against their seals making them less leaky; upon depressurization, they are pulled away from their seals, increasing the leakage.

The measurement of the asymmetry parameter was done as indicated above for both the tight and loose configuration. To measure the flexing parameter, we plotted the apparent leakage squared against the square of the frequency, as shown in Fig 6. Looking at Fig. 6, we can see that for high frequencies ($w > 10$ rad/s) the apparent leakage is dominated by the flexing and the plot becomes linear. From this linear section the value of the flexing parameter, λ, can be found.

The asymmetry and linear flexing parameters were measured in order to subtract out their effects. Their values for our test house discussed above are tabulated below.

PARAMETER	VALUE TIGHT	VALUE LOOSE	UNITS
α	.0152±.001	.004±.003	Pa^{-1}
λ	.0032±.001	.0032±.001	m^3/Pa

These constants were used with the measured pressures to produce a plot of the corrected leakage function vs pressure. Fig. 2 is the leakage function of the house in the loose configuration and Fig. 3 is the leakage function of the house in the tight configuration. Each plotted point represents a one-minute average at a certain frequency and displacement. The solid line represents a smooth weighted average of all of the points on the graph.

Fig. 4 and 5 show the air flow through the envelope vs applied pressure curves for the loose and tight configurations, respectively. The open points are calculated air flows from the average leakage curves, and the solid points are the DC measurements made with fan pressurization.

REFERENCES

1. M.H. Sherman, D.T. Grimsrud, R.C. Sonderegger, The Low Pressure Leakage Function of a Building, Presented at the DOE/ASHRAE Conference on the Thermal Performance Exterior Envelope of Buildings, Orlando, FL, December 1979.
   Lawrence Berkeley Laboratory Report #9162 (1979)

2. W.H. Card, A. Sallman, R.W. Graham, E.E. Drucker, Air Leakage Measurement of Building by an Infrasonic Method, Tech. Rpt. TR-78-1, Syracuse University (1978)

3. Recommendations for the calculation of wind effects on buildings

and structures , European Convention for Constructional Steelwork, T12, (1978)

4. D.T. Grimsrud, M.H. Sherman, R.C. Diamond, P.E. Condon and A.H. Rosenfeld, Infiltration-Pressurization Correlations: Detailed Measurements on a California House, ASHRAE Transactions 85:I 1979, Lawrence Berkeley Laboratory Report No. 7824, 1978.

FIGURE CAPTIONS

FIG. B:1 Sketch of experimental set-up and apparatus. Fig. 1a is a schematic of the piston motor and flywheel assembly. The piston is driven by a shaft connected to an 18-inch diameter flywheel that is driven through a gear box by a variable-speed motor. Fig. 1b is a schematic of the pressure sensor and physical filter. The reference end of the differential pressure sensor is connected to a thermally insulated volume that has a high-resistance leak in it. This volume and leak combination is an effective low-pass filter with a time constant of roughly 5 minutes. Thus the reference end of the pressure sensor is at the average interior pressure.

FIG. B:2 The leakage function of the structure (loose configuration) plotted vs the applied pressure. Each point represents a one-minute average reading at a particular frequency and displacement. Points of the same displacement have the same symbol. The curve is the weighted average of all the data points.

FIG. B:3 The leakage function of the structure (tight configuration) plotted vs the applied pressure. Each point represents a one-minute average reading at a particular frequency and displacement. Points of the same displacement have the same symbol. The curve is the weighted average of all the data points.

FIG. B:4 The air flow through the envelope vs the applied pressure for the structure (loose configuration). Both the AC pressurization graph as derived from the low-pressure leakage function, and the DC pressurization are shown. The error bars are calculated from the measurement errors and displayed for each point.

FIG. B:5 The air flow through the envelope vs the applied pressure for the structure (tight configuration). Both the AC pressurization graph as derived from the low-pressure leakage function, and the DC pressurization are shown. The error bars are calculated from the measurement errors and displayed for each point.

FIG. B:6 The apparent leakage squared plotted against the frequency squared for the smallest displacement. From the high-frequency slope, the total capacity can be inferred.

FIG. B:7 The DC leakage curves for both loose and tight configurations. The error bars are derived from the measurement error and equipment calibration errors.

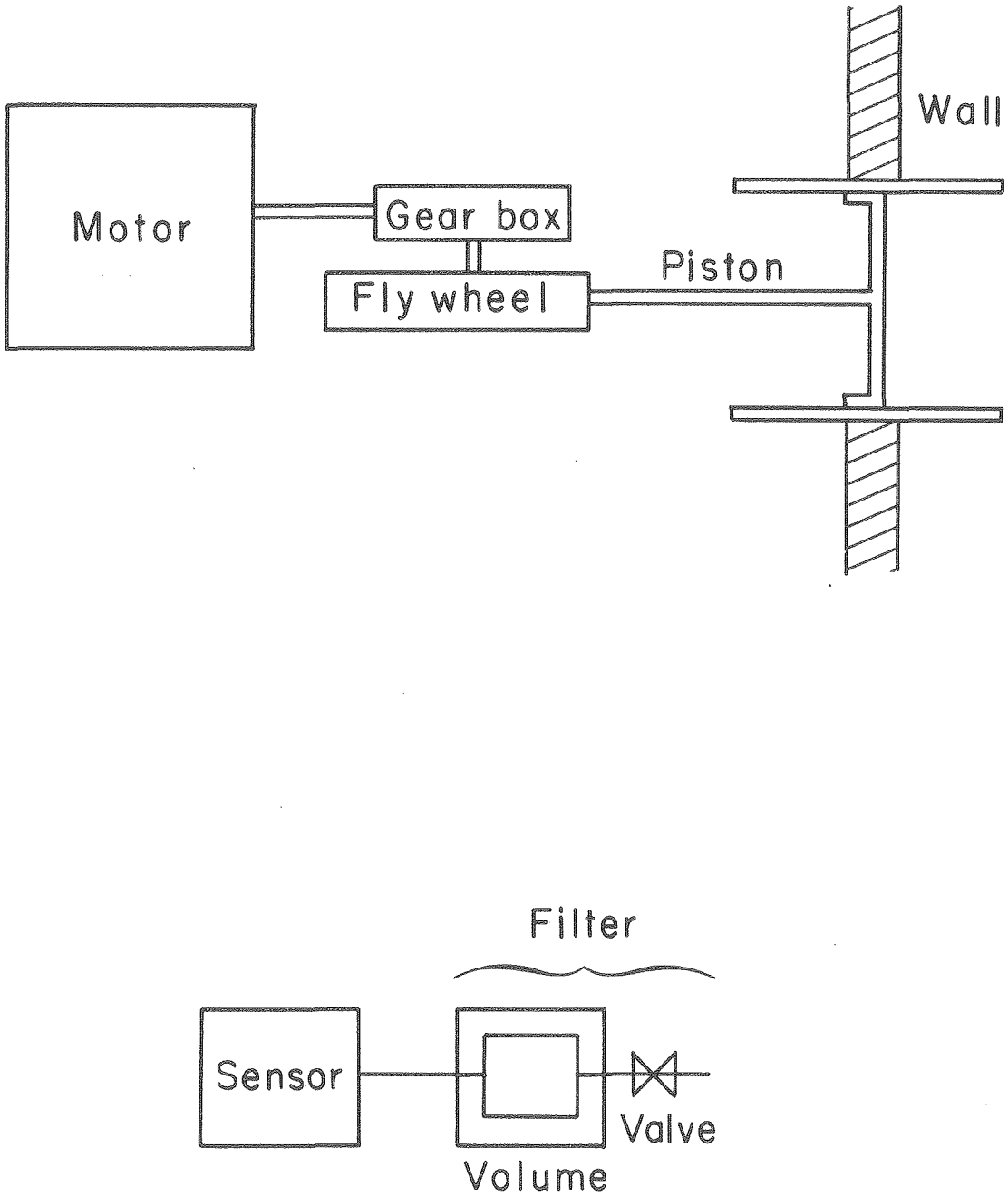

FIG. B:1 Sketch of experimental set-up and apparatus

XBL7910-4409

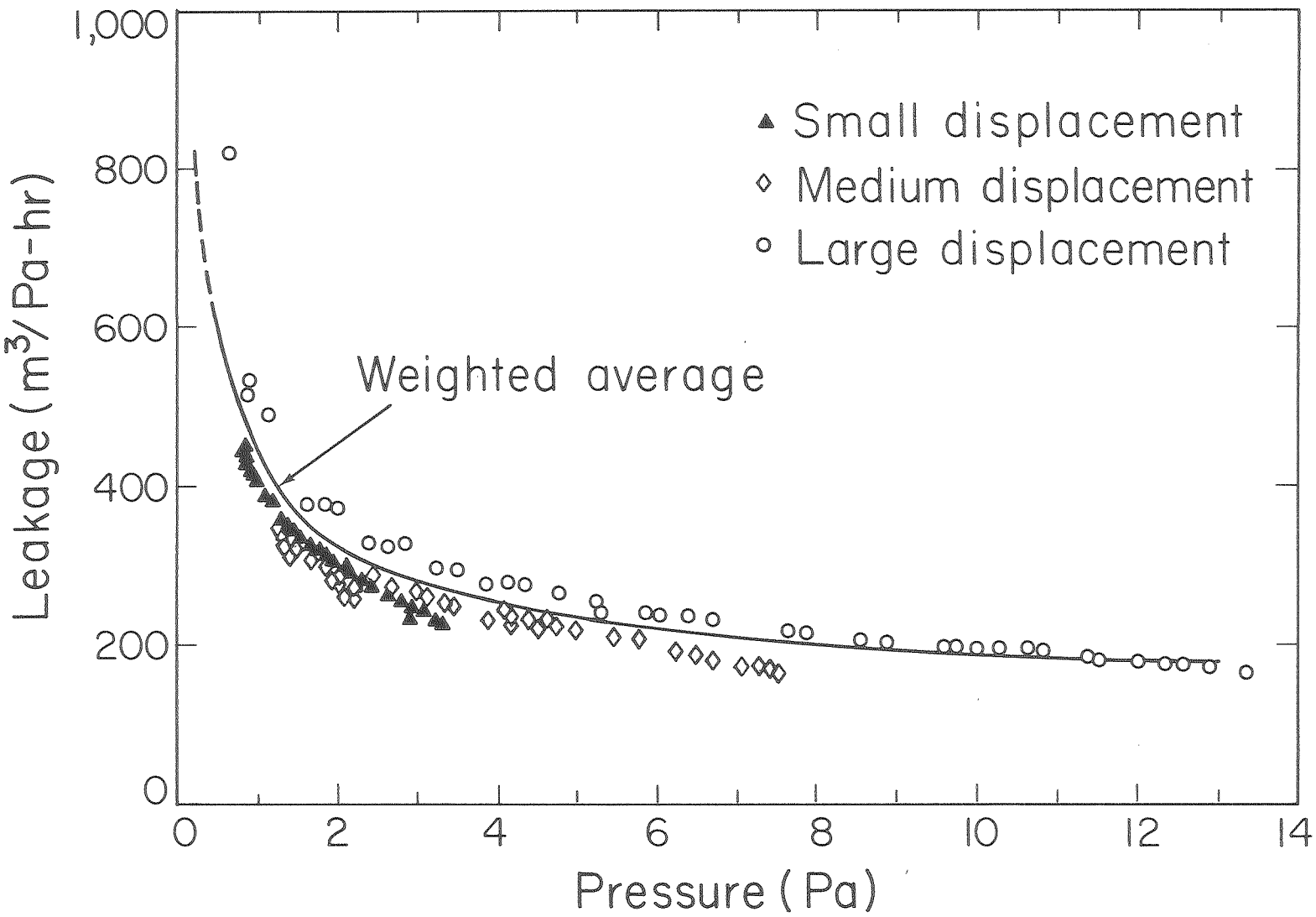

FIG. B:2 The leakage function of the structure in the loose configuration in plotted vs the applied pressure.

XBL 7910-4412

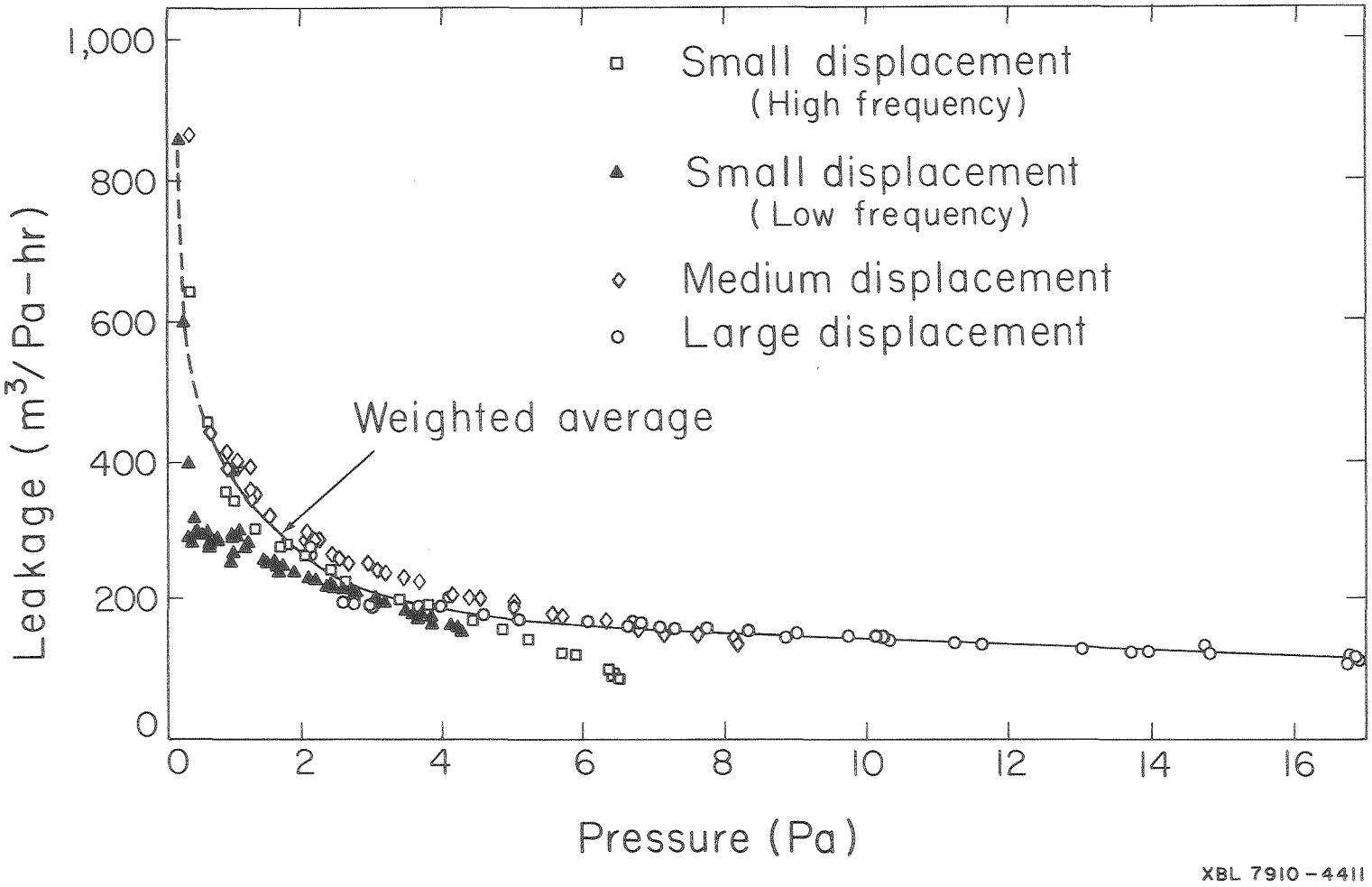

FIG. B:3 The leakage function of the structure (tight configuration) plotted vs the applied pressure.

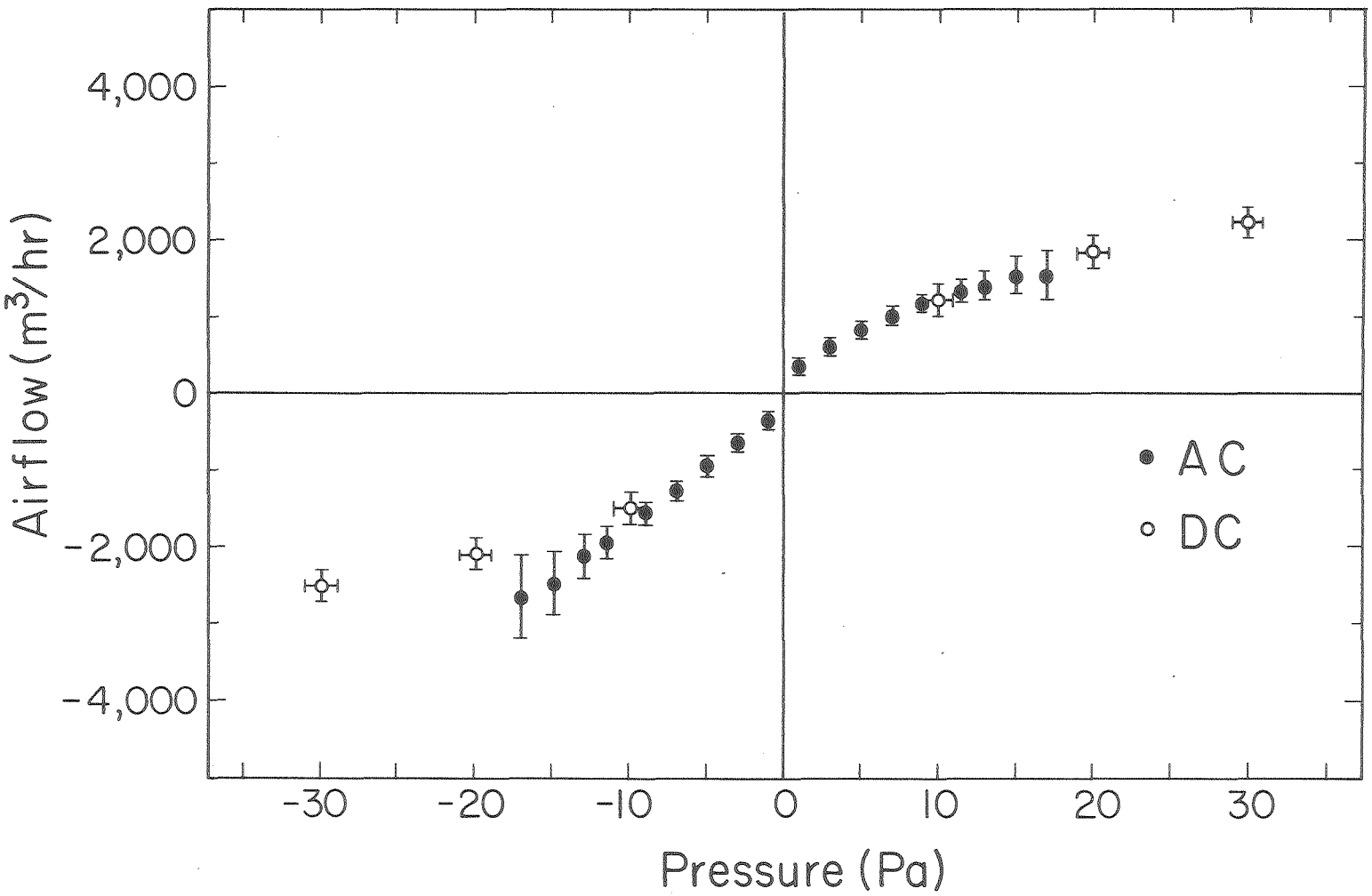

XBL 7910-4410

FIG. B:4 The air flow through the envelope is graphed vs the applied pressure for the structure in the loose configuration.

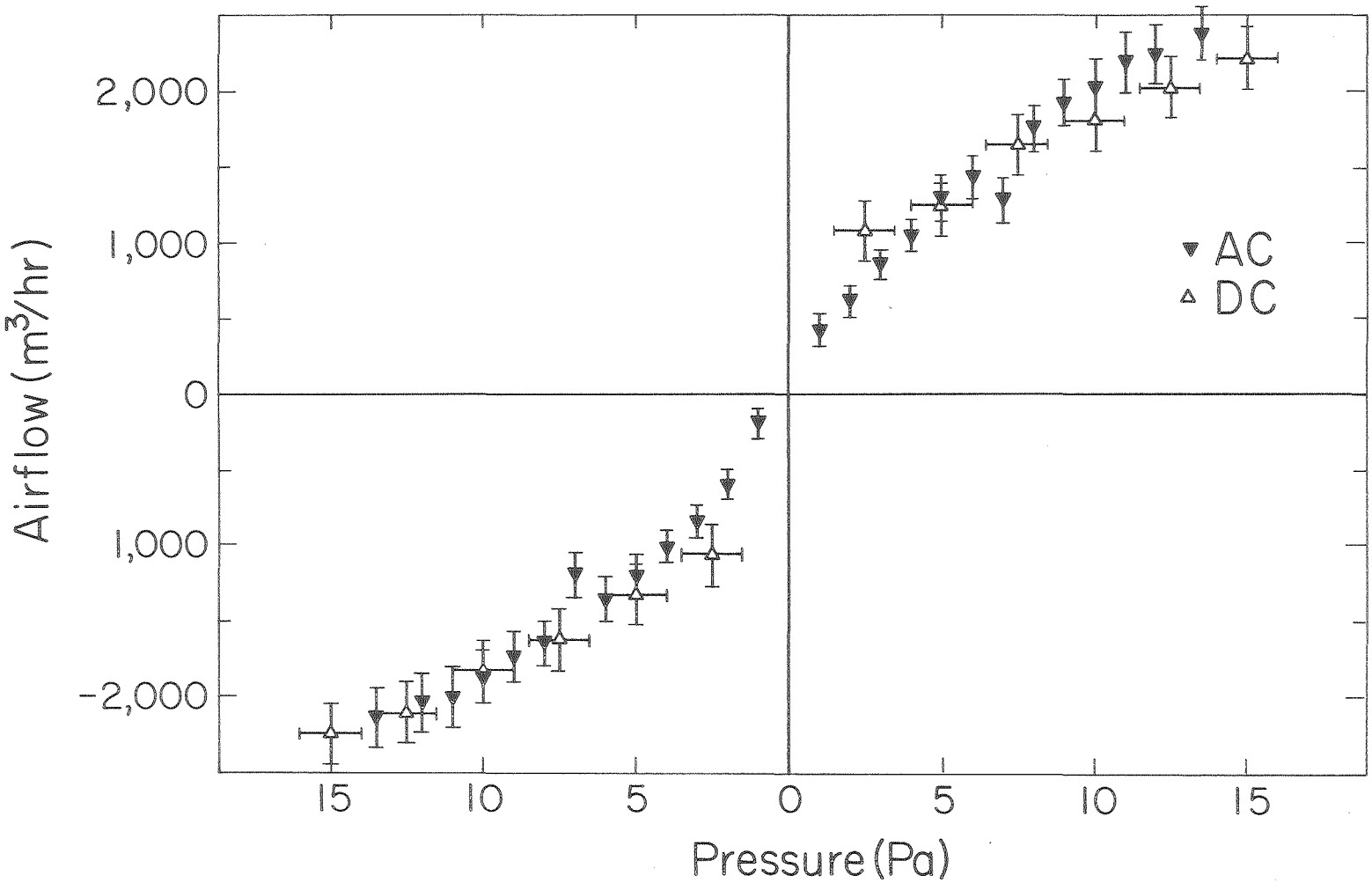

XBL 7910-4414

FIG. B:5 The air flow through the envelope is graphed vs the applied pressure for the structure in the tight configuration.

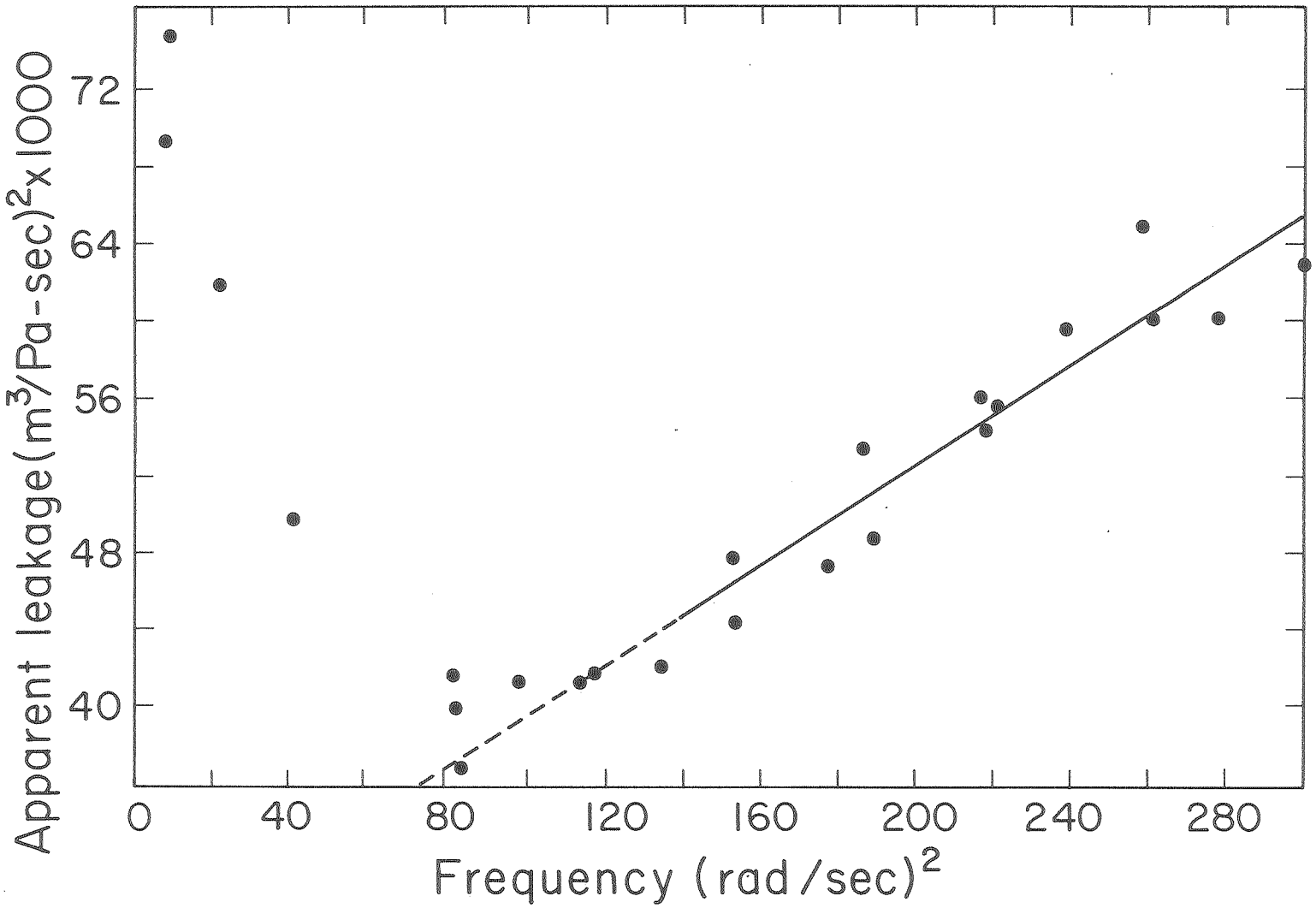

FIG. B:6 The apparent leakage squared is plotted against the frequency squared for the smallest displacement.

XBL 7910-4413

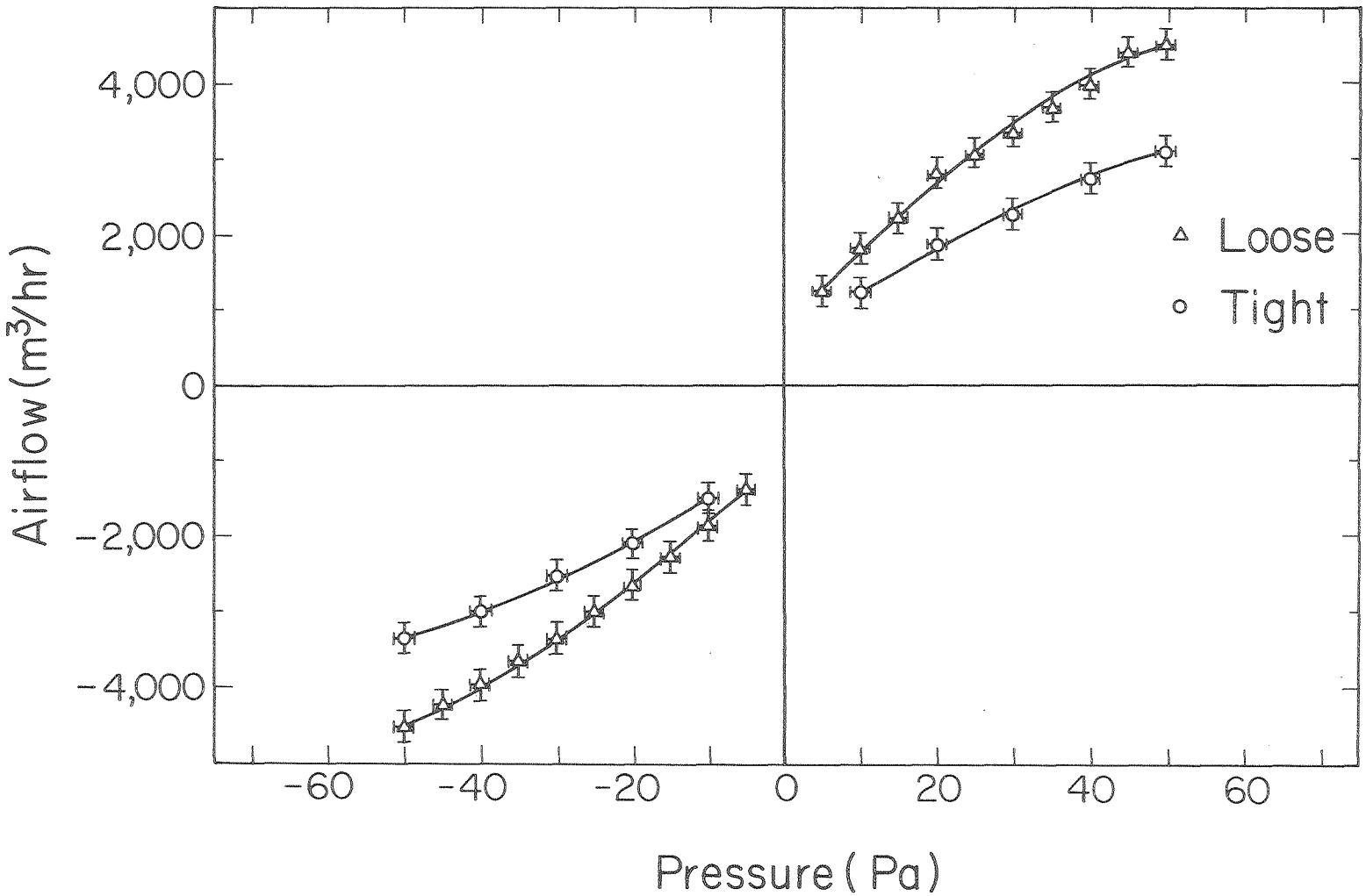

FIG. B:7 The DC leakage curves for both the loose and tight configurations. XBL 7910-4415

APPENDIX C

CALCULATION OF ISOLATED INFILTRATION

Infiltration is caused by differential pressures across the envelope of a structure; these pressures are, in turn, caused by the action of the weather on the structure. Weather-induced pressures can be separated into two types: Stack Effect pressures are created by an indoor-outdoor temperature difference, and Wind Effect pressures are created by the dynamic forces exerted by the wind on a stationary object. In this Appendix we calculate the infiltration separately for each of these two effects.

The pressures induced by the stack and wind effects cause flow through the leakage sites in the building envelope. As discussed in the text, we use a leakage model that assumes the flow to be dominated by inertial effects, implying that an effective area can be defined to characterize the leakage:

$$Q_j = A_j\sqrt{\frac{2}{\rho}\Delta P_j} \qquad (C.1)$$

where

Q_j	is the flow through the jth leakage site [m^3/s],
A_j	is called the effective leakage area of the jth site [m^2],
ΔP_j	is the pressure drop across the jth site [Pa] and
ρ	is the mean density of air[1.2 kg/m^3].

Although every leakage site can be given an effective leakage area, in any real situation it will be practically impossible to measure all of the sites in the envelope individually. Hence, we will limit the number of leakage variables by considering each face of the structure (i.e. floor, walls, ceiling) to have a single leakage area. Furthermore, we will treat the stack and wind effects separately (i.e. without taking each other into account).

PART I — Stack Effect

The stack effect pressure is caused by the existence of bodies of air whose differing temperatures cause differing densities. From the condition of hydrostatic equilibrium we know that the change in pressure with respect to height is proportional to the density.

$$\frac{dP}{dh} = -\rho g \qquad (C.2)$$

where

P	is the static pressure [Pa],
h	is the height [m],
ρ	is the density of that body of air [kg/m^3] and
g	is the acceleration of gravity [9.8 m/s^2].

In the case of a structure, the inside and outside bodies of air will usually be of different temperatures; therefore, there will be a differential surface pressure that changes with height:

$$\frac{d\Delta P}{dh} = -\rho g \left(1 - \frac{\rho'}{\rho}\right) \qquad (C.3)$$

where

ΔP	is the differential surface pressure [Pa],
ρ	is the density of outside air [1.2 kg/m^3],
ρ'	is the density of inside air [kg/m^3],.

Using the ideal gas law, we can replace the density difference factor with a temperature difference factor:

$$\frac{d\Delta P}{dh} = -\rho g \frac{\Delta T}{T} \qquad (C.4)$$

where

ΔT	is the inside-outside temperature difference [K] and
T	is the inside temperature [295K].

We can now integrate this expression to find the actual pressure difference:

$$\Delta P = \Delta P_o - \rho\ g\ h \frac{\Delta T}{T} \tag{C.5}$$

where

ΔP_o is the constant of integration [Pa].

This constant of integration corresponds to an internal pressure shift; it will be fixed by the requirement that the volume of air entering the structure must be equal to the volume of air leaving it.

We now rewrite that expression,

$$\Delta P = P_s\ (\beta^o - \beta) \tag{C.6}$$

where

P_s is the stack pressure [Pa],

β is the (dimensionless) height and

β^o is the (dimensionless) height of the neutral level.

In the above expression we have used the following definitions:

$$P_s = \rho\ g\ H \frac{\Delta T}{T} \tag{C.7.1}$$

$$\beta = \frac{h}{H} \tag{C.7.2}$$

$$\Delta P_o = P_s\ \beta^o \tag{C.7.3}$$

where

the neutral level is the height at which the inside and outside static pressures are equal. H is the height of the structure [m] and (Note that we have substituted the height of the neutral level for the internal pressure shift as our unknown constant of integration.)

We now have an expression that relates the differential pressure to the stack pressure, the neutral level, and the position on the structure. In order to calculate the air flow through the envelope, we must integrate the differential pressures with the air leakage over the entire envelope, making sure to keep track of the infiltration and exfiltration separately.

We are assuming that the floor and ceiling are each at a single height and that their leakage can be considered uniform, thus eliminating the need for integration to calculate the flow through these surfaces. Rewriting the expressions by using the definition that the floor is at $\beta=0$ and, therefore, the ceiling is at $\beta=H$, we get:

$$Q^{-}_{ceiling} = A_c \sqrt{\frac{2}{\rho} P_s \ (\beta^o - 1)} \qquad (C.8.1)$$

$$Q^{+}_{floor} = A_f \sqrt{\frac{2}{\rho} P_s \ (\beta^o)} \qquad (C.8.2)$$

$$Q^{+}_{ceiling} = Q^{-}_{floor} = 0 \qquad (C.8.3)$$

where

A_c is the effective leakage area of the ceiling[m^2] and

A_f is the effective leakage area of the floor[m^2].

The superscripts +/- imply infiltration/exfiltration, respectively.

In stack-dominated flow there is no infiltration through the ceiling nor is there any exfiltration through the floor because of the sign of the pressure difference across them.

We can find the infiltration through the walls by integrating from the floor to the neutral level, and the exfiltration by integrating from the neutral level to the ceiling:

$$Q_w^+ = A_w \sqrt{\frac{2}{\rho} P_s} \int_0^{\beta^o} \sqrt{\beta^o - \beta}\, d\beta \tag{C.9.1}$$

$$Q_w^- = A_w \sqrt{\frac{2}{\rho} P_s} \int_{\beta^o}^{1} \sqrt{\beta - \beta^o}\, d\beta \tag{C.9.2}$$

where

Q_w is the infiltration/exfiltration through a wall [m^3/s]

A_w is the effective leakage area of the walls [m^2].

If we now make the useful definitions,

$$A_o = A_w + A_c + A_f \tag{C.10.1}$$

$$R = \frac{A_c + A_f}{A_o} \tag{C.10.2}$$

$$X = \frac{A_c - A_f}{A_o} \tag{C.10.3}$$

where

A_o is the total (effective) leakage area [m^2],

R is the fraction of leakage in the floor and ceiling and

X is the effective leakage distribution parameter.

we can rewrite the expressions for the total stack infiltration and exfiltration:

$$Q_{stack}^+ = A_o \sqrt{2gh\frac{\Delta T}{T}} \left[\frac{R - X}{2} \sqrt{\beta^o} + \frac{2}{3} (1 - R) (\beta^o)^{3/2} \right] \tag{C.11.1}$$

$$Q_{stack}^- = A_o \sqrt{2gh\frac{\Delta T}{T}} \left[\frac{R + X}{2} \sqrt{1 - \beta^o} + \frac{2}{3} (1 - R) (1 - \beta^o)^{3/2} \right] \tag{C.11.2}$$

Treating air as an incompressible gas requires that the infiltration and exfiltration be equal. Therefore, the relationship between the neutral level (β^o) and the vertical leakage distribution parameter (X) is fixed:

$$X = \frac{\frac{4}{3}(1-R)\left[(\beta^o)^{3/2} - (1-\beta^o)^{3/2}\right] + R\left[\sqrt{\beta^o} - \sqrt{1-\beta^o}\right]}{\sqrt{\beta^o} + \sqrt{1-\beta^o}} \qquad (C.12)$$

Using this expression, any one of the parameters from the set $\{\beta^o, X, R\}$ can be found from the other two.

Because the expressions for infiltration and exfiltration are equal, it does not matter what linear combination we use to find the actual air flow; for ease of calculation and minimization of errors we use the average of the two expressions:

$$Q_{stack} = \frac{A_o}{3}\sqrt{2gh\frac{\Delta T}{T}}\,(R+2)\,\frac{\sqrt{\beta^o}\,\sqrt{1-\beta^o}}{\sqrt{\beta^o}+\sqrt{1-\beta^o}} \qquad (C.13)$$

While it is possible to measure the neutral level directly,[1] in most cases it will be the variable X that will be available. Accordingly, we have used approximation methods to find an expression for the infiltration that contains X instead of the neutral level:

$$Q_{stack} = \frac{A_o\sqrt{gh\frac{\Delta T}{T}}}{3}\,(1+R/2)\left[1 - \frac{X^2}{(2-R)^2}\right]^{3/2} \qquad (C.14)$$

Summary

In this part of the Appendix we have derived formulae for calculating infiltration due to the presence of an indoor-outdoor temperature difference. Below is a listing of these equations with some definitions

of terms.

$$Q_{stack} = A_o \, f_s^* \sqrt{\Delta T} \tag{C.15.1}$$

$$Q_{stack} = A_o \, f_s \sqrt{gH\frac{\Delta T}{T}} \tag{C.15.2}$$

where

f_s^* is the reduced stack parameter [m/s/$\sqrt{K}$] and

f_s is the (dimensionless) stack parameter.

As is obvious from these two equations,

$$f_s^* = f_s \sqrt{\frac{gH}{T}} \tag{C.16}$$

The stack parameter has two different expressions that are essentially equal: the exact expression which requires knowledge of the height of the neutral level,

$$f_s = \frac{(1+R/2)}{3} \left[\frac{\sqrt{8}\,\sqrt{\beta^o}\,\sqrt{1-\beta^o}}{\sqrt{\beta^o}+\sqrt{1-\beta^o}} \right] \tag{C.17.1}$$

and the approximate expression which requires knowledge only of the relative leakiness of the floor and the ceiling.

$$f_s = \frac{(1+R/2)}{3} \left[1 - \frac{X^2}{(2-R)^2} \right]^{3/2} \tag{C.17.2}$$

Note that X=0 implies $\beta^o = 1/2$ which implies that both terms in brackets are equal to unity. Furthermore, there is an exact relationship between X and β^o as given previously.

PART II — Wind Effect

The wind pressure is caused by the loss of kinetic energy associated with the deceleration of wind when it strikes a fixed object. This relation is given by the expression,

$$\frac{dP}{dv} = -\rho v \qquad (C.18)$$

where

P is the static pressure [Pa] and

v is the real free-stream wind speed [m/s].

Care must be taken in determinating the velocity in the above expression. There are two factors which complicate the measurement of the free-stream wind speed: terrain and shielding.

Terrain effects result from the fact that the measurement of wind speed may not occur at the same height or in the same general geographic terrain as the infiltration measurements (i.e. both the height and the geography can affect the free-stream wind speed.) Conventionally, we define the wind speed, v, to be the free-stream wind speed at the ceiling height of the structure. This convention for defining wind speed necessitates a method for converting wind speed obtained from a weather-tower measurement to a local free-stream wind speed. To do this, we make use of standard wind-engineering formulae:[2]

$$v = v_o \alpha \left(\frac{H}{10}\right)^{\gamma} \qquad (C.19)$$

where

v is the actual wind speed

v_o is the wind speed at standard conditions

α, γ are constants that depend on terrain class

To calculate the wind speed at one site from measured data at another site, we first use the above formula to calculate the standard wind speed for the measurement site; then the standard wind speed is used to calculate the wind speed at the desired site. Standard conditions are defined to be a height of 10 m and a terrain of class II. The following formulae are useful in calculating the actual wind speed:

$$v = v_o \, \alpha \left(\frac{H}{10}\right)^{\gamma} \tag{C.20.1}$$

$$v' = v_o \, \alpha' \left(\frac{H'}{10}\right)^{\gamma'} \tag{C.20.2}$$

$$v = v' \left[\frac{\alpha \left(\frac{H}{10}\right)^{\gamma}}{\alpha' \left(\frac{H'}{10}\right)^{\gamma'}} \right] \tag{C.20.3}$$

In these expressions, the primed quantities are from a wind measurement site. Values for the two parameters dependent on terrain class are shown in Table A.1.

From the above expression, we can define a terrain factor, f_T, that converts measured wind speed into effective wind speed:

$$f_T = \left[\frac{\alpha \left(\frac{H}{10}\right)^{\gamma}}{\alpha' \left(\frac{H'}{10}\right)^{\gamma'}} \right] \tag{C.21}$$

Although we can now calculate the free-stream wind speed, we are not yet able to calculate the wind pressures felt by the structure because we have not taken into account local shielding. Buildings and other obstructions within a few house-heights of the site will tend to slow or otherwise block the wind from having its full impact on the structure. To account for this phenomenon, we use a set of shielding coefficients* to convert the free-stream wind pressure into that actually felt by the structure.

Thus,

$$\frac{dP}{dv} = - C \rho v \qquad (C.22)$$

where

C is the shielding coefficient.

In the general case, the shielding coefficient will be a function of incident wind angle and position on the surface of the structure; however, full-scale studies [3] have shown that the pressure distribution on flat faces can be adequately described by using the average pressure on the face. Thus, there is one (angle-dependent) shielding coefficient for each face of the structure.*

$$\frac{dP_j}{dv} = C_j \rho v \qquad (C.23)$$

where

P_j is the static pressure on the jth face [Pa]

C_j is the shielding coefficient for the jth face

Integrating this equation yields,

$$P_j = P^j + C_j \; 1/2 \; \rho \; v^2 \qquad (C.24)$$

where

P^j is the jth constant of integration [Pa].

---

* The term shielding coefficient is equivalent to the more standard term of exterior pressure coefficient; the only difference lies in the interpretation. We use the term shielding coefficient to mean the ratio of the average exterior wind pressure to the stagnation pressure at the ceiling height.

Leakage through the envelope allows the internal pressure to be affected by the wind; thus, there will be an internal shielding coefficient analogous to the external ones above:

$$P_o = P^o + C_o \; 1/2 \; \rho \; v^2 \qquad (C.25)$$

where

P^o is the interior constant of integration [Pa] and

C_o is the internal shielding coefficient.

Note that the internal shielding coefficient is not an independent quantity; like the neutral level in the stack effect case, it is fixed by the equality of infiltration and exfiltration.

Since at zero wind speed the pressure across the envelope is zero, all of the integration constants must be equal. That is,

$$P^j = P^o \qquad \text{for all } j \qquad (C.26)$$

Furthermore, if we construct the differential surface pressure across the structure, the constant of integration will disappear altogether:

$$\Delta P_j = P_j - P_o \qquad (C.27.1)$$

$$= (C_j - C_o) \; 1/2 \; \rho \; v_2 \qquad (C.27.2)$$

ϕ The shielding coefficients are functionally dependent on the angle between the incident wind and the orientation of the structure. Since we will eventually average the shielding coefficients over angle, we have suppressed their explicit dependence on angle.

To find the infiltration, we use these equations with the leakage function (Eq A.1):

$$Q^{+}_{wind} = v \sum_j A_j \sqrt{\overline{C_j} - \overline{C_o}} \qquad \text{for } C_j > C_o \qquad (C.28.1)$$

$$Q^{-}_{wind} = v \sum_j A_j \sqrt{\overline{C_o} - \overline{C_j}} \qquad \text{for } C_j < C_o \qquad (C.28.2)$$

where

Q^{+}_{wind} is the infiltration due to the wind [m^3/s] and

Q^{-}_{wind} is the exfiltration due to the wind [m^3/s].

Conceptually, we can solve the problem in the same way as in the stack effect case: equate the infiltration and exfiltration to find C_o and then take the average of the infiltration and exfiltration to find the air flow. While the latter can be done, i.e.,

$$Q_{wind} = \frac{v}{2} \sum_j A_j \sqrt{\left| \overline{C_j} - \overline{C_o} \right|} \qquad (C.29)$$

the former cannot. The internal shielding coefficient, which is a function of the other shielding coefficients and leakage areas, cannot be found in general but, rather, must be calculated numerically for specific values of the leakage areas and shielding coefficients.

Rather than accept the situation and require detailed knowledge about shielding and leakage, we shall make some physically reasonable assumptions and use approximation techniques to get a general solution. In most cases the ceiling and floor of a structure are well shielded (i.e. there is usually an attic, basement or slab that protects these horizontal surfaces from direct wind effects). Accordingly, we assume that their shielding coefficients are negligible. In general, directional effects are not interesting; therefore, we average over incident wind angle, yielding,

$$Q_{wind} = \frac{A_o}{2} v \left[(1 - R) \langle \sqrt{| C_j - C_o |} \rangle + R \langle \sqrt{| C_o |} \rangle \right] \quad (C.30)$$

where

$\langle \ldots \rangle$ indicate an average over direction

We have reduced the problem to the evaluation of average shielding coefficients, which are independent of the leakage areas. We must now evaluate the shielding coefficients to finish the calculation of the wind effect. In most cases, the shielding coefficients of a structure will not be known; therefore, we propose to use wind tunnel data for a typically shaped structure within a turbulent boundary layer. Such a study was done at Colorado State University by Akins, et. al.[4]

It would be far more convenient to have an algebraic expression in closed form that describes the wind effect; accordingly, we have used the wind tunnel data to numerically fit these expressions to a functional form that describes the data to within 5%:

$$Q_{wind} = A_o v (1 - R) 1/3 C' \quad (C.31)$$

where

C' is the generalized shielding coefficient.

The aforementioned study considered only the case of the "self-shielded" structure. In any real situation, however, there will be local obstructions in the neighborhood of the building; we, therefore, propose to break the shielding into five classes, where class I is the "self-shielded" case and the remaining classes scale down the value of the shielding coefficients equally. Because we are assuming that all of the shielding coefficients scale the same way, C' but not n will be affected by a change in shielding class. Table C.2 contains the values of the generalized shielding coefficient C' for all five shielding classes.

We are now in a position to defined the reduced wind parameter in a manner similar to that used for the reduced stack parameter; i.e.,

$$Q_{wind} = f_w^* A_o v' \tag{C.32}$$

where

f_w^* is the reduced wind parameter:

$$f_w^* = C' (1 - R)^{1/3} \left[\frac{\alpha \left(\frac{H}{10}\right)^{\gamma}}{\alpha' \left(\frac{H'}{10}\right)^{\gamma'}} \right] \tag{C.33}$$

Summary

In this part of the Appendix we have derived formulae for calculating infiltration due to the presence of steady-state wind impinging on the surface of the building, and we are now in a position to summarize the results. Below is a listing of these equations with some convenient definitions of terms.

$$Q_{wind} = A_o f_w^* v' \tag{C.34.1}$$

$$Q_{wind} = A_o f_w v \tag{C.34.2}$$

where

f_w^* is the reduced wind parameter and

f_w is the wind parameter.

These two parameters are related by the terrain factor

$$f_w^* = f_w f_T \tag{C.35}$$

The wind parameter is an approximate quantity that contains information

about the general shielding and the leakage distribution:

$$f_w = C' \, (1 - R)^{1/3} \qquad (C.36)$$

The quantities necessary for the calculating the terrain factor and the generalized shielding coefficient are in tables at the end of this Appendix.

REFERENCES

1. M.H. Sherman, D.T. Grimsrud, R.C. Diamond, Infiltration-Pressurization Correlation: Surface Pressures and Terrain Effects, ASHRAE Trans. 85 Part II:DE-79-1, 1979.

2. European Convention for Constructional Steelwork, "Recommendations for the Calculation of Wind Effects on Buildings and Structures", Technical General Secretariat, Brussels, Belgium, September 1978.

3. S. Kim, K.C. Mehta, Full Scale Measurements on a Flat Roof Area, in Proceedings of the Fifth Int. Conf. Wind Engineering, Boulder, Colorado, July 1979.

4. R.E. Akins, J.A. Peterka, and J.E. Cermak, Average Pressure Coefficients for Rectangular Buildings, in Proceedings of the Fifth Int. Conf. Wind Engineering, Boulder, Colorado, July 1979.

TABLES

C.1: Terrain parameters for standard terrain classes

Class	γ	α	Description
I	0.10	1.30	Ocean or other body of water with at least 5 km of unrestricted expanse
II	0.15	1.00	Flat terrain with some isolated obstacles (e.g. buildings or trees well separated from each other
III	0.20	0.85	Rural areas with low buildings, trees, etc.
IV	0.25	0.67	Urban, industrial or forest areas
V	0.35	0.47	Center of large city (e.g. Manhattan)

Table C.2: Generalized shielding coefficient vs. local shielding

Shielding Class	C′	Description
I	0.324	No obstructions or local shielding whatsoever
II	0.285	Light local shielding with few obstructions
III	0.240	Moderate local shielding, some obstructions within two house heights
IV	0.185	Heavy shielding, obstructions around most of perimeter
V	0.102	Very heavy shielding, large obstruction surrounding perimeter within two house heights

APPENDIX D
DATA TABLES

This Appendix contains tables of data from 15 different sites around the country. Chapters IV and V refer to this data for comparison of models. Physical descriptions, geometric data, and measured leakage area are all displayed, as are the predicted and measured infiltrations for each site.

All data was extracted from the literature;[1-4] there are 15 sites taken from these three sources all of which were measured before the model was developed. The data extracted from reference 2 was collected by the authors.

Terrain Factor

The terrain factor displayed in these tables contains the terrain parameters and heights from both the wind measurement site and the test site. Specifically,

$$f_T = \frac{\alpha \left[\frac{H}{10}\right]^{\gamma}}{\alpha' \left[\frac{H'}{10}\right]^{\gamma'}}$$

where

f_T is the terrain factor,

H is the height [m] and

α, γ are the terrain parameters.

The terrain parameters can be found in Table C.1 of Appendix C. The primed quantities refer to the wind measurement site and the unprimed quantities refer to the test site.

Leakage Area

Generally, the leakage data extracted from the literature was not presented as "effective leakage area". In some cases, the leakage curves (for pressurization and depressurization) were given; in others only the flow rate at a specified pressure was provided. We had to devise a methodology for taking this type of data and converting it to effective leakage area for each case:

Low-Pressure Leakage Data. If leakage data was provided down to our reference pressure of 4 Pa (see Chapter III), we can use the leakage model (i.e.,

$$Q = A \sqrt{\frac{2}{\rho} \Delta P} \qquad (D.1)$$

where

Q is the air flow rate [m^3/s],

A is the effective leakage area [m^2] and

ΔP is the pressure drop [Pa])

to find the leakage area at the reference pressure:

$$A = Q(\Delta P_r) \sqrt{\frac{\rho}{2 \Delta P_r}} \qquad (D.2)$$

where

ΔP_r is the reference pressure [4 Pa].

High Pressure Leakage Data. If only high-pressure leakage data is provided (i.e. the leakage curve was measured but not down to the reference pressure), we use an empirical formula to extrapolate the data down to the reference pressure. The leakage data is fit to a power law function of the form,

$$Q = C \left[\Delta P \right]^n \qquad (D.3)$$

where

C,n are found through linear regression.

After finding the two unknown parameters, we extrapolate down to find the flow at the reference pressure and use that in the previous formula to find the effective leakage area.

Flow at Specified Pressure. If the only leakage data available is the leakage at a specified pressure, we cannot fit the data to any functional form. Some data[3] suggests that for a wide variety of envelope types the exponent in the above equation is 0.65. Accordingly, we will substitute 0.65 for n in the above expression and use the stated air flow and pressure to find C and, as in the previous case, the effective leakage area.

Infiltration Measurements

All of the infiltration measurements in this data were short-term tracer measurements using the decay technique. No attempt was made to quantify the effective volume of any of the test spaces; therefore, the physical volume was used to convert from air change rate to the infiltration.

In most cases, mixing problems were minimized by making sure that the tracer gas was well mixed before the decays had begun. This was done, whenever possible by using, the fan and duct system of the house; in lieu of that, additional mixing was supplied (e.g. mixing fans). Once the gas was well mixed, the additional mixing was stopped to prevent it from affecting the infiltration.

The error for this type of tracer gas measurement is typically about 10%.

Table 1 : Test results for test site #1

Site ID	IVANHOE
Reference No.	2
House Volume[a]	480
No. of Stories	2
Leakage Area[b]	100
Floor Area[a]	174
Terrain factor	0.85
Shielding Class	3
Reduced wind parameter	0.19
Reduced stack parameter[c]	0.16
Description	energy efficient basement active solar sealed combustion wood stove vapor barrier

Predicted and Measured Infiltration[d]				
Stack	Wind	Total Predicted	Measured	Difference
27	27	38	58	-34%
27	55	61	58	5%
27	41	49	48	2%

a) SI units

b) cm^2

c) $m/s/K^{1/2}$

d) m^3/hr

Table 2 : Test results for test site #2

Site ID	NOGAL
Reference No.	2
House Volume[a]	290
No. of Stories	1
Leakage Area[b]	960
Floor Area[a]	107
Terrain factor	0.70
Shielding Class	5
Reduced wind parameter	0.08
Reduced stack parameter[c]	0.10
Description	energy efficient slab on grade active solar and forced air vapor barrier

Predicted and Measured Infiltration[d]				
Stack	Wind	Total Predicted	Measured	Difference
60	47	76	64	19%

a) SI units

b) cm^2

c) $m/s/K^{1/2}$

d) m^3/hr

Table 3 : Test results for test site #3

Site ID	TELEMARK
Reference No.	2
House Volume[a]	480
No. of Stories	2
Leakage Area[b]	140
Floor Area[a]	197
Terrain factor	0.85
Shielding Class	2
Reduced wind parameter	0.22
Reduced stack parameter[c]	0.12
Description	energy efficient basement radiant oil fired heat — solar hot water vapor barrier seal combustion wood stove

Predicted and Measured Infiltration[d]				
Stack	Wind	Total Predicted	Measured	Difference
31	53	61	63	-3%
30	42	52	48	8%
30	32	44	38	16%

a) SI units

b) cm^2

c) $m/s/K^{1/2}$

d) m^3/hr

Table 4 : Test results for test site #4

Site ID	TOREY PINES
Reference No.	3
House Volume[a]	233
No. of Stories	3
Leakage Area[b]	200
Floor Area[a]	220
Terrain factor	0.90
Shielding Class	4
Reduced wind parameter	0.16
Reduced stack parameter[c]	0.14
Description	energy efficient basement active solar attached vertical greenhouse vapor barrier

Predicted and Measured Infiltration[d]				
Stack	Wind	Total Predicted	Measured	Difference
43	81	92	82	12%
44	69	82	72	14%
44	81	92	98	-6%
44	92	102	98	4%
45	92	103	89	16%

a) SI units

b) cm^2

c) $m/s/K^{1/2}$

d) m^3/hr

Table 5 : Test results for test site #5

Site ID	R-10
Reference No.	3
House Volume[a]	233
No. of Stories	1
Leakage Area[b]	330
Floor Area[a]	97
Terrain factor	0.85
Shielding Class	3
Reduced wind parameter	0.15
Reduced stack parameter[c]	0.09
Description	ranch style baseboard electric resistance heating

Predicted and Measured Infiltration[d]				
Stack	Wind	Total Predicted	Measured	Difference
50	80	94	105	-10%

a) SI units

b) cm^2

c) $m/s/K^{1/2}$

d) m^3/hr

Table 6 : Test results for test site #6

Site ID	T1
Reference No.	12
House Volume[a]	337
No. of Stories	1
Leakage Area[b]	330
Floor Area[a]	77
Terrain factor	0.77
Shielding Class	3
Reduced wind parameter	0.14
Reduced stack parameter[c]	0.10
Description	basement fireplace forced air

Predicted and Measured Infiltration[d]				
Stack	Wind	Total Predicted	Measured	Difference
64	23	68	74	-8%
12	45	46	54	-15%
51	67	84	78	8%

a) SI units

b) cm^2

c) $m/s/K^{1/2}$

d) m^3/hr

Table 7 : Test results for test site #7

Site ID	T2
Reference No.	12
House Volume[a]	433
No. of Stories	1
Leakage Area[b]	680
Floor Area[a]	100
Terrain factor	0.77
Shielding Class	3
Reduced wind parameter	0.17
Reduced stack parameter[c]	0.11
Description	basement fireplace forced air

Predicted and Measured Infiltration[d]				
Stack	Wind	Total Predicted	Measured	Difference
115	112	161	169	-5%
28	29	40	48	-17%
154	196	249	199	25%

a) SI units

b) cm^2

c) $m/s/K^{1/2}$

d) m^3/hr

Table 8 : Test results for test site #8

Site ID	HAVEN
Reference No.	2
House Volume[a]	230
No. of Stories	1
Leakage Area[b]	770
Floor Area[a]	100
Terrain factor	0.71
Shielding Class	5
Reduced wind parameter	0.07
Reduced stack parameter[c]	0.10
Description	crawl space forced air fireplace

Predicted and Measured Infiltration[d]				
Stack	Wind	Total Predicted	Measured	Difference
55	39	67	49	37%
92	58	109	71	54%
88	78	117	85	38%

a) SI units

b) cm^2

c) $m/s/K^{1/2}$

d) m^3/hr

Table 9 : Test results for test site #9

Site ID	PURDUE
Reference No.	2
House Volume[a]	240
No. of Stories	1
Leakage Area[b]	855
Floor Area[a]	93
Terrain factor	0.62
Shielding Class	4
Reduced wind parameter	0.11
Reduced stack parameter[c]	0.11
Description	crawl space forced air fireplace nonrectangular floor plan

Predicted and Measured Infiltration[d]				
Stack	Wind	Total Predicted	Measured	Difference
102	67	122	120	2%
102	67	122	125	-2%
102	136	170	154	10%
107	170	200	166	20%

a) SI units

b) cm^2

c) $m/s/K^{1/2}$

d) m^3/hr

Table 10 : Test results for test site #10

Site ID	NEILSON
Reference No.	2
House Volume[a]	250
No. of Stories	1
Leakage Area[b]	1275
Floor Area[a]	96
Terrain factor	0.62
Shielding Class	3
Reduced wind parameter	0.15
Reduced stack parameter[c]	0.12
Description	crawl space floor furnace fireplace — undampered nonrectangular floor plan

Predicted and Measured Infiltration[d]				
Stack	Wind	Total Predicted	Measured	Difference
123	138	185	175	6%
135	138	193	160	21%
110	69	130	185	-30%
123	69	141	340	-59%

a) SI units

b) cm^2

c) $m/s/K^{1/2}$

d) m^3/hr

Table 11 : Test results for test site #11

Site ID	V1
Reference No.	2
House Volume[a]	270
No. of Stories	1
Leakage Area[b]	560
Floor Area[a]	104
Terrain factor	0.81
Shielding Class	3
Reduced wind parameter	0.18
Reduced stack parameter[c]	0.12
Description	energy efficient active solar slab on grade vapor barrier wood stove

Predicted and Measured Infiltration[d]				
Stack	Wind	Total Predicted	Measured	Difference
59	76	96	84	-5%
64	80	102	89	15%

a) SI units

b) cm^2

c) $m/s/K^{1/2}$

d) m^3/hr

Table 12 : Test results for test site #12

Site ID	V2
Reference No.	2
House Volume[a]	270
No. of Stories	1
Leakage Area[b]	630
Floor Area[a]	104
Terrain factor	0.81
Shielding Class	4
Reduced wind parameter	0.14
Reduced stack parameter[c]	0.12
Description	energy efficient active solar slab on grade vapor barrier wood stove

Predicted and Measured Infiltration[d]				
Stack	Wind	Total Predicted	Measured	Difference
82	143	165	173	14%
61	67	90	78	15%

a) SI units

b) cm^2

c) $m/s/K^{1/2}$

d) m^3/hr

Table 13 : Test results for test site #13

Site ID	FELS
Reference No.	1
House Volume[a]	470
No. of Stories	2
Leakage Area[b]	1480
Floor Area[a]	152
Terrain factor	0.84
Shielding Class	5
Reduced wind parameter	0.08
Reduced stack parameter[c]	0.13
Description	basement forced air

Predicted and Measured Infiltration[d]				
Stack	Wind	Total Predicted	Measured	Difference
277	170	325	355	-8%
183	426	464	320	45%

a) SI units

b) cm^2

c) $m/s/K^{1/2}$

d) m^3/hr

Table 14 : Test results for test site #14

Site ID	SAN CARLOS
Reference No.	2
House Volume[a]	145
No. of Stories	1
Leakage Area[b]	845
Floor Area[a]	58
Terrain factor	0.81
Shielding Class	4
Reduced wind parameter	0.15
Reduced stack parameter[c]	0.11
Description	crawl space floor furnace fireplace — undampered

Predicted and Measured Infiltration[d]				
Stack	Wind	Total Predicted	Measured	Difference
0	76	76	149	-49%
47	49	68	116	-41%
47	89	101	90	12%
0	93	93	107	-13%

a) SI units

b) cm^2

c) $m/s/K^{1/2}$

d) m^3/hr

Table 15 : Test results for test site #15

Site ID	SOUTHAMPTON
Reference No.	2
House Volume[a]	1000
No. of Stories	3
Leakage Area[b]	1640
Floor Area[a]	370
Terrain factor	0.90
Shielding Class	3
Reduced wind parameter	0.20
Reduced stack parameter[c]	0.16
Description	basement and crawl space fireplace forced air nonrectangular floor plan

Predicted and Measured Infiltration[d]				
Stack	Wind	Total Predicted	Measured	Difference
94	124	156	250	38%
188	124	255	310	-18%
94	124	156	190	-18%

a) SI units

b) cm^2

c) $m/s/K^{1/2}$

d) m^3/hr

REFERENCES

1. Harrje, D.T., Blomsterberg, A.K., and Persily, A., Reduction of Air Infiltration due to Window and Door Retrofits in an Older Home, Princeton University, Center for Environmental Studies, Report No. 85, 1979.

2. Grimsrud, D.T., Sherman, M.H., Blomsterberg, A.K., and Rosenfeld, A.H., Infiltration and Air Leakage Comparisons: Conventional and Energy Efficient Housing Designs, Presented at the International Conference on Energy Use Management, Los Angeles, October 1979. Lawrence Berkeley Laboratory Report No. 9157 1979

3. Johns-Manville Research and Development Center, Demonstration of Energy Conservation through Reduction of Air Infiltration in Electrically Heated Houses, RP 1351-1, 1979.

4. Tamura, G.T., The Calculation of House Infiltration Rates, ASHRAE TRANSACTIONS, 85, 1:58-71, 1979.

APPENDIX E

LINEAR LEAKAGE INFILTRATION MODEL

We have already shown in Appendix B that the leakage of a structure typically can be characterized by an effective leakage area, or, equivalently, we can say that the leakage is dominated by inertial flow. In some situations (e.g. a very tight structure) the leakage is dominated by viscous flow; in the viscous flow limit, the leakage is proportional to the pressure drop across the leak and, hence, can be characterized by a leakage constant (definition of leakage area):

$$Q(\Delta P) = L\,\Delta P \tag{E.1}$$

where

Q	is the flow through a crack [m^3/s],
ΔP	is the pressure across the crack [Pa] and
L	is the leakage constant [$m^3/s/Pa$].

We can use this leakage function in place of our previous one to repeat the derivation of infiltration; as this is the only significant change in our assumptions, the derivation will follow analogous lines to the one in Appendix C.

To start, we define the leakage distribution parameters:

$$R = \frac{L_{ceiling} + L_{floor}}{L_o} \tag{E.2.1}$$

$$X = \frac{L_{ceiling} - L_{floor}}{L_o} \tag{E.2.2}$$

where

L_o	is the total leakage of the structure [$m^3/hr/Pa$].

Again, we break up the problem into the stack and wind regimes.

Stack Regime

The pressures across the envelope in the stack-dominated case are given by the inside-outside temperature difference (as originally derived in Appendix C):

$$\Delta P = P_s \ (\beta^o - \beta) \tag{E.3}$$

where

P_s is the stack pressure [Pa],

β is the (dimensionless) height and

β^o is the (dimensionless) height of the neutral level.

In the above expression we have used the following definitions:

$$P_s = \rho \ g \ H \frac{\Delta T}{T} \tag{E.4.1}$$

$$\beta = \frac{h}{H} \tag{E.4.2}$$

where

H is the height of the structure [m].

We can now integrate the leakage function over the pressure distribution around the envelope:

$Q^+_{ceiling} = 0$	$Q^-_{ceiling} = L_{ceiling}\ P_s\ (1 - \beta^o)$
$Q^+_{walls} = 1/2\ L_{walls}\ P_s\ \beta^{o^2}$	$Q^-_{walls} = 1/2\ L_{walls}\ P_s\ (1 - \beta^o)^2$
$Q^+_{floor} = L_{floor}\ P_s\ \beta^o$	$Q^-_{floor} = 0$

Using our definitions of the leakage distribution parameters, we can simplify the expressions for the total infiltration and exfiltration:

$$Q^+ = L_o\ P_s \left[\frac{R - X}{2}\ \beta^o + \frac{1 - R}{2}\ \beta^{o^2} \right] \qquad (E.5.1)$$

$$Q^- = L_o\ P_s \left[\frac{R + X}{2}\ (1 - \beta^o) + \frac{1 - R}{2}\ (1 - \beta^o)^2 \right] \qquad (E.5.2)$$

Using mass balance, we can equate the infiltration and exfiltration to find a relationship between the height of the neutral level and the leakage distribution:

$$X = 2\ \beta^o - 1 \qquad (E.6.1)$$

or, equivalently,

$$\beta^o = \frac{1 + X}{2} \qquad (E.6.2)$$

Compare this to the rather complicated expression derived in Appendix C relating the neutral level to the ceiling-floor leakage difference for the square-root leakage case.

We can use this expression and either of the previous two to find the total amount of air flowing in and out of the structure:

$$Q_{stack} = L_o \; P_s \; \frac{1 + R}{2} \; \beta^o \; (\; 1 - \beta^o \;) \tag{E.7.1}$$

or, equivalently,

$$Q_{stack} = L_o \; P_s \; \frac{1 + R}{8} \; (\; 1 - X^2 \;) \; . \tag{E.7.2}$$

Thus,

$$Q_{stack} = L_o \; f_s^* \; \Delta T \tag{E.8}$$

where

f_s^* is the reduced stack parameter [Pa/K].

The reduced stack parameter is, then,

$$f_s^* = \frac{\rho g H}{T} \; \frac{1 + R}{2} \; \beta^o \; (\; 1 - \beta^o \;) \tag{E.9.1}$$

or,

$$f_s^* = \frac{\rho g H}{T} \; \frac{1 + R}{8} \; (\; 1 - X^2 \;) \tag{E.9.2}$$

Wind Regime

As in Appendix C, the wind-effect pressures are given by the effective wind speed and the shielding coefficients:

$$\Delta P_j = (\; C_j - C_o \;) \; \tfrac{1}{2} \; \rho \; v^2 \tag{E.10}$$

where

C_j is the shielding coefficient of the jth face and

C_o is the "internal" shielding coefficient.

This leads to a rather straightforward set of expressions for the

wind-induced infiltration and exfiltration:

$$Q^{+}_{wind} = \tfrac{1}{2}\rho v^2 \sum_j L_j \left[C_j - C_o \right] \qquad \text{for } C_j > C_o \qquad (E.11.1)$$

$$Q^{-}_{wind} = \tfrac{1}{2}\rho v^2 \sum_j L_j \left[C_o - C_j \right] \qquad \text{for } C_j < C_o \qquad (E.11.2)$$

where

Q^{+}_{wind} is the infiltration due to the wind [m^3/s] and

Q^{-}_{wind} is the exfiltration due to the wind [m^3/s].

Again, we assume that directional effects are unimportant and that the shielding coefficients of the floor and ceiling are negligible; by equating the infiltration and exfiltration, we can derive the expression relating the internal pressure coefficient to the others:

$$C_o = (1 - R) < C_w > \qquad (E.12)$$

where

$< \ldots >$ implies an average over direction.

The expression for the total air flow into and out of the structure is

$$Q_{wind} = L_o \; \tfrac{1}{2}\rho v^2 \left[\frac{R}{2} < \left| C_o \right| > + \frac{(1 - R)}{2} < \left| C_w - C_o \right| > \right] \qquad (E.13)$$

Using the definition of C_o yields,

$$Q_{wind} = L_o \; \tfrac{1}{2}\rho v^2 \; (1 - R) \frac{\left| C_w - C_o \right|}{2} \left[1 + R \frac{< \left| C_w - C_o \right| >}{< \left| C_w \right| >} \right] \qquad (E.14)$$

Using the wind tunnel studies [1] to evaluate the shielding expressions above,

$$< C_w > = -0.211 \qquad (E.15.1)$$

$$< \left| C_w - (-0.211) \right| > = 0.514 \qquad (E.15.2)$$

and these numbers permit us to find the final expression for the wind-effect infiltration. We can, however, only directly evaluate these expressions for the case R=0; for the case of R≠0 we must calculate the appropriate quantities numerically. Instead of this we have used numerical techniques to fit the measured wind data as a function of R, the result of which is accurate to better than 1%.

$$Q_{wind} = L_o \; \tfrac{1}{2}\rho v^2 \; (1 - R) \; (1 + \tfrac{1}{2} R) \; C' \qquad (E.16)$$

where

C' is the generalized shielding coefficient (see Table E.1).

Table E.1 contains the generalized shielding coefficients for the five different classes of shielding outlined in Appendix C. Shielding class I is calculated directly from the wind-tunnel data and the others are equally spaced below that.

The above expression uses the effective wind speed as its weather variable; in most cases, however, we wish to express the infiltration in terms of the wind speed measured at a weather station. Accordingly, we make use of standard methods [2] to convert the measured wind speed to the effective wind speed (see Appendix C for details):

$$v \; \alpha \left[\frac{H}{10}\right]^{\gamma} = v' \; \alpha' \; \left[\frac{H'}{10}\right]^{\gamma'} \qquad (E.17)$$

where

v' is the measured wind speed [m/s],

α, γ are the terrain parameters of the test site and

α', γ' are the terrain parameters of the wind measurement site.

Rewriting the wind infiltration yields,

$$Q_{wind} = L_o \; \tfrac{1}{2}\rho \left[v' \; \frac{\alpha \left[\frac{H}{10}\right]^{\gamma}}{\alpha' \left[\frac{H'}{10}\right]^{\gamma'}} \right]^2 (1 - R) (1 + \tfrac{1}{2} R) C' \tag{E.18}$$

We now define the reduced wind parameter,

$$f_w^* = \tfrac{1}{2}\rho \left[\frac{\alpha \left[\frac{H}{10}\right]^{\gamma}}{\alpha' \left[\frac{H'}{10}\right]^{\gamma'}} \right]^2 (1 - R) (1 + \tfrac{1}{2} R) C' \tag{E.19}$$

so that the wind-effect infiltration becomes,

$$Q_{wind} = L_o \; f_w^* \; v'^2 \tag{E.20}$$

<u>where</u>

f_w^* is the reduced wind parameter [kg/m^3].

Combining Wind and Stack Effects

We must now use our leakage model to combine the wind and stack effects, as calculated above. Because in this Appendix our model of leakage is linear, this task is much simpler than in Appendix C.

Consider the limit of a wind-dominated situation. The pressure distribution is assumed to be uniform on any given face of the structure; if we now "turn on" the stack effect by allowing a slight inside-outside temperature difference, there will be a vertical linear pressure dependence on height. Because the leakage is linear, however, the extra infiltration caused by the addition of positive pressures will be compensated for by the decrease in infiltration by the addition of a positive pressure to a negative pressure (similarly for exfiltration). Thus, there will be no net increase in infiltration due to a small stack effect.

The same situation applies if we are in a stack-dominated regime and we "turn on" a small wind effect — there will be no increase in the net infiltration. The situation becomes more complicated when the two effects are size. Specifically, whenever all of the neutral levels are between the ceiling and the floor, the stack effect applies, and whenever all of the neutral levels are outside of the floor and ceiling, the wind effect applies. The intermediate case is difficult to determine because it depends critically on the leakage distribution and shielding factors; accordingly, we make the assumption that all of the neutral levels cross the floor or ceiling boundary at the same time (i.e. there is a sharp dividing line between stack and wind effects). Thus, simply stated, it is the larger of the two effects (stack and wind) that determine the infiltration:

$$Q = \mathrm{MAX}(Q_{stack}, Q_{wind}) \qquad (E.21)$$

Summary

We have used a derivation analogous to the one in Appendix C to derive the infiltration equations for the case of linear leakage.

The stack effect infiltration is,

$$Q_{stack} = L_o \, f_s^* \, \Delta T \qquad (E.22)$$

where

L_o is the total leakage of the structure [$m^3/s/Pa$] and

f_s^* is the reduced stack parameter [Pa/K].

The reduced stack parameter is

$$f_s^* = \frac{\rho g H}{T} \frac{1 + R}{2} \beta^o (1 - \beta^o) \qquad (E.23.1)$$

where

β^o is the (normalized) height of the neutral level

$$\beta^o = \frac{1 + X}{2} \tag{E.24}$$

The wind effect has a similar form:

$$Q_{wind} = L_o \, f_w^* v'^2 \tag{E.25}$$

where

f_w^* is the reduced wind parameter [kg/m^3].

$$f_w^* = \tfrac{1}{2}\rho \left[\frac{\alpha \left[\frac{H}{10}\right]^{\gamma}}{\alpha' \left[\frac{H'}{10}\right]^{\gamma'}} \right]^2 (1 - R) (1 + \tfrac{1}{2} R) C' \tag{E.26}$$

where

C' is the generalized shielding coefficient (see Table E.1),

α, γ are terrain parameters (see Appendix C).

Once the two infiltrations are known, they are combined using the following formula:

$$Q = \mathrm{MAX}(Q_{stack}, Q_{wind}) \tag{E.27.1}$$

or,

$$Q = L_o \, \mathrm{MAX}(f_s^* \Delta T, f_w^* v'^2) \tag{E.27.2}$$

While the functions of the reduced parameters are the same in the linear case as they were in the square-root case, the forms and dimensions of these parameters are different: the physical interpretation of the leakage constant is not as apparent as the physical interpretation of the leakage area, etc. In general, the model developed in Appendix C should be sufficient for calculating infiltration; however, in certain

specific situations is may be more advantageous to use the linear model developed herein.

REFERENCES

1. R.E. Akins, J.A. Peterka, and J.E. Cermak, Average Pressure Coefficients for Rectangular Buildings, Proceedings of the Fifth International Conference Wind Engineering, Boulder, Colorado, July 1979.

2. European Convention for Constructional Steelwork, Recommendations for the Calculation of Wind Effects on Buildings and Structures, Technical General Secretariat, Brussels, Belgium, September 1978.

Table E.1: Generalized shielding coefficient vs. local shielding

Shielding Class	C'	Description
I	0.257	No obstructions or local shielding whatsoever
II	0.199	Light local shielding with few obstructions
III	0.141	Moderate local shielding, some obstructions within two house heights
IV	0.084	Heavy shielding, obstructions around most of perimeter
V	0.026	Very heavy shielding, large obstruction surrounding perimeter within two house heights